

See discussions, stats, and author profiles for this publication at: <https://www.researchgate.net/publication/319973956>

Light Stable Isotopic Compositions of Enriched Mantle Sources: Resolving the Dehydration Paradox

Article in *Geochemistry Geophysics Geosystems* · September 2017

DOI: 10.1002/2016GC006743

CITATIONS

2

READS

268

12 authors, including:



Jacqueline Eaby Dixon
University of South Florida
60 PUBLICATIONS 2,413 CITATIONS

[SEE PROFILE](#)



Ilya Bindeman
University of Oregon
242 PUBLICATIONS 5,087 CITATIONS

[SEE PROFILE](#)



Richard Kingsley
University of Rhode Island
41 PUBLICATIONS 2,562 CITATIONS

[SEE PROFILE](#)



Petrus Le Roux
University of Cape Town
76 PUBLICATIONS 1,284 CITATIONS

[SEE PROFILE](#)

Some of the authors of this publication are also working on these related projects:



Aragonite-Calcite Isotope Exchange [View project](#)



Rhyolite generation in Yellowstone [View project](#)



Geochemistry, Geophysics, Geosystems

RESEARCH ARTICLE

10.1002/2016GC006743

Key Points:

- H_2O and δD of EM and PREMA-type basalts correlate with indicators of mantle heterogeneity with distinctive correlations for each region
- δD in enriched mantle sources reflects slab dehydration and rehydration by fluids derived from cooler, deeper parts of the slab
- A multistage metasomatic and melting model accounts for the data by extending the subduction factory through the mantle transition zone

Supporting Information:

- Supporting Information S1
- Data Set S1

Correspondence to:

J. Dixon,
jdixon@usf.edu

Citation:

Dixon, J. E., Bindeman, I. N., Kingsley, R. H., Simons, K. K., Le Roux, P. J., Hajewski, T. R., ... Wallace, P. J. (2017). Light stable isotopic compositions of enriched mantle sources: Resolving the dehydration paradox. *Geochemistry, Geophysics, Geosystems*, 18. <https://doi.org/10.1002/2016GC006743>

Received 21 NOV 2016

Accepted 15 SEP 2017

Accepted article online 21 SEP 2017

Light Stable Isotopic Compositions of Enriched Mantle Sources: Resolving the Dehydration Paradox

J. E. Dixon¹ , I. N. Bindeman², R. H. Kingsley³, K. K. Simons⁴, P. J. Le Roux⁵, T. R. Hajewski^{6,7}, P. Swart⁸, C. H. Langmuir⁹ , J. G. Ryan¹⁰, K. J. Walowski^{2,11} , I. Wada¹² , and P. J. Wallace²

¹College of Marine Science, University of South Florida, St. Petersburg, FL, USA, ²Department of Earth Sciences, University of Oregon, Eugene, OR, USA, ³Graduate School of Oceanography, University of Rhode Island, Narragansett, RI, USA,

⁴Exxon-Mobil, Houston, TX, USA, ⁵Department of Geological Sciences, University of Cape Town, Rondebosch, South Africa,

⁶Department of Geology, University of Miami, Miami, FL, USA, ⁷Now at University of Iowa Hospitals & Clinics, Iowa City, IA, USA, ⁸Division of Marine Geology and Geophysics, Rosenstiel School of Marine and Atmospheric Science, University of Miami, Miami, FL, USA, ⁹Department of Earth and Planetary Science, Harvard University, Cambridge, MA, USA, ¹⁰School of Geosciences, University of South Florida, Tampa, FL, USA, ¹¹Now at Department of Geology, Middlebury College, Middlebury, VT, USA, ¹²Department of Earth Sciences, University of Minnesota, Minneapolis, MN, USA

Abstract Volatile and stable isotope data provide tests of mantle processes that give rise to mantle heterogeneity. New data on enriched mid-oceanic ridge basalts (MORB) show a diversity of enriched components. Pacific PREMA-type basalts ($\text{H}_2\text{O}/\text{Ce} = 215 \pm 30$, $\delta\text{D}_{\text{SMOW}} = -45 \pm 5 \text{ ‰}$) are similar to those in the northern Atlantic ($\text{H}_2\text{O}/\text{Ce} = 220 \pm 30$; $\delta\text{D}_{\text{SMOW}} = -30$ to -40 ‰). Basalts with EM-type signatures have regionally variable volatile compositions. Northern Atlantic EM-type basalts are wetter ($\text{H}_2\text{O}/\text{Ce} = 330 \pm 30$) and have isotopically heavier hydrogen ($\delta\text{D}_{\text{SMOW}} = -57 \pm 5 \text{ ‰}$) than northern Atlantic MORB. Southern Atlantic EM-type basalts are damp ($\text{H}_2\text{O}/\text{Ce} = 120 \pm 10$) with intermediate $\delta\text{D}_{\text{SMOW}}$ ($-68 \pm 2 \text{ ‰}$), similar to $\delta\text{D}_{\text{SMOW}}$ for Pacific MORB. Northern Pacific EM-type basalts are dry ($\text{H}_2\text{O}/\text{Ce} = 110 \pm 20$) and isotopically light ($\delta\text{D}_{\text{SMOW}} = -94 \pm 3 \text{ ‰}$). A multistage metasomatic and melting model accounts for the origin of the enriched components by extending the subduction factory concept down through the mantle transition zone, with slab temperature a key variable. Volatiles and their stable isotopes are decoupled from lithophile elements, reflecting primary dehydration of the slab followed by secondary rehydration, infiltration, and re-equilibration by fluids derived from dehydrating subcrustal hydrous phases (e.g., antigorite) in cooler, deeper parts of the slab. Enriched mantle sources form by addition of $<1\%$ carbonated eclogite \pm sediment-derived C-O-H-Cl fluids to depleted mantle at 180–280 km (EM) or within the transition zone (PREMA).

Plain Language Summary Water in enriched oceanic basalts is mostly recycled seawater that has been added to the mantle through deep melting of subducted slab igneous crust and sediments. The stable isotopic composition of the melted slab materials reflects complex dehydration and rehydration processes, as different lithologies dehydrate at different depths depending on their position in the slab and the overall slab thermal profile.

1. Introduction

Cycling of material from Earth's surface to its interior by subduction is a fundamental planetary process. It is generally accepted that the radiogenic isotopic and trace element compositions in mantle sources of ocean island and enriched mid-ocean ridge basalts (MORB) can be explained by "pollution" of depleted mantle by varying types and amounts of subduction-modified crustal material (e.g., Hofmann, 1997; Stracke, 2012; White, 1985, 2015; Zindler & Hart, 1986) or crustal melts (e.g., Asimow et al., 2004; Cooper et al., 2004; Donnelly et al., 2004; Weiss et al., 2016). However, questions remain about the mechanisms by which these recycled crustal materials are incorporated into the mantle. Traditionally, these questions have been addressed using passive tracers, including trace element concentrations and radiogenic isotopic compositions.

Volatile cycling, especially water, is critical for many Earth system processes, including generation of arc magmas, formation, and composition of the atmosphere and ocean, and even the evolution and maintenance of life (e.g., Lane, 2015). Water is not only an important passive tracer, but it also influences mantle

melting and the transport of trace elements and their associated isotopes. Light stable isotopes are also powerful passive tracers of subduction zone processes, such as the isotopic fractionations produced during weathering (e.g., Alt et al., 1986) and dehydration (e.g., Shaw et al., 2008). The difficulty with using volatiles as tracers of mantle processes, however, is that care must be taken to see through shallow modification (loss by degassing or gain by assimilation) to detect mantle source-related variations.

Isotopic fractionation of light stable elements (e.g., H, Li, and B) during subduction may shed light on the various mechanisms that recycle crustal materials into the deep mantle. Hydrogen isotopic heterogeneity in mantle reservoirs is particularly useful due to its large fractionation and strong signals. These isotopic ratios are reported in delta notation (δ) (e.g., δD_{SMOW}), where δX is the parts per thousand (permil) deviation from a standard. For example, δD is the permil deviation of a measured ratio of deuterium to hydrogen (D/H) relative to D/H of Standard Mean Ocean Water (SMOW), where $\delta D_{SMOW} = 0 \text{ ‰}$.

Typical δD_{SMOW} for fresh MORB thought to be characteristic of the depleted upper mantle is $\sim -80 \pm 10 \text{ ‰}$ (e.g., Kyser & O'Neil, 1984; Poreda et al., 1986). As oceanic crustal rocks move away from the ridge, hydration during seafloor alteration shifts the hydrogen isotopic composition to heavier values of about $-40 \pm 20 \text{ ‰}$ (Stakes, 1991; Satake & Matsuda, 1979; Stakes & O'Neil, 1982; Sheppard & Epstein, 1970; Wenner & Taylor, 1974). During subduction, dehydration of hydrous minerals reverses these shifts, because deuterium partitions preferentially into the fluid phase ($1000 \ln \alpha = \sim +20 \pm 20 \text{ ‰}$). This produces isotopically heavier fluids exiting the slab with initial δD_{SMOW} of $\sim -20 \pm 20 \text{ ‰}$ (Graham et al., 1984; Saccoccia et al., 2001; Sakai & Tsutsumi, 1978; Suzuki & Epstein, 1976; Vennemann & O'Neil, 1996), and leaving behind a slab depleted in deuterium.

Metasomatism of the mantle wedge by these slab-derived fluids results in heavy isotopic compositions characteristic of arc and back-arc basin basalts ($\delta D_{SMOW} = -10 \text{ to } -57 \text{ ‰}$) (Hochstaedter et al., 1990; Honma et al., 1991; Marty et al., 2001; Poreda, 1985; Shaw et al., 2008). As dehydration progresses and D is increasingly removed from the slab by a distillation process, both the released fluids and the slab itself should become isotopically lighter. This theoretically results in extremely light hydrogen isotopic composition in residual mostly dehydrated slabs. Predicted δD_{SMOW} of mostly dehydrated slabs range from about $-110 \pm 10 \text{ ‰}$ (Walowski et al., 2015) to -230 ‰ (Shaw et al., 2008). This "light slab" model predicts two complementary reservoirs—a light residual slab, and a correspondingly heavy mantle wedge (or at least those portions of the wedge in contact with fluids). According to this model, incorporation of subduction-modified materials from the residual slab into the deeper mantle should create mantle sources having δD_{SMOW} that are much lighter than MORB. In contrast, incorporation of mantle wedge materials should create mantle sources having δD_{SMOW} much heavier than MORB. In support of this light slab model, Hauri (2002) presented stable isotopic analyses of melt inclusions in olivines from Koolau (Hawaii) suggesting an enriched mantle source δD_{SMOW} of -120 ‰ , similar to the values predicted by Walowski et al. (2015).

Based on trace element ratios and radiogenic isotopic compositions, some mantle end-member compositions (see section 3) are thought to include subduction-modified, mostly dehydrated igneous crust or crustal-derived melts. The light slab model predicts that these basalts should have light δD_{SMOW} values. In contrast to light slab model predictions, however, limited data on δD_{SMOW} values in those end-member basalts show that they are actually heavier ($\sim -35 \text{ ‰}$) than MORB (Kingsley et al., 2002; O'Leary et al., 2002; Poreda et al., 1986). Thus, there is an inconsistency in models for the origin of mantle enrichment depending on the data set being used. Many models based on nonvolatile trace elements and radiogenic isotopes suggest enrichments related to mostly dehydrated igneous crust and sediments (e.g., Stracke, 2012); whereas models based on hydrogen isotopic compositions suggest involvement of hydrated mantle wedge materials. This inconsistency sets up an apparent "dehydration paradox."

Other enriched mantle sources are thought to contain mantle wedge-like compositions with chemical characteristics related to sediment-derived melts and fluids, or to subcontinental lithospheric mantle (SCLM) (see section 3). These mantle sources with wedge-like compositions, therefore, should have elevated H₂O concentrations, H₂O/Ce, and δD_{SMOW} values, similar to the hydrated mantle wedge source of arc basalts. Existing stable isotopic data on enriched basalts are insufficient to test this hypothesis and is one of the motivations for the current study.

In this paper, new volatile concentration and hydrogen isotopic data are presented for mid-ocean ridge basaltic glasses from a wide range of locations (Figure 1). Each area contains enriched basalts, either related

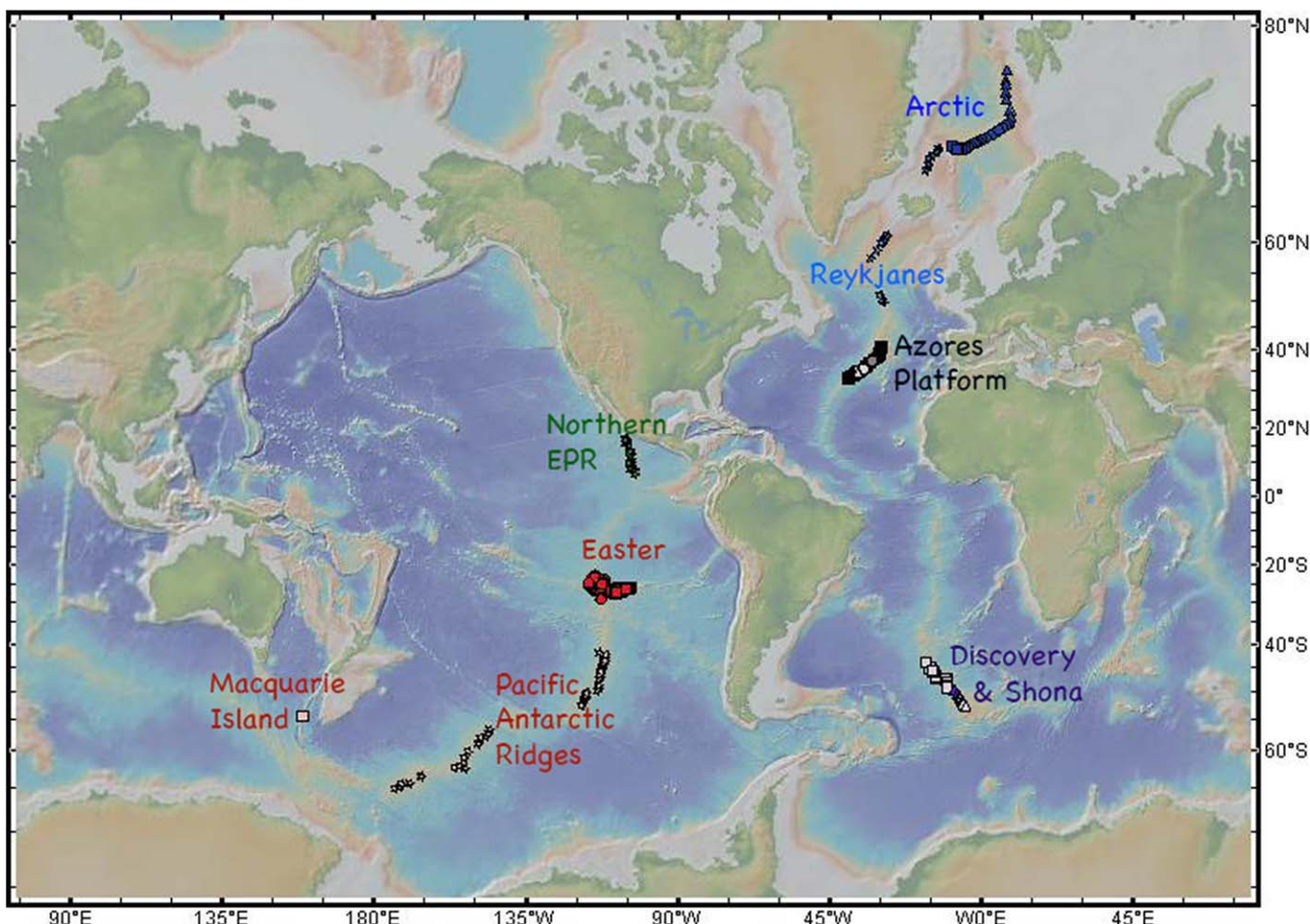


Figure 1. Sample locations (Geomapapp: <http://www.geomapapp.org/>). Close-up maps for each region are provided in supporting information S2.

to plume-ridge interaction or more dispersed heterogeneities. Plume-influenced basalts erupted in deep water, either along the mid-ocean ridge or on the margins of ocean islands, provide an important way to learn about volatiles in enriched mantle sources. While ocean islands can be representative of various mantle sources in terms of radiogenic isotopes and certain trace element ratios, sampling lavas at their exposed tops may present a highly biased picture. In particular, these samples are pervasively degassed and frequently modified by fractional crystallization and assimilation of crustal materials. In addition, studies of water in melt inclusions are often complicated by diffusion of H_2O in or out of the inclusion, as well as degassing of the host magmas.

The sample suites include the East Pacific Rise (6–17°N), the northern Mid-Atlantic Ridge, including the Arctic Ridges north of Iceland and ridges near the Azores Platform, and the southern Mid-Atlantic Ridge adjacent to the Shona and Discovery geochemical anomalies. Boron, lithium, and oxygen isotopic compositions are presented for a few locations. These and other published data are used to develop a comprehensive model for the volatile element, trace element, and radiogenic and stable isotopic composition of most basaltic melts, resolving the dehydration paradox.

The proposed model effectively extends the depth of the “subduction factory” well beyond the zone of arc magmatism. In contrast to the relatively shallow, H_2O -dominated arc magmatic system, these deeper melting systems are dominated by the phase equilibria of carbonated slab lithologies at ~200 km (where carbonated sediment melts) and at >410 km in the transition zone (where carbonated eclogite melts). For cooler slabs, water in subcrustal serpentine is carried well below depths of arc magma-genesis and is available to rehydrate the previously dehydrated slab and to buffer the isotopic composition of light elements to heavier predehydration values.

2. Analytical Techniques: Comparison of FTIR and TC/EA Techniques

Analytical results from multiple laboratories and methods, generated over four decades, are examined to investigate and understand subtle variations in basalt composition. Thus, special attention is paid to correction of interlaboratory and intertechnique biases. Where necessary, samples have been reanalyzed and/or recalibrated to account for these differences. Details of analytical techniques and the various corrections that have been applied are provided in supporting information. A summary of key issues is given below.

Dissolved water and carbon dioxide concentrations in glasses were measured using transmission infrared spectroscopy (FTIR), following the procedures of Dixon and Clague (2001). New FTIR results are presented for the Arctic Ridges north of Iceland, along with published values from the Azores Platform, south Atlantic, and EMP-ESC ridges (Dixon et al., 2002; Simons et al., 2002). Water concentrations in some bulk glasses were also measured using the TC/EA (Thermal Conversion Elemental Analyzer, or pyrolysis furnace) continuous flow system at the University of Oregon following the procedures of Bindeman et al. (2012) and Martin et al. (2017). New TC/EA results are presented here for the East Pacific Rise from 6° to 17° N, along with published data from Macquarie Island (Bindeman et al., 2012). Water concentrations measured by FTIR and TC/EA on the Azores Platform and EMP-ESC glasses show excellent agreement. For H_2O concentrations <1 wt. %, the slope of the nonweighted least square regression fit indicates that the TC/EA data are slightly lower than FTIR data by $\sim 4\%$, however the slope is not different from unity at the 2σ level. When data >1 wt. % with larger uncertainties are included, the regression fit indicates that TC/EA data are lower than FTIR data by $\sim 10\%$, with the difference in slope from unity significant at the 2σ level. (supporting information Figure S1–3). Larger uncertainties FTIR analyses of high H_2O glasses are primarily due to glass heterogeneity. Any offset in the $\delta\text{D}_{\text{SMOW}}$ values, discussed below, is unlikely to be due to incomplete water extraction during TC/EA analysis.

New $\delta\text{D}_{\text{SMOW}}$ results presented here were generated using both conventional stepped-heating manometry mass-spectrometry, analyzed at the University of Miami Stable Isotope Laboratory following the procedures of Kingsley et al. (2002), and TC/EA at the University of Oregon (Bindeman et al., 2012). Additional data are compiled from various laboratories using both conventional and TC/EA techniques. Based on reevaluation of the TC/EA mica standardization procedure, as discussed in the supporting information, a $\delta\text{D}_{\text{SMOW}}$ correction of $+16\text{ ‰}$ is applied to previously published TC/EA data on basaltic glasses from the Bindeman laboratory discussed in this study, including data from Macquarie Island (Bindeman et al., 2012). Based on analysis of a suite of glasses from the Easter Salas y Gomez Seamount Chain (ESC) using both techniques, as well as application of the revised standardization for the TC/EA data and consistent SMOW normalization for the conventional data, an offset of $10 \pm 6\text{ ‰}$ remains (supporting information Figure S1–4), with the TC/EA data lighter by $\sim 10\text{ ‰}$ than the conventional data. Data are not adjusted to reflect this offset.

3. Radiogenic Isotopic and Trace Element Ratio Characterization of Enriched Mantle Sources

Measured volatile concentrations and stable isotopic values are presented in the context of mantle heterogeneity; therefore, it is useful to first review the various mantle components and their characteristics. The original definition of four extreme mantle components was based on radiogenic Pb, Nd, and Sr isotopes in ocean island basalts (OIB) (e.g., White, 1985; Zindler & Hart, 1986; see reviews in Hofmann, 1997, 2014; Stracke, 2012; White, 2015). These include (1) DMM (depleted MORB mantle); (2) HIMU (“high μ ” where $\mu = {}^{238}\text{U}/{}^{204}\text{Pb}$; e.g., St. Helena); (3) EM1 (enriched mantle 1; e.g., Kerguelen); and (4) EM2 (enriched mantle 2; e.g., Society). In this context, “enriched” refers to time-integrated Rb/Sr, Sm/Nd, and/or (U + Th)/Pb ratios higher than primitive mantle (bulk silicate earth), but often also refers to strong enrichments in incompatible elements. These mantle end-members are well resolved on a plot of ${}^{87}\text{Sr}/{}^{86}\text{Sr}$ versus ${}^{206}\text{Pb}/{}^{204}\text{Pb}$, used to characterize regional end-members throughout this paper.

Mantle sources for normal-type MORB (NMORB) are characterized by depletions in highly incompatible elements (e.g., large-ion lithophile elements (LILE) and some high-field strength elements (HFSE) relative to more compatible elements as a result of ancient extraction of melts to form oceanic, and ultimately continental, crust (e.g., Engel et al., 1965; Hofmann, 1988, 2003; Melson et al., 1976; Sun & McDonough, 1989). Over time, melt extraction-related parent/daughter element fractionations result in the characteristic unradiogenic (low) ${}^{87}\text{Sr}/{}^{86}\text{Sr}$ and ${}^{206}\text{Pb}/{}^{204}\text{Pb}$ and radiogenic (high) ${}^{143}\text{Nd}/{}^{144}\text{Nd}$. Recent work (Gale et al., 2013a)

to establish the mean composition of ocean ridge basalts clearly shows that mantle sources for NMORB, even those far from hotspots, may contain variable amounts of other mantle components.

HIMU basalts (sometimes referred to as Extreme HIMU) are rare (St. Helena, Cook Austral Chain, Chatham Islands, and Mt. Eerebus) (Willbold & Stracke, 2006) and are not represented in this study. They are characterized by having $^{206}\text{Pb}/^{204}\text{Pb}$ greater than 20.5, low $^{87}\text{Sr}/^{86}\text{Sr}$ (Zindler & Hart, 1986), and low $^{3}\text{He}/^{4}\text{He}$ (Barfod et al., 1999; Hanyu et al., 2011; Hanyu & Kaneoka, 1997; Moreira & Kurz, 2001). Trace element compositions of HIMU basalts from different locations are remarkably homogeneous, characterized by strong depletions in incompatible elements, enrichments in Nb and Ta relative to Ba and Rb, and depletions in Pb, Rb, and Ba relative to EM basalts (Willbold & Stracke, 2006). These trace element systematics are consistent with trends caused by dehydration of oceanic crust during subduction, which results in net loss of Cs, Rb, Ba, K, LREE, Pb, and Sr due to removal of fluid-mobile elements, but in relative enrichment of Nb and Ta due to retention of Nb and Ta in residual rutile (Ayers, 1998; Brenan et al., 1994, 1995; Bromiley & Redfern, 2008; Foley et al., 2000; Keppler, 1996; Klemme et al., 2002, 2005; Kogiso et al., 1997; McCulloch & Gamble, 1991; Schmidt et al., 2004a; Stalder et al., 1998). Thus, HIMU basalts are most likely formed by direct melting of recycled ancient subduction-modified oceanic lithosphere (e.g., Chase, 1981; Chauvel et al., 1992, 1997; Fitton, 2007; Halliday et al., 1988; Hart, 1988; Hauri et al., 1994; Hauri & Hart, 1993; Hofmann, 1997, 2014; Hofmann & White, 1982; Lassiter & Hauri, 1998; Niu & Batiza, 1997; Niu et al., 1999; Palacz & Saunders, 1986; Roy-Barman & Allégre, 1995; Salters & White, 1998; Stracke et al., 2003, 2005; Vidal et al., 1984; White, 1985; Zindler & Hart, 1986).

EM1 and EM2, referred to simply as EM in this study, share the characteristics of relatively high $^{87}\text{Sr}/^{86}\text{Sr}$ and low $^{206}\text{Pb}/^{204}\text{Pb}$. In contrast to the relative homogeneity of HIMU basalts, each suite of EM has its own unique trace element fingerprint (Willbold & Stracke, 2006). Overall, EM basalts are enriched in fluid-mobile elements, including alkalis (Rb, K), Ba, Th, and Pb, and are depleted in Nb and Ta relative to similarly incompatible elements (Chauvel et al., 1992; Dostal et al., 1998; Dupuy et al., 1988; Jackson & Dasgupta, 2008; Weaver, 1991; Willbold & Stracke, 2006; White & Duncan, 1996; Workman et al., 2004). Thus, in addition to high $^{87}\text{Sr}/^{86}\text{Sr}$, EM basalts are characterized by high Ba/Nb, used here as a key geochemical indicator. Two preferred explanations for EM-type enrichments are (1) recycling of oceanic lithosphere plus overlying sediments (Chauvel et al., 1992, 2008; Cohen & O'Nions, 1982; Eisele et al., 2002; Hawkesworth et al., 1979; Hemond et al., 1994; Jackson & Dasgupta, 2008; Jackson et al., 2007; Rehkämper & Hofmann, 1997; Weis et al., 1993; White & Duncan, 1996; Woodhead & Devey, 1993), and (2) recycling of upper and lower continental crust via delamination (Arndt & Goldstein, 1989; Kay & Kay, 1993) or subduction erosion at erosive plate margins (Clift & Vannucci, 2004; Scholl et al., 1980; Stern, 2011; Stern & Scholl, 2010; von Huene & Scholl, 1993). These two mechanisms are not necessarily mutually exclusive. Varying proportions of different sediment types and/or upper and lower continental crust are the most common explanations for the differences in EM1 and EM2 compositions.

While these end-members constrain the compositional extremes, most radiogenic isotopic data from ocean islands and mid-ocean ridges adjacent to hotspots form near-linear mixing arrays that converge in a limited region of isotopic space. This common component has moderately depleted Sr and Nd signatures, radiogenic Pb isotopes, and often, but not always, elevated $^{3}\text{He}/^{4}\text{He}$ (Hauri et al., 1994). White (1985) initially assigned Hawaii as the best representative of this common component, but since then various workers have given it different acronyms and debated both its isotopic composition and significance. Acronyms include PREMA (prevalent mantle; Zindler & Hart, 1986), C (common mantle component; Hanan & Graham, 1996), FOZO (focus zone; Hart et al., 1992, 1994), and PHEM (primitive helium mantle; Farley et al., 1992). To add more confusion, the radiogenic Pb end of DMM-PREMA arrays has also been referred to as HIMU, distinct from Extreme HIMU that refers to the highest $^{206}\text{Pb}/^{204}\text{Pb}$ basalts from St. Helena and the Cook Austral Chain. The acronym PREMA is used here, replacing FOZO as used by Dixon et al. (2002), to denote the radiogenic Pb end of commonly occurring DMM-PREMA arrays of oceanic basalts. Its isotopic composition intermediate between EM and HIMU suggests involvement of recycled crustal materials in its formation.

The models for formation of enriched mantle sources cited above focus on the mechanism of wholesale mixing of recycled subduction-modified crustal lithologies into depleted mantle. A growing body of work, however, has focused on producing the incompatible element enriched characteristics of enriched sources through multistage metasomatism and melting models. In these models, depleted mantle is metasomatized

Table 1

Locations and Selected Major, Minor, and Volatile Element Concentrations for Arctic Ridge Basalts (From North to South)

Sample (EN026)	EN25D-2	EN22D-1	EN21D-1	EN19D-1	EN27D-1	EN27D-2
Location ^a	Knipovich	Knipovich	Knipovich	Knipovich	Knipovich	Knipovich
Latitude (°N) ^a	77.53	76.86	76.56	75.96	75.52	75.52
Longitude (°W) ^a	−7.67	−7.37	−7.19	−7.28	−7.50	−7.50
Depth (m) ^a	2925	3450	2810	3258	2600	2600
⁸⁷ Sr/ ⁸⁶ Sr ^b	0.702902	0.702864	0.702746	0.702863	0.703462	0.703493
²⁰⁶ Pb/ ²⁰⁴ Pb ^b	18.218	18.248	18.174	18.312	18.553	18.552
MgO (wt. %) ^a	7.95	7.27	7.50	7.72		7.01
H ₂ O (wt. %, FTIR) ^c	0.456 (4)	0.566 (28)	0.602 (31)	0.594 (33)		
CO ₂ (ppm, FTIR) ^c	364 (13)	179 (11)	150 (7)	184 (12)		
Ba (ppm) ^d	96.0	99.1	69.3	93.0	106.7	98.7
Nb (ppm) ^d	10.1	10.6	7.35	9.77	9.31	9.00
La (ppm) ^d	6.63	8.09	5.83	8.07	7.46	6.92
Ce (ppm) ^d	15.7	19.8	15.3	21.0	18.7	17.1
Ba/Nb	9.50	9.32	9.43	9.52	11.5	11.0
H ₂ O/Ce	291	286	393	283		
δD _{SMOW} (‰, conv.) ^e		−28.6 (5.0)	−45.1 (5.0)			
δ ¹⁸ O (‰) ^f		5.61 (8)	5.54 (8)			
Sample (EN026)	EN29D-1	EN30D-1	EN31D-1	EN32D-1	EN32D-3	EN16D-1
Location ^a	Knipovich	Knipovich	Knipovich	Mohns	Mohns	Mohns
Latitude (°N) ^a	74.65	74.19	73.74	73.52	73.52	73.41
Longitude (°W) ^a	−8.51	−8.84	−8.37	−8.11	−8.11	−7.39
Depth (m) ^a	2878	3210	3290	2288	2288	2623
⁸⁷ Sr/ ⁸⁶ Sr ^b	0.702928	0.703137	0.703018	0.703173	0.703173	0.702853
²⁰⁶ Pb/ ²⁰⁴ Pb ^b	18.115	18.342	18.277	17.619	17.927	17.556
MgO (wt. %) ^a	8.25	7.77	7.82		8.27	8.28
H ₂ O (wt. %, FTIR) ^c	0.397 (22)	0.457 (16)	0.257 (3)	0.386 (11)	0.264 (5)	0.214 (9)
CO ₂ (ppm, FTIR) ^c	188 (7)	199 (8)	177 (8)	169 (10)	164 (7)	350 (35)
Ba (ppm) ^d	64.4	117	56.5		41.1	24.8
Nb (ppm) ^d	6.32	10.7	5.06		2.98	2.00
La (ppm) ^d	5.22	7.84	4.46		2.92	2.35
Ce (ppm) ^d	13.48	18.2	12.3		8.49	7.24
Ba/Nb	10.2	10.9	11.2		13.8	12.4
H ₂ O/Ce	295	251	208		311	296
δD _{SMOW} (‰, conv.) ^e		−48.5 (5.0)	−48.9 (5.0)	−56.7 (5.0)		−51.4 (5.0)
δ ¹⁸ O (‰) ^f			5.55 (8)			5.54 (8)
Sample (EW026 or TR139)	EN16D-2	EN15D-1	TR33D-2	EN14D-1	TR32D-1	EN12D-2
Location ^a	Mohns	Mohns	Mohns	Mohns	Mohns	Mohns
Latitude (°N) ^a	73.41	73.22	73.01	72.81	72.61	72.32
Longitude (°W) ^a	−7.39	−6.44	−5.18	−4.26	−3.38	−1.48
Depth (m) ^a	2623	2840	2900	2540	3020	2525
⁸⁷ Sr/ ⁸⁶ Sr ^b	0.702865	0.703202	0.703154	0.703013	0.703101	0.703196
²⁰⁶ Pb/ ²⁰⁴ Pb ^b	17.956	18.382	18.288	17.919	18.227	18.501
MgO (wt. %) ^a		7.93	10.40	7.77	8.15	7.60
H ₂ O (wt. %, FTIR) ^c	0.222 (5)	0.464 (14)	0.394 (12)	0.289 (16)	0.395 (13)	0.648 (12)
CO ₂ (ppm, FTIR) ^c	211 (18)	294 (11)	224 (11)	204 (13)	182 (4)	317 (9)
Ba (ppm) ^d	22.7	93.5	72.7	51.5	74.5	222
Nb (ppm) ^d	1.77	8.99	6.70	4.15	6.79	23.6
La (ppm) ^d	1.95	6.62	5.65	3.81	5.06	15.1
Ce (ppm) ^d	6.24	15.2	13.86	10.4	12.3	30.1
Ba/Nb	12.8	10.4	10.9	12.4	11.0	9.4
H ₂ O/Ce	356	306	284	277	322	215
δD _{SMOW} (‰, conv.) ^e		−52.1 (5.0)	−52.1 (5.0)	−55.5 (5.0)	−52.9 (5.0)	−48.4 (5.0)
δ ¹⁸ O (‰) ^f		5.53 (8)	5.58 (8)	5.51 (8)	5.65 (8)	

Table 1. (continued)

Sample (EW026 or TR139)	EN12D-3	TR31D-2	EN11D-1	EN10D-1	EN10D-3	TR30D-1
Location ^a	Mohns	Mohns	Mohns	Mohns	Mohns	Mohns
Latitude (°N) ^a	72.32	72.18	71.99	71.89	71.89	71.82
Longitude (°W) ^a	−1.48	−0.23	0.65	1.39	1.39	2.08
Depth (m) ^a	2525	2462	2340	2900	2900	2550
⁸⁷ Sr/ ⁸⁶ Sr ^b	0.703204	0.703066	0.703190	0.703206	0.703185	0.703212
²⁰⁶ Pb/ ²⁰⁴ Pb ^b	18.460	17.970	18.363	18.288	18.294	18.643
MgO (wt. %) ^a		7.66	7.67	7.60	7.59	
H ₂ O (wt. %, FTIR) ^c	0.548 (9)	0.378 (8)	0.645 (15)	0.531 (20)	0.501 (28)	1.101 (66)
CO ₂ (ppm, FTIR) ^c	329 (14)	147 (7)	200 (9)	196 (8)	172 (11)	0 (40)
Ba (ppm) ^d	200	61.0	122	83.9	94.9	339
Nb (ppm) ^d	17.3	5.21	12.1	7.84	8.50	39.3
La (ppm) ^d	11.0	4.75	8.56	6.02	7.15	23.5
Ce (ppm) ^d	22.6	12.6	19.3	14.6	17.3	46.1
Ba/Nb	11.6	11.7	10.1	10.7	11.2	8.6
H ₂ O/Ce	243	300	334	364	290	239
δD _{SMOW} (‰, conv.) ^e		−60.3 (5.0)	−47.5 (5.0)		−55.8 (5.0)	−45.6 (5.0)
δ ¹⁸ O (‰) ^f	5.62 (8)	5.55 (8)	5.62 (8)		5.49 (8)	
Sample (EW026 or TR139)	TR30D-2	EN9D-1	EN8D-1	EN8D-2	EN7D-1	EN7D-2
Location ^a	Mohns	Mohns	Mohns	Mohns	Jan Mayen	Jan Mayen
Latitude (°N) ^a	71.82	71.64	71.53	71.53	71.43	71.43
Longitude (°W) ^a	2.08	3.06	3.94	3.94	4.79	4.79
Depth (m) ^a	2550	2220	2925	2925	2488	2488
⁸⁷ Sr/ ⁸⁶ Sr ^b	0.703206	0.703089	0.703202	0.703190	0.703173	0.703449
²⁰⁶ Pb/ ²⁰⁴ Pb ^b	18.624	18.538	18.579	18.600	18.677	18.822
MgO (wt. %) ^a		7.64	7.75	3.90	4.06	7.87
H ₂ O (wt. %, FTIR) ^c	1.295 (85)	0.646 (12)	1.75 (12)	1.77 (23)	0.759 (2)	
CO ₂ (ppm, FTIR) ^c	0 (40)	223 (17)	0 (40)	0 (40)	127 (5)	
Ba (ppm) ^d	293	147	278	286	146	1139
Nb (ppm) ^d	29.7	16.1	30.6	31.1	15.8	110
La (ppm) ^d	21.0	10.5	18.7	19.3	10.4	53.6
Ce (ppm) ^d	41.1	22.5	41.6	42.9	22.7	109
Ba/Nb	9.9	9.1	9.1	9.2	9.2	10.4
H ₂ O/Ce	315	288	420	413	335	
δD _{SMOW} (‰, conv.) ^e		−44.1 (5.0)	−41.8 (5.0)		−41.1 (5.0)	−32.7 (5.0)
δ ¹⁸ O (‰) ^f			5.57 (8)		5.57 (8)	5.46 (8)
Sample (EW026)	EN6D-1	EN5D-1	EN4D-3	EN3D-2	EN2D-1	EN1D-1
Location ^a	Jan Mayen					
Latitude (°N) ^a	71.33	71.24	71.26	71.19	71.41	71.48
Longitude (°W) ^a	5.43	5.78	6.48	7.09	7.49	8.63
Depth (m) ^a	1725	750	690	1100	890	1675
⁸⁷ Sr/ ⁸⁶ Sr ^b	0.703232	0.703482	0.703451	0.703413	0.703406	0.703423
²⁰⁶ Pb/ ²⁰⁴ Pb ^b	18.785	18.89	18.848	18.855	18.840	18.845
MgO (wt. %) ^a		10.66	6.53	7.13	7.26	4.96
H ₂ O (wt. %, FTIR) ^c						
CO ₂ (ppm, FTIR) ^c						
Ba (ppm) ^d	587	527	905	858	1053	1184
Nb (ppm) ^d	62.0	61.9	83.5	83.2	103	117
La (ppm) ^d	25.1	32.4	44.4	47.5	59.9	52.9
Ce (ppm) ^d	49.4	66.7	92.2	98.2	125	109
Ba/Nb	9.5	8.5	10.8	10.3	10.2	10.1
H ₂ O/Ce						
δD _{SMOW} (‰, conv.) ^e						
δ ¹⁸ O (‰) ^f						

Table 1. (continued)

Sample (TR139 or AK)	TR27D-5	TR27D-6	AK1351-1C	AK1350-1B	AK1349-1A	TR23D-1
Location ^a	Kolbein.	Kolbein.	Kolbein.	Kolbein.	Kolbein.	Kolbein.
Latitude (°N) ^a	71.33	71.33	71.06	70.66	70.36	69.73
Longitude (°W) ^a	12.64	12.64	12.98	14.31	15.42	15.59
Depth (m) ^a	1205	1205	525	1200	925	917
⁸⁷ Sr/ ⁸⁶ Sr ^b	0.703074	0.703086	0.703090	0.703047	0.702964	0.702795
²⁰⁶ Pb/ ²⁰⁴ Pb ^b	18.864	18.932	18.879	18.114	18.301	18.032
MgO (wt. %) ^a	4.88		9.80	7.69	8.75	7.21
H₂O (wt. %, FTIR)^c	0.956 (37)	0.931				0.184 (4)
CO₂ (ppm, FTIR)^c	0 (40)	0 (40)				0 (40)
Ba (ppm) ^d	241	268	110	15.4	32.5	11.0
Nb (ppm) ^d	26.5	29.8	11.2	1.64	3.28	1.12
La (ppm) ^d	16.5	18.8	7.18	1.94	2.76	1.16
Ce (ppm) ^d	33.4	37.8	15.1	6.27	7.05	5.17
Ba/Nb	9.1	9.0	9.8	9.4	9.9	9.8
H₂O/Ce	287	246				356
δD_{SMOW} (‰, conv.)^e		-54.6 (5.0)				-56.3 (5.0)
δ¹⁸O (‰)^f		5.62 (8)				5.53 (8)
Sample (TR139)	TR24D-1	TR25D-3				
Location ^a	Kolbein.	Kolbein.				
Latitude (°N) ^a	69.73	69.15				
Longitude (°W) ^a	15.74	16.22				
Depth (m) ^a	1038	1145				
⁸⁷ Sr/ ⁸⁶ Sr ^b	0.702764	0.702691				
²⁰⁶ Pb/ ²⁰⁴ Pb ^b	17.987	17.912				
MgO (wt. %) ^a						
H₂O (wt. %, FTIR)^c	0.171 (9)	0.154 (8)				
CO₂ (ppm, FTIR)^c	117 (4)	98 (7)				
Ba (ppm) ^d	9.90	8.20				
Nb (ppm) ^d	0.95	0.68				
La (ppm) ^d	1.26	1.06				
Ce (ppm) ^d	4.36	3.60				
Ba/Nb	10.4	12.1				
H₂O/Ce	392	428				
δD_{SMOW} (‰, conv.)^e	-	-				
δ¹⁸O (‰)^f	-	-				

Note. New data in bold font. Values in parentheses are 1σ standard deviations in the last or last two decimal places based on multiple analyses of glass samples (H_2O and CO_2 concentrations) or standards (stable isotopic data).

^aLocations, depths, and major elements for Arctic basalts are from Sigurdsson (1981) and Neumann and Schilling (1984).

^bRadiogenic isotopic compositions from Schilling et al. (1999).

^cTotal dissolved water and carbon dioxide analyzed by FTIR (supporting information S1.1).

^dTrace element data from Trønnes et al. (1999) and Kelley et al. (2013).

^e $\delta\text{D}_{\text{SMOW}}$ by conventional stepped-heating/manometry/mass-spectrometry at the University of Miami Stable Isotope Laboratory (supporting information S1.2).

^f $\delta^{18}\text{O}$ by laser-fluorination at the California Institute of Technology (supporting information S1.8).

by low degree partial melts derived from downwelling subducted crustal materials, followed by transport and repose in the deep mantle to produce characteristic radiogenic isotopic compositions, and ultimately followed by a second stage of higher extent melting of metasomatized peridotite during upwelling at ridge crests or within mantle plumes (e.g., Asimow et al., 2004; Cooper et al., 2004; Donnelly et al., 2004; Weiss et al., 2016). These metasomatic models explain major, trace element, and oxygen isotopic variations and provide an alternative to direct recycling of crustal lithologies (e.g., Cooper et al., 2004; Donnelly et al., 2004). Another class of models calls upon generation of metasomatizing melts by melting of ambient mantle during mantle upwelling or at the interface between the low-velocity zone and the cooling and thickening oceanic lithosphere (autometasomatism) (Galer & O’Nions, 1986; Halliday et al., 1995; McKenzie & O’Nions, 1983, 1995; Niu et al., 2002; Niu & O’Hara, 2003; Roden et al., 1984; Workman et al., 2004) or by melting of recycled components within upwelling mantle (Sobolev et al., 2007). Volatiles and stable isotopes

Table 2

Locations and Selected Major, Minor and Volatile Element Concentrations for Azores Platform (FAZAR/Mid-Atlantic Ridge) Basalts (From South to North)

Sample (All127-)	D1-2	D55-1b	D55-3	D5-5	D54-3	D7-6
Location ^a	HA-1	OH-3	OH-3	OH-3	OH-3	OH-2
Latitude (°N) ^a	33.176	33.727	33.727	33.912	34.058	34.356
Longitude (°W) ^a	39.246	37.784	37.784	37.706	37.648	37.100
Depth (m) ^a	2712	3736	3736	3018	3335	2941
⁸⁷ Sr/ ⁸⁶ Sr ^b	0.702745	0.702973			0.702937	0.702760
²⁰⁶ Pb/ ²⁰⁴ Pb ^b	18.090	18.577			18.455	18.768
MgO (wt. %) ^a	7.89	9.13		9.86	7.27	9.35
H ₂ O (wt. %, FTIR) ^c	0.169 (7)	0.145 (3)	0.139 (2)	0.131 (4)	0.242 (1)	0.097 (4)
CO ₂ (ppm, FTIR) ^c	130 (30)	265 (6)	216 (9)	180 (13)	104 (7)	125 (8)
Ba (ppm) ^d	3.94	13.7	13.7	12.54	35.1	9.48
Nb (ppm) ^d		2.46	2.38		5.46	1.69
La (ppm) ^d	1.83	1.88	1.92	2.05	3.71	1.38
Ce (ppm) ^d	6.26	5.12	5.18	5.79	9.37	3.84
Ba/Nb		5.56	5.76		6.43	5.61
H ₂ O/Ce	270	283	268	226	258	253
H ₂ O (wt. %, TC/EA) ^e	0.14 (2)	0.10 (1)	0.17 (2)	0.09 (1)	0.32 (3)	0.09 (1)
δD _{SMOW} (‰, TC/EA) ^e	-89.0 (5.0)	-83.4 (3.0)	-77.8 (3.0)	-85.1 (3.0)	-95.5 (3.0)	-79.5 (3.0)
δ ⁷ Li (‰) ^f	3.45 (20)					
Vesicles (vol. %) ^c				1	2	2
Sample (All127-)	D52-3	D8-5	D50-1	D50-2	D9-10	D46a
Location ^a	OH-1	OH-1	OH-1	OH-1	35°N	35°N
Latitude (°N) ^a	34.578	34.709	34.842	34.842	35.220	35.243
Longitude (°W) ^a	36.515	36.494	36.433	36.433	34.765	34.820
Depth (m) ^a	2971	2734	2235	2235	1657	1930
⁸⁷ Sr/ ⁸⁶ Sr ^b	0.702907	0.702824		0.702936	0.703677	0.703438
²⁰⁶ Pb/ ²⁰⁴ Pb ^b	18.704	18.481		18.614	19.060	19.170
MgO (wt. %) ^a	7.43	9.61		8.88	5.71	7.49
H ₂ O (wt. %, FTIR) ^c	0.234 (1)	0.119 (12)	0.220 (15)	0.241 (2)	0.792 (59)	0.645 (20)
CO ₂ (ppm, FTIR) ^c	148 (3)	161 (16)	104 (6)	121 (2)	118 (29)	144 (3)
Ba (ppm) ^d	38.6	6.20	32.5	32.0	471	207
Nb (ppm) ^d	6.56	1.52	5.77	5.81	77.3	33.7
La (ppm) ^d	4.21	1.86	3.74	3.87	47.3	20.5
Ce (ppm) ^d	10.42	5.18	9.37	9.53	95.6	41.1
Ba/Nb	5.88	4.08	5.64	5.50	6.09	6.14
H ₂ O/Ce	225	230	235	253	83	157
H ₂ O (wt. %, TC/EA) ^e	0.08 (1)	0.24 (2)	0.24 (2)			0.58 (3)
δD _{SMOW} (‰, TC/EA) ^e	-96.1 (7.3)	-75.7 (3.0)	-75.7 (3.0)			-71.4 (3.0)
δ ⁷ Li (‰) ^f						
Vesicles (vol. %) ^c	1	2		60	30	
Sample (All127-)	D49-3	D45a	D44-1	D43-1	D43-3A	D41-1
Location ^a	35°N	35°N	35°N	35°N	35°N	35°N
Latitude (°N) ^a	35.257	35.302	35.318	35.520	35.520	35.671
Longitude (°W) ^a	36.263	34.865	34.862	34.784	34.784	34.281
Depth (m) ^a	3684	2487	2383	3146	3146	2697
⁸⁷ Sr/ ⁸⁶ Sr ^b	0.702936	0.703664	0.704040			
²⁰⁶ Pb/ ²⁰⁴ Pb ^b	18.720	18.465	17.820			
MgO (wt. %) ^a	7.78	8.36	7.72	7.65	7.28	6.49
H ₂ O (wt. %, FTIR) ^c	0.274 (3)	0.395 (20)	1.290 (28)	0.419 (6)	0.499 (33)	0.523 (13)
CO ₂ (ppm, FTIR) ^c	234 (5)	140 (11)	73 (7)	175 (5)	148 (26)	123 (5)
Ba (ppm) ^d	43.0		443	118		
Nb (ppm) ^d	8.02	18.5	71.9	17.3		
La (ppm) ^d	4.96	12.5	45.3	10.2		
Ce (ppm) ^d	11.7	25.3	87.0	20.6		
Ba/Nb	5.36		6.16	6.82		
H ₂ O/Ce	234	156	148	203		
H ₂ O (wt. %, TC/EA) ^e	0.25 (2)	0.36 (4)	1.04 (7)		0.0.34 (3)	0.47 (5)

Table 2. (continued)

Sample (All127-)	D49-3	D45a	D44-1	D43-1	D43-3A	D41-1
δD_{SMOW} (‰, TC/EA) ^e	−72.3 (5.7)	−70.4 (3.0)	−57.1 (3.0)		−75.1 (3.0)	−74.2 (3.0)
$\delta^7\text{Li}$ (‰) ^f	−	4.2 (2)	5.7 (2)			
Vesicles (vol. %) ^c	5	25	25			
Sample (All127-)	D40-6	D10-6	D10-4A	D11-6	D12-5	D13-6
Location ^a	35°N	PO-6	PO-6	PO-5	PO-4	PO-2
Latitude (°N) ^a	35.772	35.954	35.954	36.161	36.296	36.996
Longitude (°W) ^a	34.226	34.159	34.159	33.975	33.757	32.942
Depth (m) ^a	2445	2321	2321	3048	2278	2678
$^{87}\text{Sr}/^{86}\text{Sr}$ ^b	0.703940	0.703035	0.703035	0.703090	0.703196	0.703019
$^{206}\text{Pb}/^{204}\text{Pb}$ ^b	18.126	18.243	18.243	18.606	18.842	18.498
MgO (wt. %) ^a	8.01	8.14	8.24	8.75	9.35	7.85
H_2O (wt. %, FTIR) ^c	0.195 (13)	0.213 (7)	0.213 (8)	0.266 (16)	0.186 (13)	0.241 (14)
CO_2 (ppm, FTIR) ^c	184 (12)	210 (19)	215 (8)	168 (12)	168 (15)	165 (23)
Ba (ppm) ^d	35.2	31.7	32.4	42.5	21.5	44.8
Nb (ppm) ^d	5.28	5.42	5.22	7.61		
La (ppm) ^d	3.88	3.98	4.08	4.74	2.94	3.54
Ce (ppm) ^d	9.75	9.64	9.74	10.86	7.59	8.80
Ba/Nb	6.67	5.85	6.21	5.58		
$\text{H}_2\text{O}/\text{Ce}$	200	221	219	245	245	274
H_2O (wt. %, TC/EA) ^e		0.20 (2)	0.19 (2)	0.21 (2)	0.18 (2)	
δD_{SMOW} (‰, TC/EA) ^e		−87.5 (3.0)	−84.8 (3.0)	−74.1 (3.0)	−88.8 (3.0)	
Vesicles (vol. %) ^c	10	2	2		2	5
Sample (All127-)	D14-2	D38-3	D36-12	D36-24	D15-avg	D17-5
Location	PO-2	Lucky Str.	Lucky Str.	Lucky Str.	Lucky Str.	KP-5
Latitude (°N) ^a	37.053	37.122	37.264	37.264	37.297	37.841
Longitude (°W) ^a	32.906	32.349	32.269	32.269	32.271	31.521
Depth (m) ^a	2963	2870	1867	1867	1600	926
$^{87}\text{Sr}/^{86}\text{Sr}$ ^b	0.703302	0.702953	0.702961		0.702945	0.703280
$^{206}\text{Pb}/^{204}\text{Pb}$ ^b	18.818	18.921	18.870		18.860	19.151
MgO (wt. %) ^a	6.99	7.48	7.48	7.74	8.08	8.20
H_2O (wt. %, FTIR) ^c	0.345 (23)	0.326 (8)	0.348 (4)	0.288 (7)	0.285 (8)	0.441 (62)
CO_2 (ppm, FTIR) ^c	145 (14)	141 (2)	88 (6)	121 (10)	140 (15)	39 (7)
Ba (ppm) ^d	57.9	54.8	59.8	55.4	60.0	210
Nb (ppm) ^d		8.37	9.02	8.54	8.66	24.3
La (ppm) ^d	3.72	5.00	5.37	4.90	5.15	14.2
Ce (ppm) ^d	9.80	11.2	12.48	11.43	11.5	28.4
Ba/Nb		6.55	6.63	6.49	6.93	8.64
$\text{H}_2\text{O}/\text{Ce}$	352	291	279	252	248	155
H_2O (wt. %, TC/EA) ^e	0.37 (4)	0.37 (4)		0.29 (3)		0.48 (2)
δD_{SMOW} (‰, TC/EA) ^e	−78.2 (3.0)	−81.8 (3.0)		−81.3 (3.0)		−71.0 (3.0)
$\delta^7\text{Li}$ (‰) ^f	3.8 (2)	3.7 (2)				4.8 (2)
Vesicles (vol. %) ^c	3	3	35		50	30
Sample (All127-)	D21-5	RC63	D22-6	D29-1	D27-4	D26-1
Location	KP-3	KP-3	KP-2	KP-2	KP-1	KP-1
Latitude (°N) ^a	38.495	38.828	39.044	39.437	39.504	39.907
Longitude (°W) ^a	30.262	30.087	30.028	29.849	29.739	29.674
Depth (m) ^a	1950	1240	1386	1905	2287	2093
$^{87}\text{Sr}/^{86}\text{Sr}$ ^b	0.703372	0.703504	0.703434	0.703335	0.703144	0.703039
$^{206}\text{Pb}/^{204}\text{Pb}$ ^b	19.651	19.479	19.447	19.416	18.999	18.629
MgO (wt. %) ^a	5.85	8.16	6.42	7.66	7.98	7.63
H_2O (wt. %, FTIR) ^c	1.220 (73)	0.764 (10)	0.922 (69)	0.801 (2)	0.455 (11)	0.364 (20)
CO_2 (ppm, FTIR) ^c	20 (5)	32 (10)	29 (4)	89 (3)	107 (19)	191 (42)
Ba (ppm) ^d	256	199	224	188		48.3
Nb (ppm) ^d	37.0	29.4	30.3	28.9		7.07
La (ppm) ^d	23.4	17.8	19.39	17.85	8.00	5.01
Ce (ppm) ^d	49.0	38.1	40.49	37.28	17.92	11.75

Table 2. (continued)

Sample (All127-)	D21-5	RC63	D22-6	D29-1	D27-4	D26-1
Ba/Nb	6.92	6.77	7.39	6.50		6.83
H ₂ O/Ce	249	201	228	215	254	310
H₂O (wt. %, TC/EA)^e	1.09 (5)	0.73 (4)	0.96 (5)	0.70 (3)	0.41 (2)	0.29 (3)
δD_{SMOW} (‰, TC/EA) ^e	-46.6 (3.0)	-50.9 (3.0)	-45.2 (3.0)	-58.1 (3.0)	-64.3 (3.0)	-82.8 (3.0)
$\delta^7\text{Li}$ (‰) ^f	4.10		3.7			3.24
Vesicles (vol. %) ^c	20	20	28		21	15

Note. New data in bold font. Values in parentheses are 1σ standard deviations in the last or last two decimal places based on multiple analyses of glass samples (H₂O and CO₂ concentrations) or standards (stable isotopic data).

^aLocations, depths, and major elements from Dosso et al. (1999).

^bRadiogenic isotopic compositions from Dosso et al. (1999).

^cDissolved H₂O and CO₂ concentrations by FTIR and vesicularity from Dixon et al. (2002).

^dTrace element data from Gale et al. (2013a).

^eH₂O concentration and δD_{SMOW} glass measured by High Temperature Conversion/Elemental Analyzer (TC/EA) at the University of Oregon (supporting information S1.4 and S1.5).

^fLithium was measured by MC-ICP-MS at Lamont-Doherty Earth Observatory (supporting information S1.7).

provide a critical role in evaluating these issues, because they provide the geochemical fingerprint of the origin of the proposed metasomatizing agent. Whatever the model, volatiles and their isotopes provide critical and relatively uninvestigated constraints.

All samples considered in this study are shown on two plots in the supporting information: Figures S2-2 (⁸⁷Sr/⁸⁶Sr versus ²⁰⁶Pb/²⁰⁴Pb) and S2-3 (Ba/Nb versus ²⁰⁶Pb/²⁰⁴Pb). Sources of trace element and radiogenic isotopic data are listed in the captions for these figures. High ⁸⁷Sr/⁸⁶Sr, low ²⁰⁶Pb/²⁰⁴Pb, and high Ba/Nb are used as indicators of an EM-type source, and high ²⁰⁶Pb/²⁰⁴Pb, low ⁸⁷Sr/⁸⁶Sr, and low Ba/Nb as indicators of a PREMA-type source.

In the following sections, key data are summarized for each study area, focusing on regional differences between north Atlantic (section 4) and south Atlantic and Pacific (section 5) ridges. Sections 4 and 5 address the question “How do volatiles and stable isotopes vary within each region as a function of mantle heterogeneity?” Sample locations and provenance, regional geochemical trends, including water concentrations and evidence for shallow modification, are provided in supporting information S2. New $\delta^{18}\text{O}$, $\delta^7\text{Li}$, and $\delta^{11}\text{B}$ data are discussed in supporting information S3. Because the behavior of Ba and Nb, and of H₂O and Ce, are similar during mantle melting and magma differentiation, Ba/Nb and H₂O/Ce of basalts are assumed to be representative of their mantle source. New volatile, δD_{SMOW} , $\delta^{18}\text{O}$, $\delta^7\text{Li}$, and $\delta^{11}\text{B}$ analyses, along with selected published major, trace, and radiogenic isotopic compositions, for all samples are listed in Tables (1–4). Full data tables are provided in supporting information. Section 6 provides a summary of key trends to be used as constraints on regional source end-member compositions and mixing components. Details of end-member modeling are described in supporting information S4.

Table 3
Southern Mid-Atlantic Ridge Data

Sample (EW93-09)	2D-1g	3D-1g	4D-3g	5D-5g	7D-1g	8D-1g
Location ^a	Discov.	Discov.	Discov.	Discov.	Discov.	Discov.
Latitude (°S) ^a	47.548	47.795	47.967	48.240	48.760	48.963
Longitude (°W) ^a	349.82	349.85	349.92	350.01	349.93	350.03
Depth (m) ^a	2493.5	2549.0	2895.0	3452.5	3217.5	3893.5
⁸⁷ Sr/ ⁸⁶ Sr ^b	0.704127		0.703762	0.703976	0.705093	0.704286
²⁰⁶ Pb/ ²⁰⁴ Pb ^b	18.064	18.114	18.069	18.084	17.773	17.798
MgO (wt. %) ^a	6.24	7.21	7.60	7.08	6.79	7.38
H ₂ O (wt. %, FTIR) ^c	0.483 (7)	0.378 (6)	0.296 (4)	0.436 (9)	0.503 (14)	0.295 (13)
CO ₂ (ppm, FTIR) ^c	160 (15)	181 (11)	173 (16)	219 (30)	190 (13)	192 (13)
Ba (ppm) ^d	201	148	106	177	340	104
Nb (ppm) ^d	15.9	12.1	8.62	14.3	20.8	7.58
La (ppm) ^d	15.5	12.6	9.31	14.3	17.7	8.70
Ce (ppm) ^d	34.5	28.3	21.7	32.3	36.4	21.4

Table 3. (continued)

Sample (EW93-09)	2D-1g	3D-1g	4D-3g	5D-5g	7D-1g	8D-1g
Ba/Nb	12.6	12.2	12.3	12.4	16.3	13.7
H ₂ O/Ce	140	134	136	135	138	138
δD_{SMOW} (‰, conv.) ^e		−64 (5)		−69 (5)	−58 (5)	−6.4 (0.9)
$\delta^{11}B$ (‰) ^f						
Vesicles (vol. %)	0.1	4.0	5.5	0.8	1.5	1.0
Sample (EW93-09)	9D-1g	25D-1g	26D-1g	28D-3g	33D-1g	34D-1g
Location ^a	Discov.	Discov.	Discov.	Discov.	Discov.	Discov.
Latitude (°S) ^a	49.147	47.348	47.353	46.900	45.990	45.847
Longitude (°W) ^a	350.09	349.68	346.6	346.55	345.92	345.81
Depth (m) ^a	3892.0	2032	3857	3417	3381	3443
⁸⁷ Sr/ ⁸⁶ Sr ^b	0.704604	0.705728	0.703072	0.703196	0.704475	0.703544
²⁰⁶ Pb/ ²⁰⁴ Pb ^b	17.811	18.098	18.034	18.066	17.992	17.983
MgO (wt. %) ^a	7.16	7.51	7.06	8.47	7.83	8.35
H ₂ O (wt. %, FTIR) ^c	0.392 (5)	0.148 (4)	0.226 (4)	0.177 (2)	0.301 (15)	0.125 (5)
CO ₂ (ppm, FTIR) ^c	281 (12)	90 (24)	242 (29)	151 (11)	237 (38)	299 (24)
Ba (ppm) ^d	106	70.4	20.1	28.1	183	15.5
Nb (ppm) ^d	8.19	5.44	2.2	2.99	16.6	1.59
La (ppm) ^d	9.15	5.48	4.42	4.39	12.16	2.76
Ce (ppm) ^d	22.1	13.0	13.8	13.3	26.4	9.03
Ba/Nb	12.9	12.9	9.14	9.40	11.0	9.75
H ₂ O/Ce	177	114	164	134	114	138
δD_{SMOW} (‰, conv.) ^e		−69 (5)				
$\delta^{11}B$ (‰) ^f		−7.0 (5)	−11.7 (5)	−8.5 (4)	−7.6 (5)	−7.4 (5)
Vesicles (vol. %)	0.2	4.5	5.0	0.8	0.9	0.5
Sample (EW93-09)	37D-1g	41D-1g	11D-1g	14D-1g	15D-1g	17D-1g
Location ^a	Discov.	Discov.	Shona1	Shona1	Shona1	Shona1
Latitude (°S) ^a	45.233	44.020	49.443	50.267	50.578	50.757
Longitude (°W) ^a	344.93	343.92	352.03	352.94	353.57	353.66
Depth (m) ^a	3534	3522	3868	3347	2980	2943
⁸⁷ Sr/ ⁸⁶ Sr ^b	0.704121	0.703273	0.702562	0.702644	0.702741	0.702680
²⁰⁶ Pb/ ²⁰⁴ Pb ^b	17.974	17.894	18.133	18.355	18.489	18.71
MgO (wt. %) ^a	8.11	8.36	8.02	7.41	7.81	7.82
H ₂ O (wt. %, FTIR) ^c	0.277 (4)	0.165 (4)	0.159 (4)	0.180 (5)	0.205 (4)	0.281 (8)
CO ₂ (ppm, FTIR) ^c	233 (27)	248 (35)	192 (18)	189 (23)	162 (20)	138 (11)
Ba (ppm) ^d	104	21.3	11.2	15.4	30.6	38.9
Nb (ppm) ^d	9.71	2.37	1.34	2.7	4.97	5.58
La (ppm) ^d	8.35	3.49	3.07	3.68	4.79	5.61
Ce (ppm) ^d	20.5	11.2	10.6	11.9	13.7	15.5
Ba/Nb	10.7	8.99	8.36	5.70	6.16	6.97
H ₂ O/Ce	135	148	149	151	150	182
δD_{SMOW} (‰, conv.) ^e		−67 (5)				
$\delta^{11}B$ (‰) ^f		−6.9 (0.9)	−7.8 (0.9)	−7.8 (0.9)	−9.8 (1.6)	−7.5 (1.0)
Vesicles (vol. %)	5.0	3.5	0.5	0.5	1.0	1.5
Sample (EW93-09)	19D-1g	18D-1g	20D-1g	21D-1g	22D-3g	23D-1g
Location ^a	Shona1	Shona2	Shona2	Shona2	Shona2	Shona2
Latitude (°S) ^a	51.062	51.053	51.428	51.822	52.458	52.157
Longitude (°W) ^a	353.84	353.80	354.22	354.5	355.43	354.66
Depth (m) ^a	1743	1991	1719	2025	3059	2609
⁸⁷ Sr/ ⁸⁶ Sr ^b	0.702740	0.703231	0.703440	0.703115	0.703576	0.703058
²⁰⁶ Pb/ ²⁰⁴ Pb ^b	18.923	18.415	18.593	18.721	18.182	18.480
MgO (wt. %) ^a	7.19	8.31	6.77	7.10	4.83	6.09
H ₂ O (wt. %, FTIR) ^c	0.347 (16)	0.200 (5)	0.333 (19)	0.364 (21)	0.649 (19)	0.369 (39)
CO ₂ (ppm, FTIR) ^c	77 (8)	143 (9)	81 (13)	119 (10)	125 (16)	
Ba (ppm) ^d	21.1	52.8	79.5	89.5	122	62.5
Nb (ppm) ^d	2.88	5.93	9.05	9.85	15.5	8.80
La (ppm) ^d	3.75	5.83	8.45	8.91	14.58	9.07
Ce (ppm) ^d	10.76	14.68	20.80	21.71	36.13	24.50

Table 3. (continued)

Sample (EW93-09)	19D-1g	18D-1g	20D-1g	21D-1g	22D-3g	23D-1g
Ba/Nb	7.33	8.90	8.78	9.09	7.87	7.10
H ₂ O/Ce	323	136	160	168	180	151
δD_{SMOW} (‰, conv.) ^e	−66 (5)	−64 (5)	−67 (5)	−62 (5)		
$\delta^{11}B$ (‰) ^f	−3.8 (5)					
Vesicles (vol. %)	2	10.0	0.3	0.8		

Note. New data are in bold font. Values in parentheses are 1σ standard deviations in the last or last two decimal places based on multiple analyses of glass samples (H₂O and CO₂ concentrations) or standards (stable isotopic data).

^aLocations, depths, and major elements for southern Atlantic basalts are from Douglass et al. (1995). Discov. is Discovery segment. Shona1 is Shona group 1. Shona2 is Shona group 2.

^bRadiogenic isotopic compositions from Douglass et al. (1999) and Gale et al. (2013a).

^cTotal dissolved water and carbon dioxide analyzed according to method given in Dixon and Clague (2001). Details provided in Supporting Information S1.1.

^dTrace element data from Douglass et al. (1999) and Kelley et al. (2013).

^e δD_{SMOW} by conventional stepped-heating/manometry/mass-spectrometry at the University of Miami Stable Isotope Laboratory. Details in supporting information S1.2.

^fIn situ boron isotopic compositions were measured by laser ablation, multiple-multiplier ICP-MS at the Department of Terrestrial Magnetism, Carnegie Institute of Washington following Le Roux et al. (2004). Details in supporting information S1.6.

4. Arctic and Northern Mid-Atlantic Ridges

4.1. Arctic Ridges North of Iceland

Previous studies of Arctic basalts model the radiogenic isotopic compositions by binary mixing between a PREMA-type source at Jan Mayen and a more depleted source at the northern end of the Mohns Ridge and the Knipovich Ridge (Blichert-Toft et al., 2005; Schilling et al., 1999). Though significantly depleted in incompatible elements, the Mohns Ridge end-member has slightly elevated ⁸⁷Sr/⁸⁶Sr and elevated Ba/Nb at unradiogenic ²⁰⁶Pb/²⁰⁴Pb compared to depleted basalts south of the Azores Platform. Arctic ridge basalts are generated by relatively low extents of partial melting, particularly in the vicinity of the Jan Mayen Platform (Schilling et al., 1999; Waggoner, 1990), which may increase ratios of highly to less incompatible elements,

Table 4

Locations and Selected Major, Minor and Volatile Element Concentrations for Northern East Pacific Rise Basalts

Sample (CHEPR)	CH59-1	CH59-2	CH59-4	CH121-2	CH18-4	CH19-3
Location ^a	SOFZ	SOFZ	SOFZ	SOFZ	SOFZ	SOFZ
Latitude (°N) ^a	8.00	8.00	8.00	12.53	12.89	12.82
Longitude (°W) ^a	−102.84	−102.84	−102.84	−103.91	−103.97	−103.90
Depth (m) ^a	2828	2828	2828	2629	2700	2764
⁸⁷ Sr/ ⁸⁶ Sr ^a		0.702407	0.702389	0.702500	0.702554	0.702517
²⁰⁶ Pb/ ²⁰⁴ Pb ^a		18.221	18.224	18.360	18.395	18.446
MgO (wt. %) ^a	7.04	7.25	7.28	7.17	7.23	8.73
Ba (ppm) ^a	11.2	7.74	8.14	9.25	17.1	5.15
Nb (ppm) ^a	3.06	2.83	2.77	2.99	4.46	1.74
La (ppm) ^a	4.22	4.11	4.12	3.95	4.86	2.64
Ce (ppm) ^a	14.0	13.58	13.5	12.5	14.3	8.71
Ba/Nb	3.67	2.73	2.94	3.09	3.83	2.96
H ₂ O (wt. %, TC/EA) ^b	0.25 (3)			0.20 (2)	0.24 (2)	0.13 (1)
H ₂ O/Ce	179			160	168	149
δD_{SMOW} (‰, TC/EA) ^b	−76.3 (3.0)			−75.0 (3.0)	−78.1 (3.0)	−72.3 (3.0)
Sample (CHEPR)	CH2-2	CH21-1	CH22-1	CH24-1	CH24-4	CH26-1
Location ^a	SOFZ	SOFZ	SOFZ	SOFZ	SOFZ	SOFZ
Latitude (°N) ^a	14.14	12.78	12.76	12.67	12.67	12.49
Longitude (°W) ^a	−104.22	−103.94	−103.93	−103.91	−103.91	−103.91
Depth (m) ^a	2780	2623	2620	2625	2625	2635

Table 4. (continued)

Sample (CHEPR)	CH2-2	CH21-1	CH22-1	CH24-1	CH24-4	CH26-1
$^{87}\text{Sr}/^{86}\text{Sr}^a$	0.702600	0.702598	0.702470	0.702531	0.702560	0.702564
$^{206}\text{Pb}/^{204}\text{Pb}^a$	18.498	18.308	18.421	18.442	18.449	18.375
MgO (wt. %) ^a	7.80	8.39	8.95	7.94	7.78	6.40
Ba (ppm) ^a	25.83	17.2	8.63	7.59	10.1	32.0
Nb (ppm) ^a	6.34	4.39	2.13	2.45	2.78	8.22
La (ppm) ^a	6.11	4.71	2.81	3.18	3.43	8.02
Ce (ppm) ^a	16.8	13.1	8.83	10.2	10.9	22.6
Ba/Nb	4.07	3.93	4.05	3.10	3.63	3.90
H_2O (wt. %, TC/EA) ^b	0.26 (3)	0.23 (2)	0.16 (2)	0.16 (2)	0.15 (2)	0.44 (4)
$\text{H}_2\text{O}/\text{Ce}$	155	176	181	157	137	195
$\delta\text{D}_{\text{SMOW}}$ (‰, TC/EA) ^b	-71.6 (3.0)	-80.0 (3.0)	-68.0 (3.0)	-75.1 (3.0)	-80.6 (3.0)	-69.5 (3.0)
Sample (CHEPR)	CH38-2	CH45-2	CH57-1	CH61-1	CH66-3	CH8-1
Location ^a	SOFZ	SOFZ	SOFZ	SOFZ	SOFZ	SOFZ
Latitude (°N) ^a	11.32	10.49	6.80	8.36	8.41	13.44
Longitude (°W) ^a	-103.78	-103.61	-102.65	-102.89	-104.18	-104.13
Depth (m) ^a	2548	2802	2740	2715	2570	2620
$^{87}\text{Sr}/^{86}\text{Sr}^a$	0.702807	0.702563	0.702580	0.702441	0.702609	0.702508
$^{206}\text{Pb}/^{204}\text{Pb}^a$	18.310	18.372	18.353		18.509	18.341
MgO (wt. %) ^a	6.40	6.54	7.38	7.93	7.49	7.02
Ba (ppm) ^a	29.5	20.1	14.1	5.94	20.4	15.4
Nb (ppm) ^a	6.48	4.79	4.20	2.07	4.06	4.12
La (ppm) ^a	5.88	5.30	4.73	2.95	4.42	4.55
Ce (ppm) ^a	17.2	16.3	14.4	9.68	12.6	13.7
Ba/Nb	4.55	4.20	3.36	2.87	5.02	3.73
H_2O (wt. %, TC/EA) ^b	0.33 (3)	0.27 (3)	0.28 (3)	0.16 (2)	0.19 (2)	0.21 (2)
$\text{H}_2\text{O}/\text{Ce}$	192	166	195	165	151	154
$\delta\text{D}_{\text{SMOW}}$ (‰, TC/EA) ^b	-75.5 (3.0)	-83.0 (3.0)	-72.3 (3.0)	-67.9 (3.0)	-88.9 (3.0)	-79.3 (3.0)
Sample (CHEPR)	CH9-2	CH9-3	CH98-1	CH99-1	D20-1	D22A
Location ^a	SOFZ	SOFZ	SOFZ	SOFZ	NOFZ	NOFZ
Latitude (°N) ^a	13.36	13.36	10.14	10.16	15.85	15.71
Longitude (°W) ^a	-104.08	-104.08	-104.35	-104.35	-105.44	-105.43
Depth (m) ^a	2605	2605	2565	2565	2319	2314
$^{87}\text{Sr}/^{86}\text{Sr}^a$	0.702610	0.703047	0.702447	0.702440	0.702956	0.703118
$^{206}\text{Pb}/^{204}\text{Pb}^a$	18.426	18.452	18.216	18.211	17.921	17.784
MgO (wt. %) ^a	7.12	6.49	7.39	7.78		7.59
Ba (ppm) ^a	32.1	38.5	9.28	8.37	40.2	35.8
Nb (ppm) ^a	6.22	7.32	2.66	2.22	4.79	3.86
La (ppm) ^a	5.73	6.63	3.35	2.75	4.47	3.77
Ce (ppm) ^a	15.3	18.2	10.7	8.82	12.2	10.6
Ba/Nb	5.16	5.26	3.49	3.77	8.40	9.27
H_2O (wt. %, TC/EA) ^b	0.30 (3)	0.38 (4)	0.15 (2)	0.12 (1)	0.17 (2)	0.14 (1)
$\text{H}_2\text{O}/\text{Ce}$	196	209	140	136	139	132
$\delta\text{D}_{\text{SMOW}}$ (‰, TC/EA) ^b	-70.8 (3.0)	-59.3 (3.0)	-78.1 (3.0)	-88.1 (3.0)	-87.7 (3.0)	-93.6 (3.0)
Sample (PANRI)	RC104	RC19	RC20	RC25	RC45	D69-1
Location ^a	NOFZ	NOFZ	NOFZ	NOFZ	NOFZ	NOFZ
Latitude (°N) ^a	16.93	17.13	17.05	16.63	15.87	15.91
Longitude (°W) ^a	-105.37	-105.39	-105.39	-105.34	-105.44	-105.45
Depth (m) ^a	2705	2747	2732	2682	2312	2312
$^{87}\text{Sr}/^{86}\text{Sr}^a$	0.702553	0.702586	0.702584	0.702653	0.702995	0.703044
$^{206}\text{Pb}/^{204}\text{Pb}^a$	18.059	18.138	18.122	18.062	17.626	17.758
MgO (wt. %) ^a	8.52	7.91	7.30	7.10	7.09	
Ba (ppm) ^a	9.07	16.8	13.6	12.9	34.8	38.0
Nb (ppm) ^a	1.72	3.08	2.53	2.87	3.70	4.19
La (ppm) ^a	2.43	3.77	3.28	3.80	3.58	4.06
Ce (ppm) ^a	7.94	11.5	10.3	11.5	10.1	11.3
Ba/Nb	5.27	5.46	5.36	4.50	9.39	9.07
H_2O (wt. %, TC/EA) ^b	0.16 (2)	0.19 (2)	0.17 (2)	0.18 (2)	0.11 (1)	0.10 (1)

Table 4. (continued)

Sample (PANRI)	RC104	RC19	RC20	RC25	RC45	D69-1
H₂O/Ce	202	165	165	157	109	89
δD_{SMOW} (‰, TC/EA) ^b	−78.7 (3.0)	−79.5 (3.0)	−80.3 (3.0)	−81.8 (3.0)	−96.3 (3.0)	−97.8 (3.0)
Sample (PANRI)	RC38	RC43	RC95	RC83		
Location ^a	NOFZ	NOFZ	NOFZ	NOFZ		
Latitude (°N) ^a	15.99	15.91	16.02	15.74		
Longitude (°W) ^a	−105.44	−105.44	−105.42	−105.39		
Depth (m) ^a	2351	2314	2612	2250		
⁸⁷ Sr/ ⁸⁶ Sr ^a		0.702890	0.702758	0.702816		
²⁰⁶ Pb/ ²⁰⁴ Pb ^a	18.342	18.185	18.202	18.358		
MgO (wt. %) ^a	7.94	6.61	6.78	7.72		
Ba (ppm) ^a	21.5	54.8	44.9	82.7		
Nb (ppm) ^a	4.42	6.47	5.71	11.4		
La (ppm) ^a	3.94	6.23	5.73	9.03		
Ce (ppm) ^a	10.9	16.43	15.64	22.3		
Ba/Nb	4.85	8.47	7.86	7.29		
H₂O (wt. %, TC/EA)^b	0.14 (1)	0.21 (2)	0.21 (2)	0.39 (4)		
H₂O/Ce	128	128	134	175		
δD_{SMOW} (‰, TC/EA) ^b	−86.4 (3.0)	−86.8 (3.0)	−92.6 (3.0)	−66.2 (3.0)		

Note. Values in parentheses are 1σ standard deviations in the last or last two decimal places based on multiple analyses of glass samples (H_2O and CO_2 concentrations) or standards (stable isotopic data).

^aLocations, depths, major and trace elements, and radiogenic isotopes from Castillo et al. (2000) and Gale et al. (2013a). SOFZ and NOFZ are south and north of the Orozco Fracture Zone, respectively.

^b H_2O concentration and δD_{SMOW} glass measured by High Temperature Conversion/Elemental Analyzer (TC/EA) at the University of Oregon (supporting information S1.3. Reported 1σ standard deviations based on replicate analysis of standards for δD_{SMOW} are $\pm 3\text{ ‰}$ and for H_2O concentrations are $\pm 5\%$ relative for $H_2O > \sim 0.5\text{ wt. \%}$ and 10% relative for $H_2O < 0.4\text{ wt. \%}$.

such as La/Sm, H_2O/Ce , and Ba/Nb. However, this is unlikely to create the relatively high Ba/Nb of the Mohns and Knipovich Ridge basalts. Thus, the compositions of the Arctic Ridge basalts can be modeled by pseudobinary mixing between two end-members—one having PREMA, and the other DMM + EM, characteristics (Figures 2a and 2b).

H_2O/Ce in Arctic Ridge basalts varies from 210 to 430 (mean $310 \pm 58 1\sigma$), consistent with the relatively high H_2O/Ce of North Atlantic basalts ($240\text{--}280 \pm 50 1\sigma$) reported in Michael (1995). These values are greater than typical of MORB from the south Atlantic and Pacific ($\sim 170 \pm 15$) (Michael, 1995). H_2O/Ce does not correlate systematically with $^{206}Pb/^{204}Pb$ (Figure 2c) or Ba/Nb (not shown). Given the similarity in partitioning behavior during magmatic processes, H_2O/Ce in basalts should provide information of the H_2O/Ce in the mantle source; however, variations may occur as a function of mantle mineralogy. Increased scatter in H_2O/Ce in Arctic Ridge basalts may be due to the overall low extents of melting for Arctic Ridge basalts (Schilling et al., 1999; Waggoner, 1990) or the presence of residual garnet in the Jan Mayen-influenced mantle source (Hauri et al., 2006).

δD_{SMOW} ranges from -60 ‰ near the Spar Fracture Zone on the Kolbeinsey Ridge to a heavier value of -29 ‰ on the Knipovich Ridge. The binary mixing relationship along the Mohns Ridge defined on the basis radiogenic isotopes is also present in the δD_{SMOW} variation, grading from PREMA-type with heavy δD_{SMOW} of -33 ‰ to the DMM-EM-type Mohns Ridge basalts with lighter δD_{SMOW} of -60 ‰ (Figure 2d).

4.2. Azores Platform

Azores Platform basalts form a general mixing array between DMM and PREMA (Figures 2a and 2b). In contrast, basalts from the $35^\circ N$ anomaly form a mixing array between PREMA and an EM component, with samples 9-10, 45-3, and 44-1 having the highest $^{87}Sr/^{86}Sr$ (Figure 2a). An exception is 49-3, which falls within the Azores platform array. Figure 2b also shows that the some of the more depleted Reykjanes Ridge basalts have elevated Ba/Nb similar to the Arctic Ridge basalts.

H_2O/Ce (253 ± 33) in Azores platform basalts with $<25\%$ vesicles are consistent with previously reported values for the North Atlantic (Michael, 1995). The overall correlation of H_2O/Ce with indicators of mantle

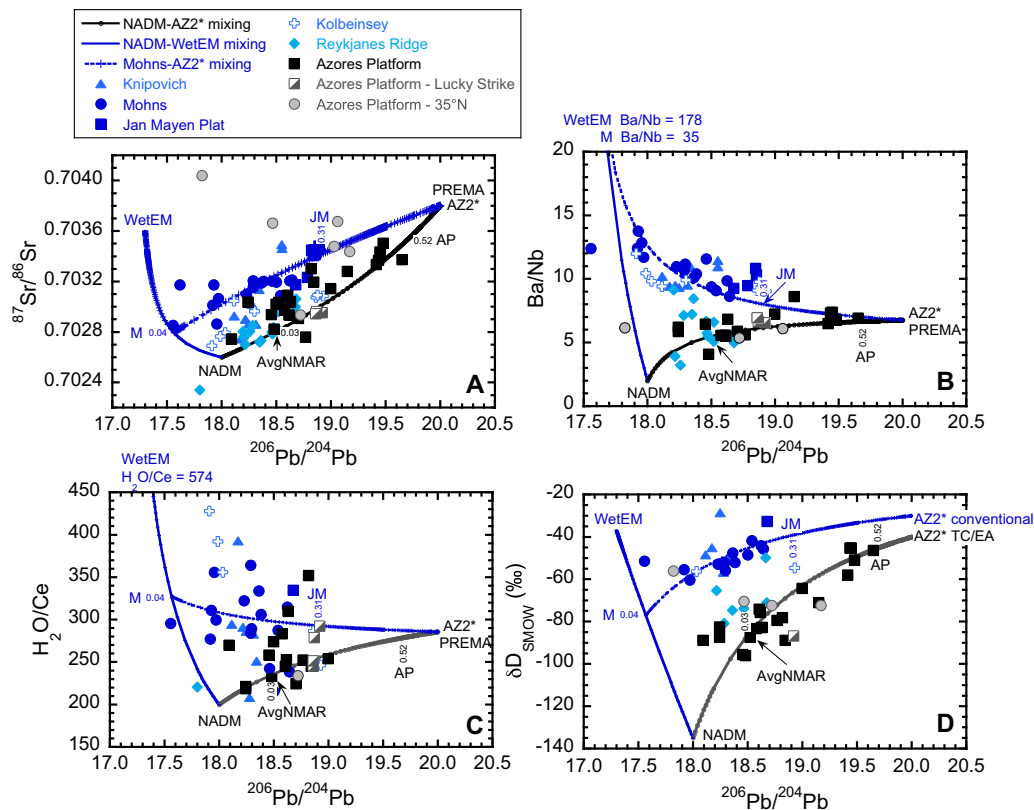


Figure 2. Arctic Ridges and Azores Platform: (a) $^{87}\text{Sr}/^{86}\text{Sr}$ versus $^{206}\text{Pb}/^{204}\text{Pb}$. Azores Platform basalts form DM-PREMA array. Data sources given in caption to supporting information Figure S2-2. (b) Ba/Nb versus $^{206}\text{Pb}/^{204}\text{Pb}$. Arctic Ridge basalts trend toward higher Ba/Nb with decreasing $^{206}\text{Pb}/^{204}\text{Pb}$ consistent with involvement of an EM-type component. Data sources given caption to supporting information Figure S2-3. (c) $\text{H}_2\text{O}/\text{Ce}$ versus $^{206}\text{Pb}/^{204}\text{Pb}$. Arctic Ridge basalts have higher $\text{H}_2\text{O}/\text{Ce}$ at lower $^{206}\text{Pb}/^{204}\text{Pb}$ than Azores Platform basalts. (d) $\delta\text{D}_{\text{SMOW}}$ versus $^{206}\text{Pb}/^{204}\text{Pb}$. Heavier $\delta\text{D}_{\text{SMOW}}$ for the Arctic Ridges is greater than the 1 ‰ offset between conventional and TC/EA analyses. $\delta\text{D}_{\text{SMOW}}$ data from: Arctic Ridges (this study; conventional stepped-heating/manometry/mass-spectrometry); Reykjanes Ridge (Poreda et al., 1986; conventional); Azores Platform, Lucky Strike, 35°N (this study; TC/EA); 34°50' (Pineau et al., 2004). Calculations of end-member compositions and mixing curves are discussed in supporting information S4. NADM is North Atlantic Depleted Mantle; AvgNMAR is average northern Atlantic Mid-Atlantic Ridge basalt (99.97% NADM + 0.03% AZ2*); AP is PREMA-type mantle source for enriched Azores basalts (AP = 99.48% NADM + 0.52% AZ2*); AZ2* is PREMA-type C-H-O-Cl fluid end-member for Azores basalts; WetEM is EM-type C-H-O-Cl end-member fluid for Arctic basalts; M is Mohns end-member (M = 99.96% NADM + 0.04% WetEM); JM is mantle source for Jan Mayen basalts (JM = 99.69% Mohns + 0.31% AZ2*).

enrichment is poor (Figure 2d). However, the most depleted Azores Platform basalts have the lowest $\text{H}_2\text{O}/\text{Ce}$ (213 ± 16) and the most enriched have the highest $\text{H}_2\text{O}/\text{Ce}$ (~ 350), and the mean value (253 ± 33) is lower than that for the Arctic Ridges (310 ± 58).

$\delta\text{D}_{\text{SMOW}}$ values for Azores platform basalts correlate positively with $^{206}\text{Pb}/^{204}\text{Pb}$ (Figure 2d). Water degassing from enriched basalts on the shallowest portions of the Azores Platform may have resulted in $\sim 6\text{--}12$ ‰ shift to lighter values in these samples (supporting information S2).

$\delta\text{D}_{\text{SMOW}}$ for the Reykjanes Ridge (Poreda et al., 1986) and the mid-Atlantic Ridge at 34°50'N (Pineau et al., 2004), both using vacuum-crushing and step-heating techniques, agree well with the TC/EA data for the Azores Platform (Figures 2d). Poreda et al. (1986) were the first to show correlations between $\delta\text{D}_{\text{SMOW}}$ and indicators of mantle enrichment, in that case $(\text{La}/\text{Sm})_{\text{N}}$. Some of the more depleted Reykjanes Ridge samples, however, have elevated Ba/Nb, suggesting additional involvement of small amounts of an EM component similar to the Mohns Ridge samples.

4.3. Summary of North Atlantic Volatile and Stable Isotopic Values

DMORB from the Azores Platform have northern Atlantic-type $\text{H}_2\text{O}/\text{Ce}$ of $\sim 240 \pm 40$ and $\delta\text{D}_{\text{SMOW}}$ of -90 ± 10 ‰. EM-influenced MORB from Mohns-Jan Mayen array are wetter ($\text{H}_2\text{O}/\text{Ce} = \sim 300 \pm 50$) and

heavier δD_{SMOW} (-60 ‰) than non-EM-influenced MORB further south, implying that the EM component is wetter and heavier than the MORB source. This EM component is not isolated in plume-influenced areas and is likely dispersed in the upper mantle. Basalts with PREMA-type compositions associated with the Azores Platform and Jan Mayen plumes share a common end-member H_2O/Ce ($\sim 285 \pm 15$) and δD_{SMOW} (-30 to -40 ‰). Parallel trends of δD_{SMOW} and δ^7Li with $^{206}Pb/^{204}Pb$ in Azores Platform basalts (supporting information S2, Figure S3-2 and 3) indicate that the observed trends are not the result of diffusion of light elements out of enriched mantle sources, as proposed for Samoa (Workman et al., 2006). Neither EM- nor PREMA-type mantle compositions in the north Atlantic are consistent with the light slab model.

5. Southern Atlantic and Pacific Ridges

5.1. Southern Pacific

Hydrogen isotopes have been previously studied in three southern Pacific regions: (1) Easter Microplate (EMP) and Easter Salas y Gomez Seamount Chain (ESC; supporting information Figure S2-16 and 17) (Cheng et al., 1999; Kingsley et al., 2002; Kingsley & Schilling, 1998); (2) the Pacific-Antarctic Ridge 41° to $65^\circ S$ (PAR, supporting information Figure S2-16) (Clog et al., 2013; Hamelin et al., 2010, 2011; Vlastélic et al., 2000); and (3) Macquarie Island (supporting information Figure S2-16) (Bindeman et al. 2012; Kamenetsky et al., 2000). The overlapping radiogenic isotopic compositions for these three regions (Figure 3a) suggest influence by a common component with high $^{206}Pb/^{204}Pb$ similar to that for the Easter Salas y Gomez (SYG) plume, even for ridges far from hotspots. The PAR basalt compositions cluster around values representative of average EPR basalts with a mean $^{206}Pb/^{204}Pb$ of roughly 18.6 ± 0.2 and Ba/Nb of 3.0 ± 0.7 (Figures 3a and 3b). EMP basalts range to more depleted compositions with a few having $^{206}Pb/^{204}Pb$ as low as 17.5. Radiogenic isotopic and Ba/Nb compositions of Macquarie Island basalts are intermediate between average EPR and the enriched ESC basalts but with higher Ba/Nb at a given $^{206}Pb/^{204}Pb$ (Figures 3a and 3b).

Samples that have suffered modification of water, Cl, Ba/Nb , and δD_{SMOW} due to degassing or assimilation of brines are discussed in the supporting information (S2) and are not considered further here. For minimally modified samples, H_2O/Ce and δD_{SMOW} roughly increase with proximity to the SyG plume (Figures 3c and 3d) (Kingsley et al., 2002; Simons et al., 2002) and with increasing $^{206}Pb/^{204}Pb$.

Water concentrations and hydrogen isotopic compositions in PAR basalts were measured using the conventional techniques (Clog et al., 2013). H_2O/Ce (180 ± 23) and δD_{SMOW} ($-61 \pm 15\text{ ‰}$) in PAR basalts represent a similar, but more limited, compositional range than the EMP samples (Kingsley et al., 2002; Simons et al., 2002) and do not correlate systematically with indicators of brine assimilation (Cl concentration), mantle enrichment ($(La/Sm)_N$ and $^{206}Pb/^{204}Pb$), or latitude (Clog et al., 2013).

The Macquarie Island H_2O concentrations and δD_{SMOW} data were generated using the TC/EA technique (Bindeman et al., 2012). Macquarie Island δD_{SMOW} values (with 16 ‰ added to published values) of -50 ‰ to -64 ‰ are slightly heavier than average Pacific MORB. Combined with their high $^{206}Pb/^{204}Pb$, these observations are consistent with the idea that these basalts are variably influenced by a high $^{206}Pb/^{204}Pb$ PREMA-type mantle end-member with relatively high δD_{SMOW} values (possibly similar to the SYG plume source). This interpretation differs from the conclusion by Bindeman et al. (2012) that Macquarie Island glasses plot narrowly within the canonical $-80 \pm 10\text{ ‰}$ value for the MORB mantle (Kysar & O'Neil, 1984).

5.2. Southern Mid-Atlantic Ridge (Shona and Discovery Anomalies)

This section of the ridge contains two distinct geochemical, gravity, and bathymetric anomalies. The northern “Discovery” anomaly is centered at $47.5^\circ S$ and is influenced by the Discovery plume (Douglass et al., 1995, 1999). The southern “Shona” anomaly is centered at $51.5^\circ S$ (Douglass et al., 1995, 1999; Le Roex et al., 1987) (supporting information Figure S2-17).

Discovery anomaly lavas show a wide range of $^{87}Sr/^{86}Sr$ and Ba/Nb at relatively constant $^{206}Pb/^{204}Pb$, consistent with mixing of DMM and EM components (Andres et al., 2002; Douglass & Schilling, 2000) (Figures 4a and 4b). Shona anomaly glasses form two Pb-Sr isotopic groups consistent with variable contributions of PREMA and EM-type components. Shona Group I lava compositions show mixing mainly between DMM and an enriched component with PREMA influence similar to the SYG plume component. Shona Group II lava compositions show additional influence of an EM component (Andres et al., 2002).

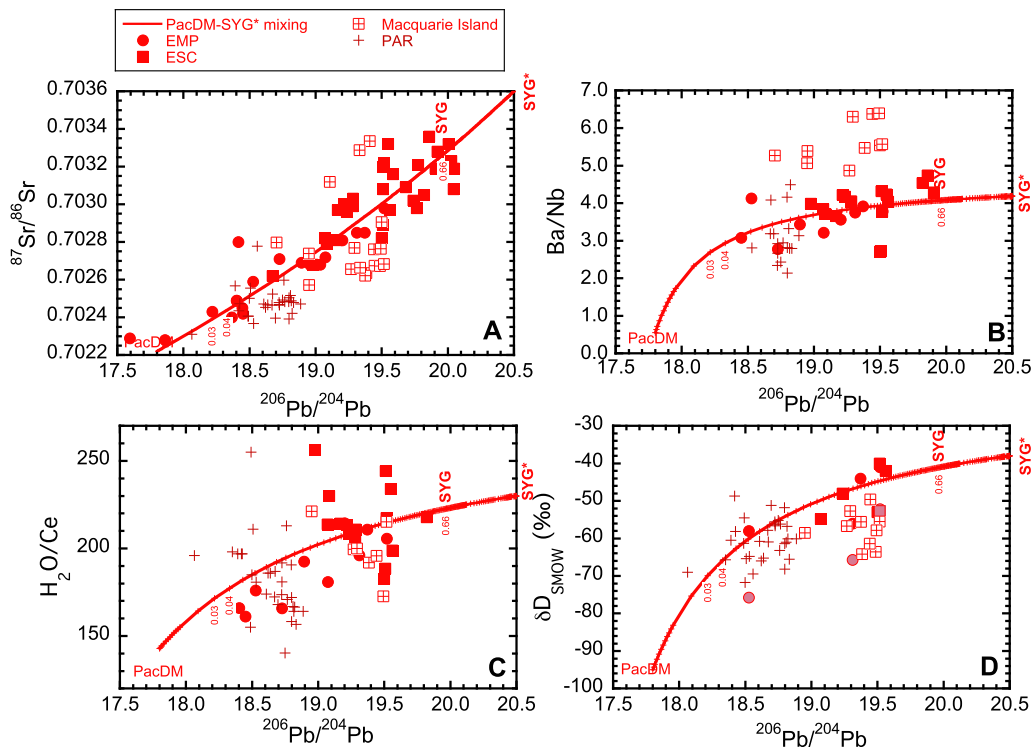


Figure 3. Published Pacific data: (a) $^{87}\text{Sr}/^{86}\text{Sr}$ versus $^{206}\text{Pb}/^{204}\text{Pb}$ showing mixing array between Pacific Depleted Mantle (PacDM) and Salas y Gomez (SYG*) PREMA-like end-member. Pacific Antarctic Ridges with mean $^{206}\text{Pb}/^{204}\text{Pb}$ of 18.6 ± 0.2 represent average EPR basalts compositions. Macquarie Ridge basalts are significantly more enriched than average EPR with a component similar to the SYG* PREMA-like end-member. Data sources given in caption to supporting information Figure S2-2. (b) Ba/Nb versus $^{206}\text{Pb}/^{204}\text{Pb}$. Average EPR have Ba/Nb of ~ 3 . Macquarie Island basalts have Ba/Nb greater than PAR and EMP-ESC basalts. PREMA-like SYG* component has low Ba/Nb (4) and high $^{206}\text{Pb}/^{204}\text{Pb}$ (20.9). Data sources given in caption to supporting information Figure S2-3. (c) $\text{H}_2\text{O}/\text{Ce}$ versus $^{206}\text{Pb}/^{204}\text{Pb}$. Mean $\text{H}_2\text{O}/\text{Ce}$ values for PAR (180 ± 23) are consistent with regional Pacific values of 160 to 194 (Michael, 1995). Mean Macquarie Island value (199 ± 16) are similar to ESC basalts influenced by PREMA-like SYG* end-member with $\text{H}_2\text{O}/\text{Ce}$ of 223. H_2O data from: ESC-EMP (Simons et al., 2002; FTIR, degassed ESC basalts excluded); Macquarie Island (Bindeman et al., 2012); Pacific-Antarctic Ridges (Clog et al., 2013). (d) $\delta\text{D}_{\text{SMOW}}$ versus $^{206}\text{Pb}/^{204}\text{Pb}$. Mean PAR basalt $\delta\text{D}_{\text{SMOW}}$ ($-60 \pm 5 \text{ } \text{\textperthousand}$) represents average Pacific MORB composition. Mean Macquarie Island basalt ($-45 \pm 5 \text{ } \text{\textperthousand}$) enriched with PREMA-like SYG* component similar to ESC basalts ($-48 \pm 7 \text{ } \text{\textperthousand}$). $\delta\text{D}_{\text{SMOW}}$ of PacDM end-member significantly lighter ($-95 \text{ } \text{\textperthousand}$) than estimates for average MORB mantle. $\delta\text{D}_{\text{SMOW}}$ data from: EMP-ESC (Kingsley et al., 2002, conventional with up to $-6 \text{ } \text{\textperthousand}$ correction to published values (filled red circles and squares) and this study, TC/EA (pink circles and squares)); Macquarie Island (Bindeman et al., 2012; TC/EA with $+16 \text{ } \text{\textperthousand}$ correction to published values (open red squares with cross)); PAR (Clog et al., 2013, conventional (red plus)). Data for brine-modified basalts are excluded. Calculations of end-member compositions and mixing curves are discussed in supporting information S4 and listed in Table S4-1. PacDM is Pacific depleted mantle; SYG* is C-O-H-Cl fluid end-member; SYG is mantle end-member for Salas y Gomez basalts (SYG = 99.34% PacDM + 0.66% SYG*); AvgEPR1 = 99.97% PacDM + 0.03% SYG*, AvgEPR2 = 99.96% PacDM + 0.04% SYG*, with the compositional range of “average EPR” mantle extending to about $+ 0.06\%$ SYG*.

Dixon et al. (2002) showed that EM-type Shona Group II and Discovery glasses ($^{87}\text{Sr}/^{86}\text{Sr} > 0.703$) have distinctly lower H_2O concentrations and lower $\text{H}_2\text{O}/\text{Ce}$ than the PREMA-type Shona Group I and EMP-ESC glasses (Figure 4c). The Discovery glasses form a distinct binary mixing line such that samples with the highest EM-like radiogenic Sr isotopic compositions having H_2O concentrations and $\text{H}_2\text{O}/\text{Ce}$ about half that of the Easter glasses (Figure 4c). In contrast to the North Atlantic, EM components in the mantle sources for the Shona and Discovery lavas are associated with lower water concentrations and lower ratios of water to similarly incompatible elements.

The Shona and Discovery glasses have $\delta\text{D}_{\text{SMOW}}$ ranging from -58 to $-69 \text{ } \text{\textperthousand}$ (Figure 4d) similar to values for average Pacific MORB. $\delta\text{D}_{\text{SMOW}}$ values of Shona and Discovery basalts are relatively constant, unlike the EMP-ESC glasses that trend toward heavier $\delta\text{D}_{\text{SMOW}}$ values, suggesting that both the EM and depleted end-members in the South Atlantic have similar $\delta\text{D}_{\text{SMOW}}$ values of $\sim 64 \pm 5 \text{ } \text{\textperthousand}$. Similarly, Discovery basalts have

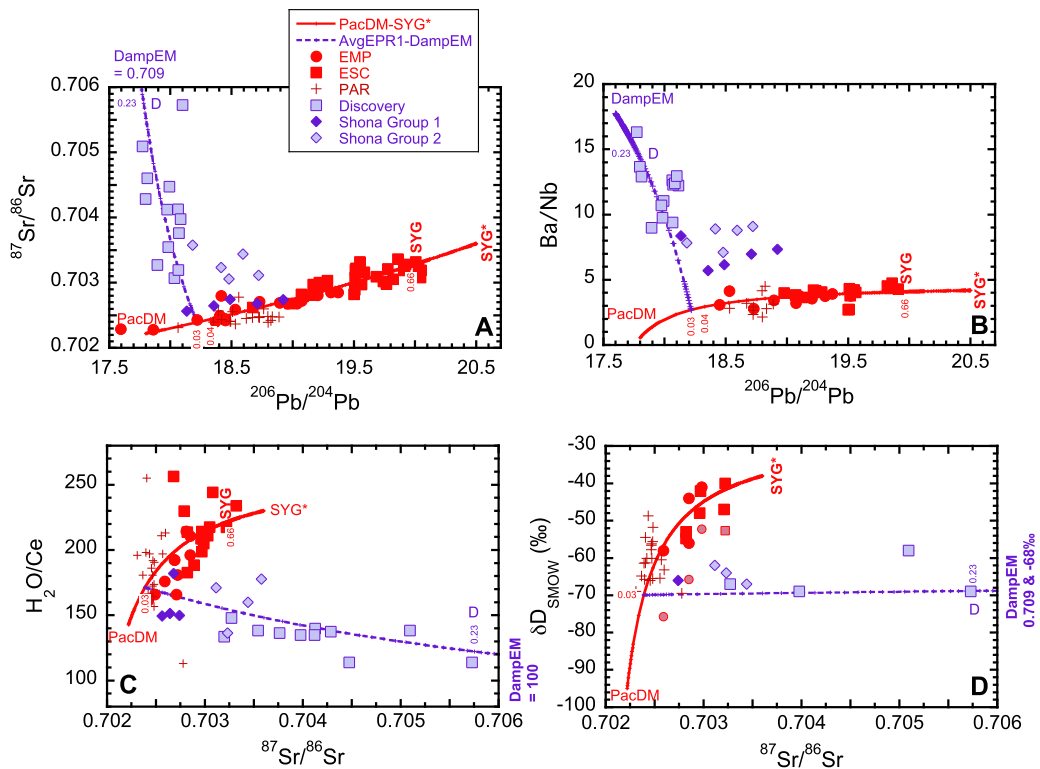


Figure 4. South Atlantic data: (a) $^{87}\text{Sr}/^{86}\text{Sr}$ versus $^{206}\text{Pb}/^{204}\text{Pb}$. Data sources given in caption 1B. EMP-ESC basalts are shown for comparison. Discovery basalts have large range in $^{87}\text{Sr}/^{86}\text{Sr}$ at constant $^{206}\text{Pb}/^{204}\text{Pb}$ consistent with mixing between average EPR mantle (EPR1) and EM-component (DampEM). Shona Group 1 basalts fall on PacDM-SYG* mixing curve. Shona Group 2 basalts have values intermediate between PacDM-SYG* and EPR1-DampEM mixing curves. Data sources listed in caption to supporting information Figure S2-2. (b) Ba/Nb versus $^{206}\text{Pb}/^{204}\text{Pb}$. Discovery basalts consistent with addition of high Ba/Nb DampEM component. Both Shona Groups 1 and 2 basalts have Ba/Nb higher than the PacDM-SYG* mixing curve and intermediate between PacDM-SYG* and EPR1-DampEM mixing curves. Data sources given in caption to supporting information Figure S2-3. (c) $\text{H}_2\text{O}/\text{Ce}$ versus $^{87}\text{Sr}/^{86}\text{Sr}$. In contrast to EM-influenced basalts in the northern Atlantic, $\text{H}_2\text{O}/\text{Ce}$ in Discovery basalts correlate negatively with $^{87}\text{Sr}/^{86}\text{Sr}$ trending toward the DampEM endmember with $\text{H}_2\text{O}/\text{Ce}$ of 100. Shona Group 1 basalts fall near PacDM-SYG* mixing curve. Shona Group 2 basalts have values intermediate between PacDM-SYG* and EPR1-DampEM mixing curves. Data from Dixon et al. (2002). (d) δD_{SMOW} versus $^{87}\text{Sr}/^{86}\text{Sr}$. Southern Atlantic δD_{SMOW} data from: (this study, conventional (purple and lavender symbols)). In contrast to EM-influenced basalts in the northern Atlantic, δD_{SMOW} in Discovery and Shona basalts are relatively constant at variable $^{87}\text{Sr}/^{86}\text{Sr}$. Calculations of end-member compositions and mixing curves are discussed in supporting information S4 and listed in Table S4-1. Other data sources and PacDM, SYG*, and SYG end-members described in Figure 3 caption. DampEM is C-O-H-Cl fluid end-member for Discovery EM-type basalts; D is mantle source for Discovery basalts (D = 99.77% PacDM + 0.23% DampEM).

relatively constant $\delta^{11}\text{B}$ values of $\sim -7.2 \pm 1.0 \text{ ‰}$ (section S3.3, supporting information Figure S3–4, 5, and 6). These values are within the range reported for OIB and are also consistent with the boron isotopic composition of dehydrated sediments (-1 to -8 ‰) (Ishikawa & Nakamura, 1993).

5.3. Northern East Pacific Rise

Northern EPR basalts are from 6° to 17°N (supporting information Figure S2-6a). There are no distinct plumes in this region, however on and off-axis EPR basalts, as well as small seamounts, have large chemical variations over small spatial scales (Batiza & Vanko, 1984; Bideau and Hékinian, 1995; Castillo et al., 2000; Niu et al., 1999; Perfit et al., 1994; Reynolds et al., 1992; Reynolds & Langmuir, 2000; Zindler et al., 1984).

The nature of dispersed small-scale heterogeneities differ north and south of the Orozco fracture zone (Castillo et al., 2000). The majority of northern EPR samples south of the Orozco fracture zone ($\sim 15^\circ\text{N}$) have $^{87}\text{Sr}/^{86}\text{Sr} \sim 0.7025 \pm 0.0001$, $^{206}\text{Pb}/^{204}\text{Pb} (\sim 18.4 \pm 0.2)$, and Ba/Nb ($\sim 4 \pm 1$) consistent with average EPR basalt on a DMM-PREMA array (Figures 5a and 5b and supporting information Figure S2-5a). Samples north of the Orozco fracture zone have lower $^{206}\text{Pb}/^{204}\text{Pb}$ and higher $^{87}\text{Sr}/^{86}\text{Sr}$ and Ba/Nb consistent with

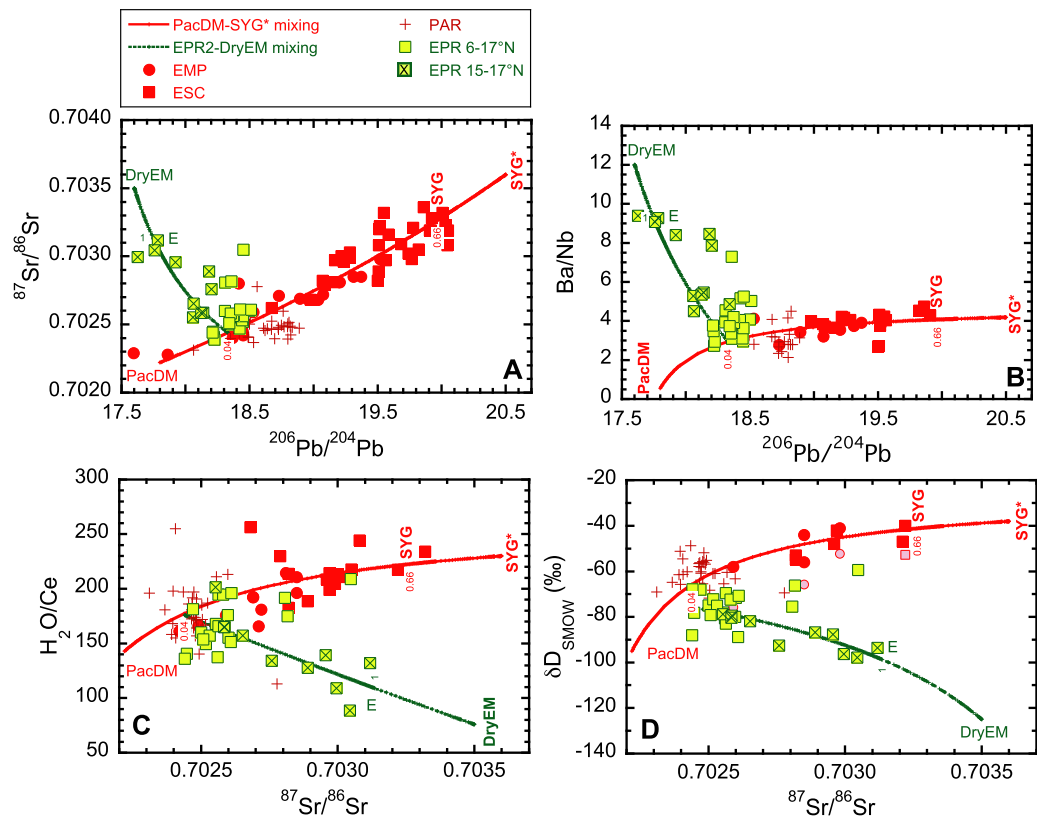


Figure 5. Northern EPR data: (a) $^{87}\text{Sr}/^{86}\text{Sr}$ versus $^{206}\text{Pb}/^{204}\text{Pb}$. No plume influences basalts from the EPR between 6 and 17°N. Enriched basalts related to dispersed heterogeneities that are dominantly PREMA-like between 6° and 14°N (south of Orozco Fracture Zone, yellow boxes) and dominantly EM-like between 15° and 17°N (north of Orozco Fracture Zone, yellow box and "X") (see supporting information Figure S2-17). Data sources given in caption to supporting information Figure S2-2. (b) Ba/Nb versus $^{206}\text{Pb}/^{204}\text{Pb}$. EM-type EPR basalts with elevated $^{87}\text{Sr}/^{86}\text{Sr}$ have enrichments in Ba/Nb. Data sources given in caption to S2-3. (c) $\text{H}_2\text{O}/\text{Ce}$ versus $^{87}\text{Sr}/^{86}\text{Sr}$. $\text{H}_2\text{O}/\text{Ce}$ in basalts south of Orozco FZ are similar to the EMP values and fall on PacDM-SYG* mixing curve. $\text{H}_2\text{O}/\text{Ce}$ in basalts north of Orozco FZ correlates negatively with $^{87}\text{Sr}/^{86}\text{Sr}$ trending toward a DryEM mixing end-member with $\text{H}_2\text{O}/\text{Ce}$ of 95. (d) $\delta\text{D}_{\text{SMOW}}$ versus $^{87}\text{Sr}/^{86}\text{Sr}$. $\delta\text{D}_{\text{SMOW}}$ values in basalts south of Orozco FZ are similar to EMP basalts. $\delta\text{D}_{\text{SMOW}}$ values in basalts north of Orozco FZ trend toward significantly lighter values as low as -98 ‰ . EPR $\delta\text{D}_{\text{SMOW}}$ data from: (this study, TC/EA (lime green symbols)). Other data sources and PacDM, SYG*, and SYG end-members described in Figure 3 caption. DryEM is the EM-type C-H-O-Cl fluid end-member for the dry EPR basalts. E is mantle source for EM-type EPR basalts (E = 99% PacDM + 1% DryEM).

involvement of an additional EM-type component. The EPR EM-type samples have $^{87}\text{Sr}/^{86}\text{Sr}$ and Ba/Nb compositions lower than those for the Discovery basalts.

EPR samples south of the Orozco fracture zone have $\text{H}_2\text{O}/\text{Ce}$ (mean 168 ± 21) consistent with values for average EPR basalts (190 ± 40 , Michael, 1995; 168 ± 95 , Saal et al., 2002; 168 ± 8 , Danyushevsky et al., 2000). $\text{H}_2\text{O}/\text{Ce}$ in samples north of Orozco are lower (mean 143 ± 31) and correlate negatively with $^{87}\text{Sr}/^{86}\text{Sr}$ and Ba/Nb (Figure 5c). Degassing of water from these EM-type basalts is unlikely given their low absolute water concentrations (<0.2 wt. %) and eruption depths greater than 2,300 m. Basalts with the highest Ba/Nb (samples RC 45 and D69-1) have extremely low $\text{H}_2\text{O}/\text{Ce}$ values of 109 and 89, respectively. These are the lowest values ever observed along the mid-ocean ridge system in basalts that have not degassed water.

$\delta\text{D}_{\text{SMOW}}$ values for EPR basaltic glasses were measured using TC/EA. Basalts south of the Orozco fracture zone (with the exception of CH9-3 and CH38-2) have a mean $\delta\text{D}_{\text{SMOW}}$ of $-77 \pm 7\text{ ‰}$. This is lighter than published data measured using conventional methods (-68 ‰ for depleted EMP basalts, Kingsley et al., 2002), but within the uncertainty of $\pm 10\text{ ‰}$ between the techniques. Samples CH9-3 and CH38-2 that fall on the DMM-PREMA mixing curve have heavier $\delta\text{D}_{\text{SMOW}}$ of -59 and -76 ‰ , consistent with the EMP-ESC trend. Samples north of the Orozco fracture zone (with the exception of RC83) have $\delta\text{D}_{\text{SMOW}}$ values extending to much lighter values, as low as -94 ‰ . Figure 5d shows the negative correlations between $\delta\text{D}_{\text{SMOW}}$

and $^{87}\text{Sr}/^{86}\text{Sr}$ and Ba/Nb defined by the light values for the north of Orozco samples. The one exception is RC83 with an adjusted $\delta\text{D}_{\text{SMOW}}$ of -54.2 ‰ ; this sample appears to also contain the local PREMA component, consistent with the model of mixed dispersed heterogeneities (Castillo et al., 2000). Thus, the EM component in the northern EPR samples is the driest and contains the lightest hydrogen ever documented along the mid-ocean ridge system.

6. Summary of $\text{H}_2\text{O}/\text{Ce}$ and $\delta\text{D}_{\text{SMOW}}$ Data in Global Basalts

The data presented above show that volatile concentrations and stable isotopic compositions of oceanic basalts correlate with indicators of mantle composition, but the correlations differ among regions. PREMA-type basalts in the Pacific (ESC, Macquarie Island; $\text{H}_2\text{O}/\text{Ce} = 215 \pm 30$, $\delta\text{D}_{\text{SMOW}} = -45 \pm 5\text{ ‰}$) are similar to those in the north Atlantic (Jan Mayen, Azores Platform; $\text{H}_2\text{O}/\text{Ce} = 220 \pm 30$; $\delta\text{D}_{\text{SMOW}} = -30$ to -40 ‰). Heavy $\delta\text{D}_{\text{SMOW}}$ in PREMA-type basalts are inconsistent with a light slab model as the origin of this material.

In contrast, basalts with EM-type signatures have regionally variable volatile compositions, consistent with their variable trace element compositions. In the North Atlantic, EM-type basalts (Mohns) are wetter ($\text{H}_2\text{O}/\text{Ce} = 330 \pm 30$) and have isotopically heavier hydrogen ($\delta\text{D}_{\text{SMOW}} = -57 \pm 5\text{ ‰}$) than DMORB. In the southern Atlantic, EM-type basalts (Discovery) are damp ($\text{H}_2\text{O}/\text{Ce} = 120 \pm 10$) with intermediate $\delta\text{D}_{\text{SMOW}}$ ($-68 \pm 2\text{ ‰}$), similar to $\delta\text{D}_{\text{SMOW}}$ for Pacific MORB. In the northern Pacific, EM-type basalts (EPR north of Orozco) are dry ($\text{H}_2\text{O}/\text{Ce} = 110 \pm 20$) and isotopically light ($\delta\text{D}_{\text{SMOW}} = -94 \pm 3\text{ ‰}$). Thus, the light slab model may be valid for the northern EPR EM-type basalts, but must be modified to explain basalts from the rest of the globe.

Average Pacific MORB, represented by PAR basalts, are drier ($\text{H}_2\text{O}/\text{Ce} = 180 \pm 20$) and contain heavier hydrogen ($\delta\text{D}_{\text{SMOW}} = -60 \pm 5\text{ ‰}$) than average depleted north Atlantic MORB ($\text{H}_2\text{O}/\text{Ce} = \sim 230 \pm 20$; $\delta\text{D}_{\text{SMOW}} = -90 \pm 10\text{ ‰}$). Thus, variations in volatile and hydrogen isotopic composition support the idea that mantle sources for NMORB, even those far from hotspots, may contain variable amounts of other mantle components (Gale et al., 2013a).

7. Summary of Mantle Mixing End-Members

Details of the mixing calculations and estimation of mantle end-member compositions are provided in supporting information S4. Mantle end-member compositions are listed in supporting information Table S4-1 and summarized in Figures 6a–6d. Building on the work of Asimow et al. (2004), proportions of mixing components are estimated using nonvolatile incompatible elements and radiogenic isotopic compositions and then used to estimate the mantle end-member volatile and stable isotopic compositions. Though the proposed end-member compositions are not unique, mantle sources for both PREMA and EM-type mantle sources can be produced by addition of $<1\%$ of sediment \pm eclogite derived C-O-H-Cl fluids generated as described by the model below. H_2O concentrations, $\text{H}_2\text{O}/\text{Ce}$, and $\delta\text{D}_{\text{SMOW}}$ in mantle sources for PREMA-type basalts are similar implying a consistency of process and volatile content. Binary mixing model results show that PREMA-type end-member C-O-H-Cl fluids have uniformly heavy $\delta\text{D}_{\text{SMOW}}$ of $\sim -37 \pm 3\text{ ‰}$, inconsistent with the light slab model. EM C-O-H-Cl fluid end-members have variable $\delta\text{D}_{\text{SMOW}}$ ranging from -30 to -125 ‰ , with only the DryEM fluid (lowest $\text{H}_2\text{O}/\text{Ce}$ and lightest $\delta\text{D}_{\text{SMOW}}$) consistent with the light slab model.

8. Resolution of Dehydration Paradox

Shaw et al. (2008) proposed a single reservoir, fractional-distillation model for dehydration of subducting slabs. However, reality is more complicated. Different regions of the downgoing lithosphere experience dehydration at different rates due to differences in lithology (sediment, MORB, gabbro, and hydrated lithospheric mantle) and differences in P-T path as a function of their different positions in the slab (e.g., van Keken et al., 2011, 2002b). In almost all recent thermal models (Syracuse et al., 2010; van Keken et al., 2011; Wada et al., 2012), the slab crust has fully or nearly fully dehydrated by the time it is beneath the arc. For most thermal conditions, the top of the slab crust has fully dehydrated within a horizontal distance of 20 km from the depth at which slab motion becomes coupled to flow of the overlying mantle wedge. Thus, any volatiles transported beyond the arc must be carried in the deeper portions of the slab. In cooler slabs,

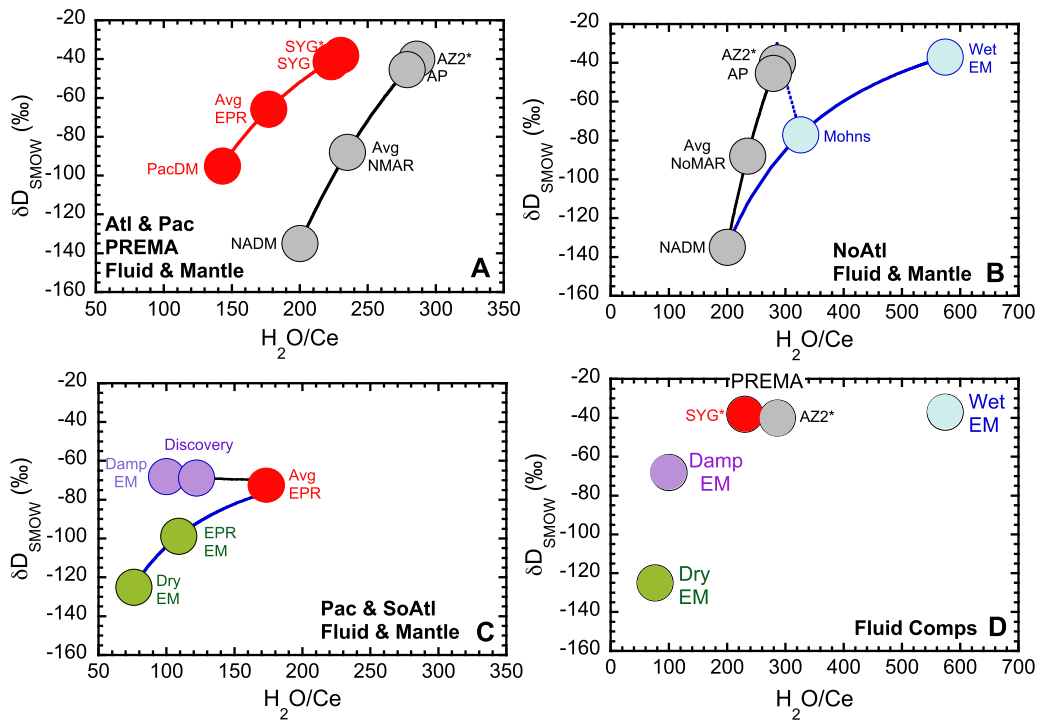


Figure 6. Summary of PREMA- and EM-type mixing components. Mantle sources for both PREMA and EM-type mantle sources can be produced by addition of $<1\%$ of C-O-H-Cl fluids to depleted mantle. (a) $\text{H}_2\text{O/Ce}$ and $\delta\text{D}_{\text{SMOW}}$ in mantle sources for PREMA-type basalts are similar implying consistency of formation and volatile content. PREMA-type end-member C-O-H-Cl fluids have uniformly heavy $\delta\text{D}_{\text{SMOW}}$ ($\sim -37 \pm 3\text{\textperthousand}$), inconsistent with the light slab model. Average North Atlantic depleted MORB ($\sim 90 \pm 10\text{\textperthousand}$) is lighter than average Pacific MORB ($\sim 60 \pm 5\text{\textperthousand}$) (Clog et al., 2013). Simple binary mixing models result in $\delta\text{D}_{\text{SMOW}}$ for North Atlantic and Pacific depleted mantle end-members to be $-135\text{\textperthousand}$ and $-95\text{\textperthousand}$ respectively. (b) The Mohns end-member mantle source, though more depleted than the Jan Mayen mantle source, shows EM-like characteristics due to small contribution (0.04%) of the WetEM fluid end-member. (c) In the southern Atlantic, EM-type basalts (Discovery) are damp ($\text{H}_2\text{O/Ce} = 120 \pm 10$) with intermediate $\delta\text{D}_{\text{SMOW}}$ ($-68 \pm 2\text{\textperthousand}$), similar to $\delta\text{D}_{\text{SMOW}}$ for Pacific MORB. In the northern Pacific, EM-type basalts (EPR north of Orozco) are dry ($\text{H}_2\text{O/Ce} = 110 \pm 20$) and isotopically light ($\delta\text{D}_{\text{SMOW}} = -94 \pm 3\text{\textperthousand}$). (d) Summary of calculated C-H-O-Cl fluid end-member compositions showing a limited range of $\text{H}_2\text{O/Ce}$ and $\delta\text{D}_{\text{SMOW}}$ in metasomatizing fluids for PREMA-type mantle sources inconsistent with the light slab model. EM C-O-H-Cl fluid end-members have variable $\delta\text{D}_{\text{SMOW}}$ ranging from -30 to $-125\text{\textperthousand}$ with only the DryEM fluid (lowest $\text{H}_2\text{O/Ce}$ and lightest $\delta\text{D}_{\text{SMOW}}$) consistent with the light slab model.

for example, serpentine formed by hydration of the subcrustal subducting mantle during bending at the trench (e.g., Faccenda et al., 2009; Ivandic et al., 2010; Peacock, 2001; Ranero et al., 2003; Ranero & Sallares, 2004; Rüpke et al., 2002), may transport water into the deeper mantle, at least to 250 km depth, beyond which dense hydrous magnesium silicates may carry water even deeper (Thompson, 1992; van Keken et al., 2002b, 2011; Wada & Wang, 2009).

Antigorite (serpentine) breaks down to form forsterite + enstatite + water at roughly 400–650°C at depths shallower than 250 km (Hilairet et al., 2006). Addition of a few weight percent of Al into the system may stabilize antigorite to even higher pressures and temperatures (up to $\sim 700^\circ\text{C}$) (Bromiley & Pawley, 2003). Subducted subcrustal serpentine will convert to chlorite, with some release of fluid, when slab-top depth is about 40–50 km for hot thermal profiles (Cascadia), and then chlorite breaks down when slab-top depth is about 80 km depth (van Keken et al., 2011; Walowski et al., 2015). For intermediate and cold thermal profiles (S. Chile and N. Honshu, respectively), chlorite is no longer stable, and serpentine breaks down when slab-top depths are about 110 km (intermediate—leaving anhydrous peridotite) and 200 km (cold—leaving phase A bearing peridotite) (Hilairet et al., 2006). In slabs cool enough for subcrustal serpentine to breakdown deeper than about 100 km, overlying mostly dehydrated sediments and igneous crust will interact with these fluids causing rehydration and re-equilibration of the stable isotopic compositions to heavier arc-like values. Similar models were developed by Walowski et al. (2015) to explain hydrogen isotopic values

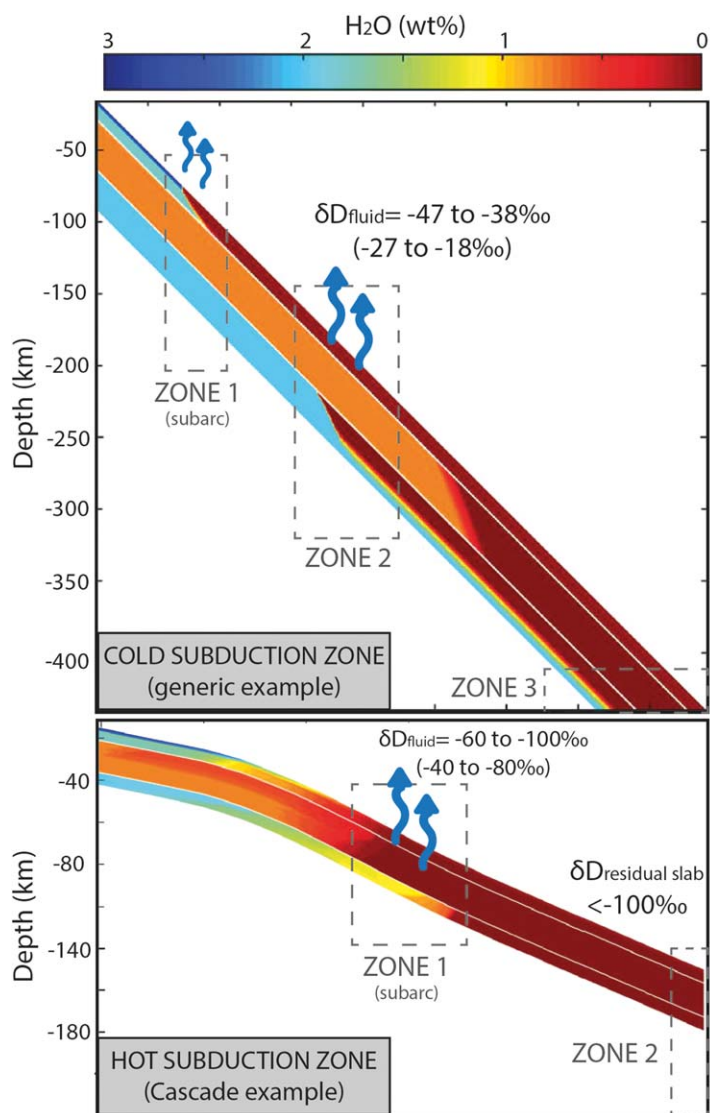


Figure 7. Thermal-petrologic slab dehydration model results for a (a) generic “cold” subduction zone (45° dip angle, 4 cm/yr convergence rate, 100 Ma slab age at the trench) compared with a (b) end-member “hot” slab subduction zone, Cascadia (based on modern Cascadia slab parameters; Walowski et al. (2015)), calculated using the methods described in Wada et al. (2012). For both models, the color gradient represents the distribution of bound H_2O remaining in the slab, and the slab thickness exaggerated is by a factor of three. The estimated $\delta\text{D}_{\text{fluid}}$ for each model was calculated using the fractionation model described in Walowski et al. (2015). Model results assume a starting $\delta\text{D}_{\text{SMOW}}$ of the serpentinized mantle materials of -60‰ (Alt & Shanks, 2006), with results in parentheses assuming a starting value of -40‰ (Barnes et al., 2009). Uncertainty in estimated δD values is $\pm 15\text{‰}$. Dashed boxes show approximate locations of Zones 1, 2, and 3 as described in Figures 7 and 8 and the text. Blue arrows show the approximate location of fluid-release pulses predicted by the dehydration models. For more details, see the supporting information of this manuscript and the supplementary materials of Walowski et al. (2015).

of arc basalts in the hot-slab southern Cascades region and by Kendrick et al. (2017) to explain water and halogens in MORB and OIB.

This process is modeled by extending the work of Walowski et al. (2015) to cooler conditions and greater depths. They used experimentally derived hydrogen isotopic fractionation factors of common phases in subducted oceanic lithosphere, excluding sediments, to predict the $\delta\text{D}_{\text{SMOW}}$ of the slab and fluids released during progressive dehydration of the slab down to depths of ~ 120 km. To extend their models to deeper depths for a cooler slab, we prescribe a hypothetical slab geometry with a 45° dip angle and a convergence rate of 4 cm/yr. For this geometry, we begin with a slab that is 100 Ma at the trench (and thus, cooler), to compare with the Cascade case (8 Ma slab age) of Walowski et al. (2015). The hydrogen isotope composition of the subducting slab (throughout its full thickness) and released fluids are calculated as a function of distance from the trench to a depth of ~ 400 km. The results (Figure 7) for the cooler 100 Ma slab place the breakdown of serpentinites in the upper mantle portion of the downgoing plate and the second pulse of released fluids at about 160 – 170 km depth, deeper than in the hot slab case. Depending on the assumed starting $\delta\text{D}_{\text{SMOW}}$ of the serpentinized mantle materials (-40‰ to -60‰) (Alt et al., 2012; Alt & Shanks, 2006; Barnes et al., 2009), the resulting fluids would be expected to have a $\delta\text{D}_{\text{SMOW}}$ of -18‰ to -47‰ . These fluids may cause flux melting of the slab top at depths significantly deeper than the zone of arc magmatism with water concentrations greater than and stable isotopic compositions heavier than predicted by the light slab model.

New boron and lithium isotopic data (supporting information S3) are consistent with this model. Both $\delta^{11}\text{B}$ (Shona Group 1) and $\delta^7\text{Li}$ (Azores Platform) correlate positively with $^{206}\text{Pb}/^{204}\text{Pb}$ in PREMA-type basalts. The estimated PREMA-type C-O-H-Cl fluid end-member has $\delta^{11}\text{B}$ of $+10\text{‰}$, consistent with derivation of boron from deep breakdown of antigorite ($+8$ to $+13.0\text{‰}$, Benton et al., 2001; Spivack & Edmond, 1987). Heavy $\delta^7\text{Li}$ for the PREMA end-member ($+5.1\text{‰}$) is consistent with previous results (Elliott et al., 2006; Krienitz et al., 2012; Nishio et al., 2005), who showed that HIMU (PREMA)-type lavas are characterized by $\delta^7\text{Li}$ up to $+7.4\text{‰}$, which they interpreted as being due to recycling of dehydrated, less-altered oceanic crust. The DampEM C-O-H-Cl fluid end-member has $\delta^{11}\text{B}$ of -6.6‰ , consistent with the boron isotopic composition of dehydrated sediments (-1 to -8‰) (Ishikawa & Nakamura, 1993) or melange serpentinites representing mantle wedge hydration at significant depths (30 to > 70 km) (Martin et al., 2016).

This approach resolves the dehydration paradox by developing a multistage dehydration model, in which the thermal parameters of the subducting slab exert an important control on the concentrations of volatiles and light stable isotopic composition of slab materials. In cooler slabs, sediments and igneous crust that have undergone near-complete dehydration and dehydration-related trace element fractionation shallower than 120 km, will have water concentrations

increased and hydrogen isotopic compositions restored by addition of fluids derived from deep dehydration of subcrustal serpentine with “arc”-like hydrogen isotopic compositions. In hotter slabs, dehydrated sediments and igneous crust will preserve the light stable isotopic signatures created by a combination of dehydration (shallower, beneath forearc) and hydrous melting (beneath arc).

9. A Multistage Melt Metasomatic Model for the Origin of Enriched Mantle End-Members

9.1. Extending the Subduction Factory to the Mantle Transition Zone

The phrase “subduction factory” has been used to describe subduction zone processes, in which raw materials (downgoing slab as factory input) are processed (metamorphism and dehydration) to produce hydrous fluids/melts and ultimately arc magmas (factory outputs) (e.g., Eiler, 2003; Kimura et al., 2009; Ryan & Chauvel, 2014; Stern, 2002). The archetypal subduction factory is a multistage metasomatism and melting model dominated by dehydration reactions that occur at depths shallower than 120 km (Zone 1) in most arcs. It is useful to consider the subduction factory extending beyond 120 km to include two additional “processing plants,” where depleted mantle is metasomatized by melts of differing compositions, and where carbon plays as important a role as water (Figures 8 and 9). Zone 2 occurs at ~200 km, where carbonated sediments may melt (Grassi & Schmidt, 2011a, 2011b). Zone 3 occurs at ~410 km, where carbonated eclogite may melt (Thomson et al., 2016). The presence of heavy hydrogen isotopic compositions in enriched mantle end-members requires that these metasomatizing melts be derived from surface-modified materials, e.g., a subducted slab, and not from the melting in the wings of the upwelling MORB melting regime or at the interface between the low-velocity zone and the cooling oceanic lithosphere (autometasomatism).

Thus, water-dominated dehydration and melting processes in Zone 1 (<120 km) generate the sources of arc magmas, whereas carbonate-dominated melting processes (>120 km) in Zones 2 (sediments) and 3 (eclogite ± sediments) generate the metasomatized peridotite that later becomes EM- and PREMA-type mantle components, respectively. Melting of subducted materials in Zones 2 and 3, and transfer of these melts to the ambient upper mantle and SCLM, are important mechanisms controlling variable water concentrations and stable isotopic compositions of oceanic basalts.

9.2. Zone 1: Dehydration-Derived Subcritical Fluids and Melts in the Source for Arc Magmatism

In Zone 1 (roughly 2–4 GPa, 60–120 km, 600–800°C), hydrous fluids (>95% H₂O) and silicate melts (H₂O < 15 wt. %) form in the subcritical zone, where separate melt and fluid phases coexist and become more miscible in each other with increasing temperature and pressure until the second critical endpoint is reached at about 5 ± 1 GPa (~150 ± 30 km) (Kessel et al. 2005; Mibe et al., 2007, 2011). Addition of hydrous fluids and melts to arc mantle sources greatly increases the water content of arc magmas resulting in H₂O/Ce as high as 20,000 (Cooper et al., 2012; Plank et al., 2009). Under Zone 1 conditions, accessory phases, including allanite, monazite, and rutile, are stable residual phases (assuming they have not been exhausted by hydrous flux melting of the slab top) and play important roles in controlling the trace element characteristics, especially rare earth elements, of fluids and melts.

Experimental results on the solid/fluid trace element bulk partitioning of allanite and monazite as a function of temperature (e.g., Brenan et al., 1995; Hermann & Rubatto, 2009; Johnson & Plank, 1999; Keppler, 1996; Kessel et al., 2005) have allowed the development of geothermometers based on H₂O/Ce in mafic arc melt inclusions (Cooper et al., 2012; Plank et al., 2009). In addition, the temperature of fluid or hydrous melt generation based on H₂O/Ce has been found to correlate with the thermal parameters of the subducting slab (Cooper et al., 2012; Ruscitto et al., 2012). They show H₂O/Ce in primary arc magmas ranging from about 20,000 to as low as 200, with the lowest values similar to oceanic basalts. Their derived geothermometer (H₂O/Ce = $2 \times 10^7 e^{-0.0109T}$; T in °C) predicts that H₂O/Ce in slab-derived fluids and hydrous melts will decrease by orders of magnitude, from >1,000,000 to <1,000, as temperature increases from 600 to 1,000°C.

In addition, rutile plays a critical role in controlling HFSE (Nb and Ta) concentrations. At depths shallower than 300 km, Nb and Ta strongly partition into rutile during melting (Bromiley & Redfern, 2008), resulting in subcritical fluids and melts generated in Zone 1 depleted in Nb and Ta relative to similarly incompatible trace elements consistent with observed compositions of arc and EM-type magmas.

Recent thermal models for the slab and mantle wedge (Syracuse et al., 2010; van Keken et al., 2011) predict slab surface temperatures beneath arc volcanic fronts that vary between 700° and 950°C, significantly higher than earlier models (Kincaid & Sacks, 1997; Peacock, 1996; Peacock & Wang, 1999). According to these more recent models, sediments and basaltic crust should be thoroughly dehydrated at 120 km depth. Given these higher slab surface temperatures, especially for the hottest (or slowest) slabs, and if dehydrating serpentine or chlorite provide a source of water fluxing, it is physically plausible to generate partial melts of water-saturated

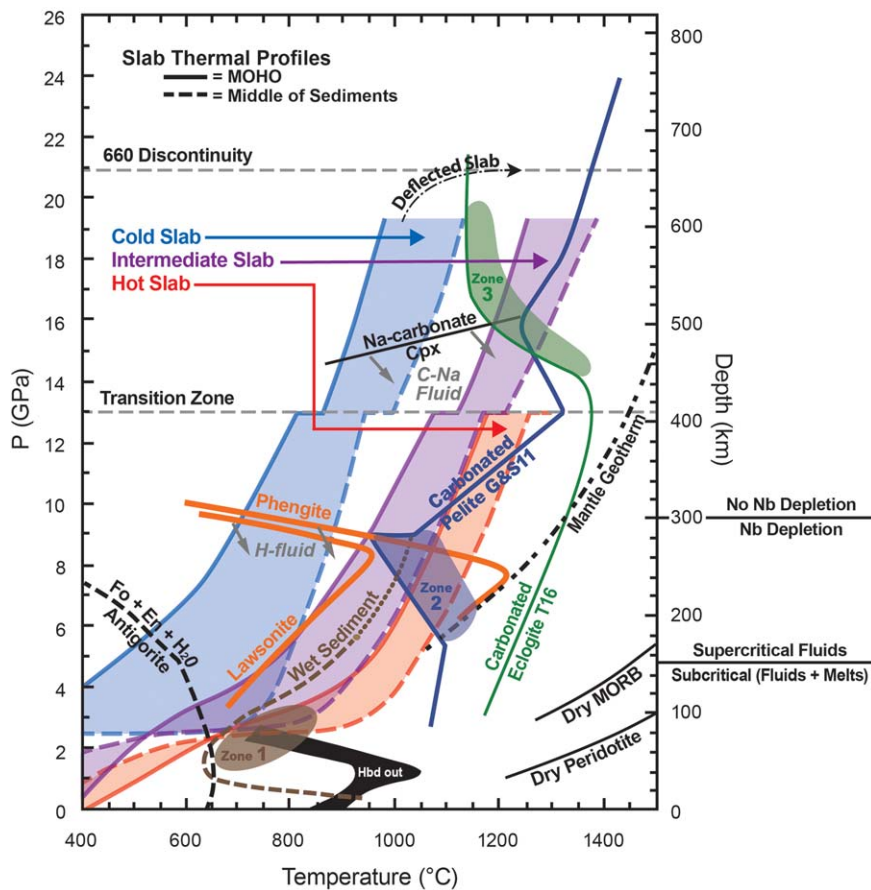


Figure 8. For warm to hot subduction paths, melting of sediments or igneous crust may occur in three zones where P-T paths intersect with a solidus that has a negative slope. In Zone 1, hydrous fluids ($>95\% \text{ H}_2\text{O}$) and silicate melts ($\text{H}_2\text{O} < 15 \text{ wt. \%}$) form separate phases that become more miscible in each other until the second critical endpoint is reached at about $5 \pm 1 \text{ GPa}$ ($\sim 150 \pm 30 \text{ km}$). Zone 2 occurs at $\sim 200 \text{ km}$ (6–9 GPa), where carbonated sediments may melt (Grassi & Schmidt, 2011a, 2011b), and Zone 3 occurs at $\sim 410 \text{ km}$ (14–17 GPa), where carbonated eclogite may melt (Thomson et al., 2016). Thus, water-dominated dehydration and melting processes in Zone 1 ($< 120 \text{ km}$) generate the sources of arc magmas, while carbonate-dominated melting processes in Zones 2 and 3 ($> 120 \text{ km}$) generate the sources for EM and PREMA enriched mantle end-members. Sub and supercritical boundary at 150 km defines depth above which a single fluid phase forms with volatile contents intermediate between subcritical “fluids” and “melts” (Kessel et al., 2005; Mibe et al., 2007, 2011). Boundary at 300 km above which rutile no longer preferentially retains Nb from Bromiley and Redfern (2008). Black-dashed curve is breakdown of antigorite (Hilairet et al., 2006). Blue curve is melting of carbonated pelitic sediments (Grassi & Schmidt, 2011a, 2011b). Green curve is melting of carbonated eclogite (Thomson et al., 2016). Hot, intermediate, and cold slab thermal profiles from Syracuse et al. (2010) and van Keken et al. (2011). Dashed curves represent the middle of the sediments (their layer 99). Solid curves represent upper mantle about 1 km below the base of the crust (their layer 109). The hot-slab P-T path is shown as ending at the transition zone to reflect flat-slab subduction (e.g., Suárez et al., 1990). Melting may occur for cooler slabs if they are deflected and reside at the top of the lower mantle long enough to thermally equilibrate with the ambient mantle. Modified from Grassi and Schmidt (2011a, 2011b).

sediments and basaltic crust, with $\text{H}_2\text{O}/\text{Ce}$ ranging from 640 to 9700, that contribute to the generation of arc magmas (Hermann & Spandler, 2008; Kessel et al., 2005; Poli & Schmidt, 2002; Schmidt et al., 2004b; Schmidt & Poli, 2014, 1998).

In particular, compositions of arc magmas in hot subduction zones, such as the Cascades, the Mexican Volcanic Belt, and Central America are consistent with addition of melts of subduction-modified sediments and igneous crust to the mantle wedge source (e.g., Cai et al., 2014; Rusciotto et al., 2010, 2014; Walowski et al., 2015). These components have geochemical characteristics similar to EM-type sources (e.g., overall enrichment in incompatible elements, enrichments in fluid-mobile elements, and depletions in HFSE). Zone 2 sediment-derived supercritical fluids may share some of trace element characteristics of Zone 1 hot slab

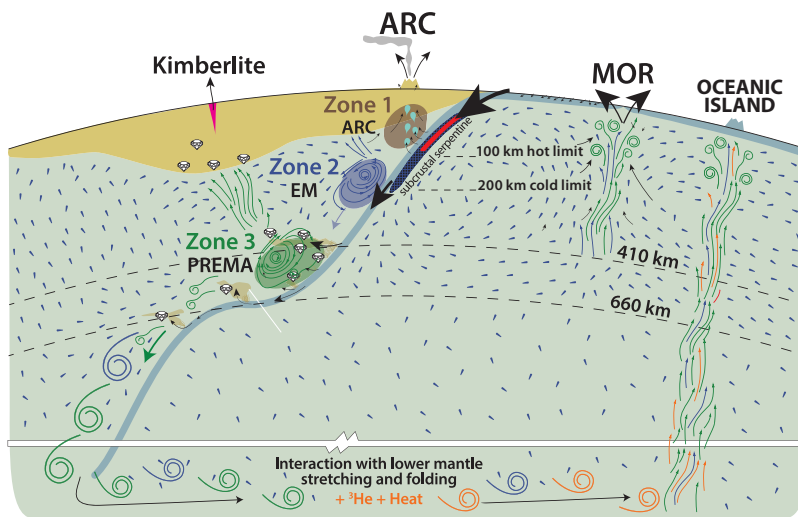


Figure 9. Multistage melting model for the origin of enriched MORB and OIB. Mantle heterogeneity produced by addition of less than a few percent sub or supercritical fluids and melts derived from dehydrating/decarbonating slab lithologies to depleted mantle. In Zone 1, subcritical fluids and melts (light blue) produce hydrous mantle sources of arc and back-arc basalts. In Zone 2, supercritical C-O-H-Cl fluids (purple) from dominantly carbonated sediments result in EM-type sources. In Zone 3, supercritical C-O-H-Cl fluids (green) derived from carbonated eclogite result in PREMA-type sources. Metasomatized mantle gets stretched and folded during mantle convection and may remain as distributed heterogeneities in the upper mantle (low ${}^3\text{He}/{}^4\text{He}$) or be transported through the lower mantle (high ${}^3\text{He}/{}^4\text{He}$, red) and returned to the surface in mantle plumes. Modified from Thomson et al. (2016).

sediment melts, including high Ba/Nb, Rb/Sr, and Ce/Pb. Binary mixing models (supporting information S4) explore the feasibility of using a hot subduction component (Ruscitto et al., 2012) as an enriched end-member component associated with the formation of EM-type sources.

9.3. Zone 2: Melting of Sediments and Formation of EM Components

Grassi and Schmidt (2011a, 2011b) identified P-T conditions at which carbonated pelitic sediments melt ($\sim 230 \pm 50$ km depths and 950° to $1,200^\circ\text{C}$) (Figure 8) associated with the breakdown of phengite, referred to here as Zone 2. Thermal profiles for sediments on top of average to hot slabs will cross the carbonated pelite melting curve allowing sediment melting. Because Zone 2 carbonated pelite melting is driven by the breakdown of phengite, even sediments that underwent melting in Zone 1 may undergo additional melting in Zone 2. Melting of carbonated sediments occurs under supercritical conditions (deeper than the second critical endpoint at 150 ± 30 km, Kessel et al. 2005; Mibe et al., 2007, 2011), thus producing a single fluid phase with volatile contents intermediate between subcritical “fluids” and “melts.” The resulting sediment-derived supercritical fluids are carbonatitic to alkali silica-undersaturated in composition, are enriched in fluid-mobile elements, are depleted in Nb and Ta due to residual rutile (Bromiley & Redfern, 2008), and have high Ba/Nb.

If accessory phases allanite and monazite have not been exhausted by fluid production in Zone 1, then estimates of slab surface temperature may be used to predict expected $\text{H}_2\text{O}/\text{Ce}$ in these fluids. The estimated EM fluid $\text{H}_2\text{O}/\text{Ce}$ values of 95–574 yield $\text{H}_2\text{O}/\text{Ce}$ geothermometer temperatures of 960°C – $1,125^\circ\text{C}$, in excellent agreement with temperatures of carbonated pelite melting in Zone 2 (950°C – $1,200^\circ\text{C}$), though these results should be viewed with some caution as the Plank et al. (2009) geothermometer is only calibrated to $\sim 1,060^\circ\text{C}$. In the hypothetical case where these phases have been exhausted, then $\text{H}_2\text{O}/\text{Ce}$ may reflect the amount of residual H_2O and Ce in the slab and their solid/melt partitioning. For cooler slabs, fluxing of the slab surface by fluids derived below 120 km from subcrustal hydrous phases may buffer H_2O concentrations and stable isotopic compositions at higher and heavier values, respectively, than predicted by a simple Raleigh fractionation model. Thus, the wet and heavy $\delta\text{D}_{\text{SMOW}}$ metasomatic fluid compositions for the northern Atlantic EM-type basalts may indicate fluid generation from a cooler slab than the one that produced the dry and light $\delta\text{D}_{\text{SMOW}}$ fluid end-member for the northern EPR EM-type basalts.

Most earlier models for the origin of EM-type mantle end-members have used mixing between depleted mantle and various proportions of subducted crustal materials or SCLM, to explain the enrichments in fluid-mobile elements and alkalis and depletions in high-field strength elements Nb and Ta (e.g., Chauvel et al., 2008; Hofmann, 2014; Jackson & Dasgupta, 2008; Willbold & Stracke, 2006). However, addition of sediment melts, instead of raw sediments, better satisfies available data (e.g., Chauvel et al. 2008), and is supported by recent experimental studies. Addition of ≤ 1 wt. % of carbonate melts of carbonated pelites to depleted mantle is capable of evolving into observed EM-type radiogenic isotopic compositions (Grassi et al., 2012). Thus, melting of carbonated sediments within Zone 2 at roughly 230 km depth is proposed as the locus of formation of EM-type enrichments. Heterogeneity in melt compositions may be introduced by varying sediment type and origin (e.g., amount of eroded upper and lower continental crust).

9.4. Zone 3: Melting of Carbonated Eclogite in the Mantle Transition Zone and Formation of PREMA Components

Zone 3 is located at near the top of and within the mantle transition zone between 410 and 660 km. Thomson et al. (2016) showed that melting of carbonated oceanic crust (eclogite) may occur at ~ 300 –700 km depth in the mantle, where average to hot slab geotherms intersect a deep depression along the melting curve (Figure 8). A 200°C drop in the solidus temperature over a narrow pressure range is caused by a change in clinopyroxene composition toward a more sodium-rich composition above 13 GPa (~ 400 km) due to dissolution of sodium-poor pyroxene components into coexisting garnet. Eventually, clinopyroxene becomes so sodium-rich that a coexisting Na-carbonate mineral stabilizes in the subsolidus assemblage, causing the depression along the solidus. Recognition of the carbonated eclogite solidus depression in this region provides a mechanism to generate deep incipient melts of subducted igneous crust and overcomes serious concerns about the feasibility of previously proposed metasomatism models.

The first partial melts of carbonated eclogites are alkaline carbonatites (e.g., Dasgupta & Hirschmann, 2006; Kisieva et al., 2012; Thomson et al., 2016) that are mobile and highly reactive with ambient mantle. With increasing extents of melting, experiments show either a gradual increase in the silicate component in the melt (Yaxley & Brey, 2004) or the formation of carbonatitic and silicate immiscible melts (e.g., Dasgupta et al., 2006, 2007; Gerbode & Dasgupta, 2010). Reaction of these incipient melts with ambient mantle provides an explanation for the occurrence of “superdeep” diamonds, originating in the deep upper mantle and transition zone, with chemical fingerprints similar to subducted oceanic crust (Bulanova et al., 2010; Harte, 2010; Stachel, 2001; Thomson et al., 2014; Weiss et al., 2015).

Zone 3 is located deeper than the 300 km limit above which changes in melt structure result in marked reduction in the partitioning of Nb and Ta into rutile (Bromiley & Redfern, 2008), and also mostly deeper than the 420 km limit of rutile stability (Okamoto & Maruyama, 2004). Thus, HFSE elements retained in the slab during fluid and melt production in Zones 1 and 2 are available to enter supercritical fluids in Zone 3. This produces enrichments in Nb and Ta relative to similarly incompatible elements, along with low Ba/Nb, characteristic of PREMA components. Addition of low degree partial melts (formed at pressures above the second critical endpoint) of carbonated subduction-modified oceanic crust at transition zone depths is capable of producing the geochemical fingerprint of PREMA-type sources (e.g., Cooper et al., 2004). In addition, Grassi et al. (2012) show that melts of carbonated pelites within Zone 3 have trace element characteristics capable of evolving to EM2 radiogenic isotopic compositions.

The uniformly heavy PREMA-type end-member fluids requires that the hydrogen isotopic values of previously dehydrated eclogite be restored to values similar to hydrothermally altered basalt entering the trench by interaction with fluids derived from dehydration of subcrustal antigorite.

9.5. Conditions for Deep Melting in Cold Slabs

The proposed model permits melting of carbonated sediment and eclogite for average to hot subduction thermal profiles (Figure 8). Such melting may have been more common earlier in Earth’s history (e.g., Sizova et al., 2010; Sleep & Windley, 1982; Stern, 2005). Cold or rapidly subducting slabs (e.g., N. Honshu) should not undergo melting in Zones 2 and 3. Only if cold slabs are deflected and stagnate in the upper mantle, most likely at the 410 or 670 km discontinuities, would they be able to warm up sufficiently to exceed the carbonated sediment and eclogite melting curves.

9.6. Second-Stage Melting of Plumes and Distributed Heterogeneities

Mantle metasomatized by melts and fluids in Zones 1–3 will get further stretched and mixed into ambient mantle during convection (e.g., Farnetani et al., 2002; Lin & van Keken, 2006; van Keken et al., 2002a). Metasomatized mantle and/or metasomatized subcontinental lithospheric mantle formed by Zones 1 and 2 melting may remain in the upper mantle and will retain a low $^3\text{He}/^4\text{He}$ signature, as observed for the Arctic Ridges north of Iceland. Slabs and entrained metasomatized mantle that make it all the way to the lower mantle may interact and mix with a less degassed high $^3\text{He}/^4\text{He}$ component, perhaps associated with the LLSVP layer at the core–mantle boundary.

Plumes that upwell from the lower mantle bring with them mixtures of recycled metasomatized and hotter ambient mantle components with contributions of long-isolated less-degassed primitive material with high $^3\text{He}/^4\text{He}$, as is the case for the Azores Platform, south Atlantic, and EMP-ESC basalts. The origin of various chemical fingerprints can be attributed to different components in the mixed source. Concentrations of noble gases will be dominated by the lower mantle component; compatible elements (Ni, Cr, and HREE) will be dominated by the peridotitic depleted mantle; and roughly half to almost all of the highly incompatible elements, including water and carbon, will be dominated by the metasomatic melt components. Autometasomatism will act to further redistribute enriched “lumps” into the upwelling mantle, as modeled for the Mid-Atlantic Ridge south of the Azores Platform (Gale et al., 2013b).

This multistage metasomatic and melting model satisfies all available data, including the combination of little to no $\delta^{18}\text{O}$ signal in most oceanic basalts indicating addition of <5% recycled material, evidence for peridotitic source mineralogy, and evidence for mantle source incompatible element enrichment.

10. Broader Implications

10.1. What Is $\delta\text{D}_{\text{SMOW}}$ of MORB Mantle?

The canonical value for $\delta\text{D}_{\text{SMOW}}$ in normal MORB and its mantle source has been $-80 \pm 10\text{‰}$ (Chaussidon et al., 1991; Craig & Lupton, 1976; Kyser & O’Neil, 1984; Pineau et al., 2004; Poreda et al., 1986). In contrast, recent analysis of southern Pacific MORB (Clog et al., 2013) led to the conclusion that the hydrogen isotopic composition of the MORB mantle should be revised to $-60 \pm 5\text{‰}$. Clog et al. (2012) proposed that many earlier results were in error due to a previously unrecognized memory effect in platinum crucibles and should be shifted to heavier values by 10–20‰.

Instead of being rooted in analytical differences, the $\delta\text{D}_{\text{SMOW}}$ in the upper mantle is likely heterogeneous as a result of variable contributions of enriched recycled components in different ocean basins. The compilation of depleted and enriched MORB data show that average depleted MORB in the north Atlantic has a mean $\delta\text{D}_{\text{SMOW}} = -90 \pm 10\text{‰}$, consistent with earlier work. The agreement of the new TC/EA analyses with previous conventional analyses from a variety of laboratories argues against systematic offsets due to platinum crucibles. This would then be consistent with the results of Clog et al. (2013) that average Pacific MORB has a $\delta\text{D}_{\text{SMOW}}$ of $\sim -60 \pm 5\text{‰}$. Their most depleted samples with lowest $^{206}\text{Pb}/^{204}\text{Pb} < 18.2$ have $\delta\text{D}_{\text{SMOW}}$ values of $\sim -75\text{‰}$, consistent with existence of a strongly depleted mantle component with $\delta\text{D}_{\text{SMOW}}$ values of -80‰ or lighter. The simple binary mixing models result in $\delta\text{D}_{\text{SMOW}}$ for North Atlantic and Pacific depleted mantle end-members to be -135‰ and -95‰ , respectively. These suggestions do not, however, provide an explanation for the difference in $\delta\text{D}_{\text{SMOW}}$ between these two depleted mantle regions.

10.2. Why Is PREMA so Homogeneous?

The limited range of H_2O concentrations, $\text{H}_2\text{O}/\text{Ce}$, and $\delta\text{D}_{\text{SMOW}}$ in PREMA-type basalts suggest a “sweet spot” in conditions associated with melting of igneous crustal materials subducted into the transition zone and lower mantle. With respect to $\text{H}_2\text{O}/\text{Ce}$, it is unlikely that $\text{H}_2\text{O}/\text{Ce}$ of fluids is controlled by accessory minerals under these conditions, therefore estimated fluid $\text{H}_2\text{O}/\text{Ce}$ more likely reflects the amount of residual H_2O and Ce in the slab and their solid/melt partitioning. Current models of water evolution in slab during subduction (e.g., van Keken et al., 2011; Wada et al., 2012) assume that all water is expelled during the transition from amphibolite to anhydrous eclogite, though intermediate hydrous lawsonite and phengite eclogite facies may retain 0.5–1 wt. % H_2O to depths >200 km in intermediate to cold slabs (van Keken et al.,

2011). These models do not consider water in nominally anhydrous minerals, nor do they allow for stable isotopic re-equilibration between slab lithologies and migrating fluids.

Nominally anhydrous pyroxene and garnet, however, may contain H₂O incorporated in the form of hydroxyl (OH⁻). Eclogite can hold up to 5,000 ppm H₂O in nominally anhydrous minerals at 100 km depth decreasing to 2,000 ppm at the top of the transition zone. Majorite garnet within the transition zone can hold 1,100 ppm H₂O (Hauri et al., 2006; Katayama et al., 2003). The maximum extent of rehydration possible will be controlled by the solubility of water in nominally anhydrous minerals, the stability fields of lawsonite and phengite, and by the C-O-H fluid composition.

Rehydration of overlying crustal eclogite, as required to explain the heavy δD_{SMOW} , in warm to cold slabs most likely occurs in the form of heterogeneously distributed veins. As the water solubility in eclogite decreases during slab descent, the water in these veins may get redistributed more uniformly throughout the eclogite to maintain saturation in nominally anhydrous minerals.

This hypothesis can be tested using a simple back-of-the-envelope calculation. Consider that H₂O and Ce concentrations in the eclogite incipient melts are controlled by clinopyroxene and garnet partition coefficients (not accessory phases) and that their partition coefficients are roughly equal. Assuming a Ce concentration of 5–6 ppm in bulk igneous crust (Stracke et al., 2003) and a H₂O concentration in eclogite of 2,000 ppm at saturation at the top of the transition zone, then the H₂O/Ce of incipient melts will be 330–400. These values are slightly higher than observed suggesting less than full water saturation in eclogite or differences in the partition coefficients. If the H₂O concentration in majorite garnet within the transition zone of 1,100 ppm is used, then the H₂O/Ce of incipient melts will be ~180–220. These values are certainly in the right ballpark and give us confidence that this is a possible mechanism for controlling H₂O concentrations and H₂O/Ce in PREMA-type mantle sources.

The fact that PREMA-type fluid and mantle compositions with H₂O/Ce < 220 and $\delta D_{SMOW} < -40 \text{ ‰}$ have yet to be observed suggests that melting of fully dehydrated eclogites associated with hot slabs is unlikely to occur in Zone 3. Either the rehydration process is a necessary condition for melting in Zone 3 or hot slabs rarely subduct to transition zone depths (e.g., Husker & Davis, 2009). The ubiquitous presence of near-saturation H₂O concentrations and heavy δD_{SMOW} in eclogites that melt in Zone 3 appears to be linked to either the possible role of water in further depressing the carbonated eclogite solidus or to the inability of hot slabs to subduct through the transition zone.

10.3. Is Subcontinental Lithospheric Mantle a Possible EM Source?

Subcontinental lithospheric mantle (SCLM) is often cited as the source for EM-type basalts (e.g., Andres et al., 2002; Debaillé et al., 2009; Ellam & Stuart, 2000; Geldmacher et al., 2008; Hanan et al., 2013; McKenzie & O’Nions, 1983; Tappe et al., 2007; Workman et al., 2004) analyzed 375 spinel lherzolite and harzburgite xenoliths to constrain the composition of the SCLM and determined it to be characterized by enrichment in light rare earth elements (LREE), flat trends in heavy rare earth elements (HREE), and low ³He/⁴He signature (6.1 ± 0.9). McDonough (1990) suggested a two-stage growth model, in which an initial melting event depleted the residue in LREE and was followed by one or more enrichment events. Studies of xenoliths show evidence for interaction with both carbonatitic and alkali silicate metasomatic melts (e.g., Agashev et al., 2013; Amundsen et al., 1987; Ionov et al., 1993, 2002; O’Reilly & Griffin, 2012). Recent work by Weiss et al. (2016) argues that the source for HIMU basalts is SCLM metasomatized by carbonatite melt before entrainment in convecting mantle.

Zone 2 melting and metasomatism is capable of generating the EM-like characteristics of SCLM and that its composition reflects multiple episodes of melt extraction, metasomatism, and solid/melt reactions during melt migration. SCLM may be dispersed into the convective upper mantle during opening of the ocean basin and will be progressively flushed out as the upper mantle melts to form MORB. Application of this concept to the northern Atlantic is discussed below.

10.4. Origin of High H₂O/Ce in the Northern Atlantic

High H₂O/Ce in northern Atlantic basalts relative to the rest of the mid-ocean ridge system are consistent with the findings of Michael (1995), who argued that the sources of H₂O in northern Atlantic basalts are more likely to be derived from recycled, subducted, altered oceanic crust than juvenile mantle, though he did not distinguish between EM and PREMA compositions. The model presented here offers a refinement

of his earlier interpretation, and specifies that the northern Atlantic mantle contains dispersed EM components formed by metasomatizing depleted mantle by melts and supercritical fluids of dominantly sediments at ~ 250 km. The ubiquitous presence of the EM component in the northern Atlantic mantle is consistent with the young age of the basin and slow spreading rates, whereby production of northern Atlantic MORB has not yet been able to flush out this dispersed heterogeneity. The PREMA component is isolated in plumes (Jan Mayen, Iceland, and Azores Platform) consistent with metasomatism taking place at deeper depths and perhaps at an earlier time. In some cases (Iceland and Azores Platform), the PREMA component is associated with high ${}^3\text{He}/{}^4\text{He}$, whereas in others (Jan Mayen), it is not. The PREMA component, generated in the transition zone, may remain in the upper mantle and not pick-up ${}^3\text{He}/{}^4\text{He}$ from the lower mantle, as is the case for the Arctic Ridges. In other cases, metasomatized mantle may be entrained by subduction into the lower mantle, perhaps all the way to the core/mantle boundary, at which point it may mix with or pick-up high ${}^3\text{He}/{}^4\text{He}$ characteristics and return to the surface in mantle plumes, as is the case for Iceland and the Azores Platform.

Michael (1995) also suggested that high $\text{H}_2\text{O}/\text{Ce}$ in MORB from the northern MAR might be related to a period of rapid subduction in the past that resulted in depressed isotherms and less dehydration in the slab. The association of high $\text{H}_2\text{O}/\text{Ce}$ with heavy $\delta\text{D}_{\text{SMOW}}$ supports this idea of involvement of fluids derived from deeper cooler portions of the slab.

11. Conclusions

An outstanding puzzle in mantle geochemistry has been the origin and evolution of Earth's volatile components. In particular, the "dehydration paradox" refers to the following conundrum. The PREMA end-member in mid-ocean ridge basalts and ocean island basalts requires involvement of a mostly dehydrated slab component to explain the trace element ratios and radiogenic isotopic compositions, but a fully hydrated slab component to explain the stable isotopic compositions.

The main contribution of this study is that volatile concentrations and stable isotopic compositions of EM and PREMA-type basalts for individual regions are distinctive and correlate systematically with other indicators of mantle composition. Estimated EM-type C-O-H-Cl fluid components have regionally variable H_2O concentrations and $\delta\text{D}_{\text{SMOW}}$, ranging from wet and heavy (Wet EM at Arctic Ridges; $\text{H}_2\text{O}/\text{Ce} = 574$, $\delta\text{D}_{\text{SMOW}} = -30\text{ ‰}$), intermediate (Damp EM at the Discovery anomaly in the southern Atlantic; $\text{H}_2\text{O}/\text{Ce} = 100$, $\delta\text{D}_{\text{SMOW}} = -68\text{ ‰}$), to dry and light (DryEM at EPR 14–17°N; $\text{H}_2\text{O}/\text{Ce} = 95$, $\delta\text{D}_{\text{SMOW}} = -120\text{ ‰}$). Only the DryEM fluid composition is consistent with the light slab model. In contrast, estimated PREMA-type C-O-H-Cl fluid components have a limited compositional range: $\text{H}_2\text{O}/\text{Ce}$ (230–290) and $\delta\text{D}_{\text{SMOW}}$ ($\sim -37 \pm 3\text{ ‰}$). Boron and lithium isotopic ratios parallel the trends observed for $\delta\text{D}_{\text{SMOW}}$ as a function of radiogenic isotope tracers of mantle heterogeneity.

Decoupling of slab volatiles and their stable isotopes from lithophile elements during subduction reflects complex dehydration processes including (1) primary dehydration of the slab surface, and (2) secondary rehydration, infiltration and re-equilibration of the slab by C-O-H-Cl fluids derived from dehydrating subcrustal hydrous phases in cooler, deeper parts of the slab. Rehydration of previously dehydrated slab materials resolves the dehydration paradox.

The "expanded subduction factory" model includes melt or fluid generation at several key depths:

1. Zone 1: (shallower than 120 km) Mantle wedge sources of arc and back-arc magmas are generated by addition of subcritical fluids and melts of the dehydrating subducting slab to depleted upper mantle peridotite.
2. Zone 2: (180–280 km) EM-type mantle compositions are generated above slabs with average to hot thermal profiles by addition of carbonated sediment-derived supercritical fluids/melts to depleted asthenospheric or subcontinental lithospheric mantle. The observed range in fluid end-member $\text{H}_2\text{O}/\text{Ce}$ is consistent with estimates of slab surface temperature of $>950^\circ\text{C}$.
3. Zone 3: (410–660 km) PREMA-type mantle sources are generated, above slabs with average to cool thermal profiles, by addition of carbonated eclogite and sediment-derived supercritical fluids to depleted mantle. Colder slabs may also produce melts if slab deflection allows additional warming. Heavy $\delta\text{D}_{\text{SMOW}}$ in PREMA end-member fluids requires involvement of seawater released by deep dehydration of

subcrustal hydrous minerals. The limited range and heavy stable isotopic compositions of PREMA end-members and their similarity to antigorite suggests that either fluxing by deep fluids in cool to cold slabs is essential to initiate melting of dehydrated igneous crustal materials within the transition zone or that dehydrated, hot slabs are unable to subduct past 410 km.

The proposed model does not exclude mixing of “raw” recycled crustal materials into depleted mantle; however, creation of mantle sources through addition of incipient recycled crustal melts is an important mechanism for enriching the mantle. Incipient melts form easily fusible veins of pyroxenite as they migrate through and react with mantle peridotite. These metasomatized regions get further stretched and mixed into ambient mantle during convection, either in the lower mantle, where they may pick up a high $^3\text{He}/^4\text{He}$ signature, or in the upper mantle, where they retain their low $^3\text{He}/^4\text{He}$ signature. This model does not contradict evidence for continued redistribution of the chemical heterogeneities by plumes and convective upwelling that ultimately bring these mixed sources to the surface. Autometasomatism will act to further redistribute enriched “lumps” into the upwelling mantle.

Acknowledgments

J.E.D. is grateful to the University of South Florida for granting a 1 week nano-sabbatical at the University of Oregon in March 2015 and a 2 month mini-sabbatical in March–April 2016 at the Carnegie Institution of Washington Department of Terrestrial Magnetism (DTM), where she was fortunate to serve as a Tuve Fellow. Work by R. Kingsley, J. Dixon, and T. Rau Hajewski was supported by NSF/OCE-0351149. This work brings together studies of MORB suites from both C. Langmuir and J.-G. Schilling funded over the years by NSF/OCE-9302574 (1993 to J. Dixon and C. Langmuir), NSF/OCE-9530373 (1995 to J. Dixon and J.-G. Schilling), NSF/OCE-0351149 (2004 to J. Dixon, R. Kingsley, and J.-G. Schilling), NSFOCE-0351125 (2006 to R. Kingsley and J.-G. Schilling for the D/H and O isotopes along the Arctic ridges), and NSF/EAR-844772 (2009 to I. Bindeman for D/H analysis of Atlantic and north Pacific samples). Ideas were refined during many helpful discussions with Erik Hauri, Peter van Keken, Steve Shirey, and Rick Carlson. The first author is extremely grateful for the thoughtful and thorough review by A. Pietruszka. The manuscript also benefited from reviews by R. Stern and an anonymous reviewer. The data used are listed in Figures 2–8 are provided in Tables (1–4) and archived in IEDA:EarthChem [<http://www.earthchem.org/library>].

References

Agashev, A. M., Ionov, D. A., Pokhilenko, N. P., Golovin, A. V., Cherepanova, Y., & Sharygin, I. S. (2013). Metasomatism in lithospheric mantle roots: Constraints from whole-rock and mineral chemical composition of deformed peridotite xenoliths from kimberlite pipe Udachnaya. *Lithos*, 160–161, 201–215.

Alt, J. C., Garrido, C. J., Shanks, W. C. III, Turchyn, A., Padrón-Navarta, J. A., López Sánchez-Vizcaíno, V., . . . Marchesi, C. (2012). Recycling of water, carbon, and sulfur during subduction of serpentinites: A stable isotope study of Cerro del Almirez, Spain. *Earth Planetary Science Letters*, 327–328, 50–60.

Alt, J. C., Honnorez, J., Laverne, C., & Emmermann, R. (1986). Hydrothermal alteration of a 1 km section through the upper oceanic crust, Deep Sea Drilling Project Hole 504B: Mineralogy, chemistry and evolution of seawater-basalt interactions. *Journal of Geophysical Research*, 91, 10309–10335. <https://doi.org/10.1029/JB091iB10p10309>

Alt, J. C., & Shanks, W. C. (2006). Stable isotope compositions of serpentinite seamounts in the Marian Forearc: Serpentinitization processes, fluid sources and sulfur metasomatism. *Earth and Planets Science Letters*, 242, 272–285.

Amundsen, H. E. F., Griffin, W. L., & O’Reilly, S. (1987). The lower crust and upper mantle beneath northwestern Spitsbergen: Evidence from xenoliths and geophysics. *Tectonophysics*, 139, 169–185.

Andres, M., Blichert-Toft, J., & Schilling, J.-G. (2002). Hafnium isotopes in basalts from the southern Mid-Atlantic Ridge from 40°S to 55°S: Discovery and Shona plume-ridge interactions and the role of recycled sediments. *Geochemistry Geophysics Geosystems*, 3(10) 8502. <https://doi.org/10.1029/2002GC000324>

Arndt, N. T., & Goldstein, S. L. (1989). An open boundary between lower continental crust and mantle: Its role in crust formation and crustal recycling. *Tectonophysics*, 161, 201–212.

Asimow, P., Dixon, J. E., & Langmuir, C. H. (2004). A hydrous melting and fractionation model for mid-ocean ridge basalts: Application to the Mid-Atlantic Ridge near the Azores. *Geochemistry Geophysics Geosystems*, 5, Q01E16. <https://doi.org/10.1029/2003GC000568>

Aubaud, C., Hauri, E. H., & Hirschmann, M. M. (2004). Hydrogen partition coefficients between nominally anhydrous minerals and basaltic melts. *Geophysical Research Letters*, 31, L20611. <https://doi.org/10.1029/2004GL021341>

Ayers, J. (1998). Trace element modeling of aqueous fluid-peridotite interaction in the mantle wedge of subduction zones. *Contributions to Mineralogy and Petrology*, 132, 390–404.

Barfod, D. N., Ballentine, C. J., Halliday, A. N., & Fitton, J. G. (1999). Noble gases in the Cameroon line and the He, Ne, and Ar isotopic compositions of high μ (HIMU) mantle. *Journal of Geophysical Research*, 104, 29509–29527.

Barnes, J. D., Sharp, Z. D., & Fischer, T. P. (2009). Chlorine isotope variations across the Izu-Bonin-Mariana arc. *Geology*, 36, 883–886.

Batiza, R., Niu, Y., & Zayac, W. C. (1990). Chemistry of seamounts near the East Pacific Rise: Implications for the geometry of sub-axial mantle flow. *Geology*, 18, 1122–1125.

Batiza, R., & Vanko, D. (1984). Petrology of young Pacific seamounts. *Journal of Geophysical Research*, 89, 11235–11260.

Benton, L. D., Ryan, J. G., & Tera, F. (2001). Boron isotope systematics of slab fluids as inferred from a serpentine seamount, Mariana forearc. *Earth and Planetary Science Letters*, 187, 273–282.

Bideau, D., & Hékinian, R. (1995). A dynamic model for generating small-scale heterogeneities in ocean floor basalts. *Journal of Geophysical Research*, 100, 10141–10162.

Bindeman, I. N., Kamenetsky, V. S., Palandri, J., & Vennemann, T. (2012). Hydrogen and oxygen isotope behaviors during variable degrees of upper mantle melting: Example from the basaltic glasses from Macquarie Island. *Chemical Geology*, 310–311, 126–136.

Blichert-Toft, J., Agranier, A., Andres, M., Kingsley, R., Schilling, J.-G., & Albarede, F. (2005). Geochemical segmentation of the Mid-Atlantic Ridge north of Iceland and ridge–hotspot interaction in the North Atlantic. *Geochemistry Geophysics Geosystems*, 6, Q01E19. <https://doi.org/10.1029/2004GC000788>

Bougault, H., Dmitriev, L., Schilling, J.-G., Sobolev, A., Joron, J. L., & Needham, H. D. (1988). Mantle heterogeneity from trace elements: MAR triple junction near 14°N. *Earth and Planetary Science Letters*, 88, 27–36.

Brenan, J. M., Shaw, H. F., Phinney, D. L., & Ryerson, F. J. (1994). Rutile-aqueous fluid partitioning of Nb, Ta, Hf, Zr, U and Th: Implications for high-field strength element depletions in island-arc basalts. *Earth and Planetary Science Letters*, 128, 327–339.

Brenan, J. M., Shaw, H., Ryerson, F., & Phinney, D. (1995). Mineral-aqueous fluid partitioning of trace elements at 900°C and 2.0 GPa: Constraints on the trace element chemistry of mantle and deep crustal fluids. *Geochimica et Cosmochimica Acta*, 59, 3331–3350. [https://doi.org/10.1016/0016-7037\(95\)00215-L](https://doi.org/10.1016/0016-7037(95)00215-L)

Bromiley, G. D., & Pawley, A. R. (2003). The stability of antigorite in the systems $\text{MgO}-\text{SiO}_2-\text{H}_2\text{O}$ (MSH) and $\text{MgO}-\text{Al}_2\text{O}_3-\text{SiO}_2-\text{H}_2\text{O}$ (MASH): The effects of Al^{3+} substitution on high-pressure stability. *American Mineralogist*, 88, 99–108.

Bromiley, G. D., & Redfern, S. A. T. (2008). The role of TiO_2 phases during melting of subduction-modified crust: Implications for deep mantle melting. *Earth and Planetary Science Letters*, 267, 301–308.

Bulanova, G. P., Walter, M. J., Smith, C. B., Kohn, S. C., Armstrong, L. S., Blundy, J., & Gobbo, L. (2010). Mineral inclusions in sublithospheric diamonds from Collier 4 kimberlite pipe, Juina, Brazil: Subducted protoliths, carbonated melts and primary kimberlite magmatism. *Contributions to Mineralogy and Petrology*, 160, 489–510.

Cai, Y., LaGatta, A., Goldstein, S. L., Langmuir, C. H., Gómez-Tuena, A., Martín-del Pozzo, A. L., & Carrasco-Núñez, G. (2014). Hafnium isotope evidence for slab melt contributions in the Central Mexican Volcanic Belt and implications for slab melting in hot and cold slab arcs. *Chemical Geology*, 377, 45–55.

Cartigny, P., Pineau, F., Aubaud, C., & Javoy, M. (2008). Towards a consistent mantle carbon flux estimate: Insights from volatile systematics ($\text{H}_2\text{O}/\text{Ce}$, δD , CO_2/Nb) in the North Atlantic mantle (14°N and 34°N). *Earth and Planetary Science Letters*, 265, 672–685.

Castillo, P. R., Klein, E., Bender, J., Langmuir, C., Shirey, S., Batiza, R., & White, W. (2000). Petrology and Sr, Nd, and Pb isotope geochemistry of mid-ocean ridge basalt glasses from the $11^\circ 45'$ to $15^\circ 00'\text{N}$ segment of the East Pacific Rise. *Geochemistry Geophysics Geosystems*, 1, 1011. <https://doi.org/10.1029/1999GC000024>

Chase, C. G. (1981). Oceanic island lead: Two-stage histories and mantle evolution. *Earth and Planetary Science Letters*, 52, 277–284.

Chaussidon, M., & Jambon, A. (1994). Boron content and isotopic composition of oceanic basalts: Geochemical and cosmochemical implications. *Earth and Planetary Science Letters*, 121, 277–291.

Chaussidon, M., & Marty, B. (1995). Primitive boron isotope composition of the mantle. *Science*, 269, 383–386.

Chaussidon, M., Sheppard, S. M. F., & Michard, A. (1991). Hydrogen, sulphur and neodymium isotope variations in the mantle beneath the EPR at $12 50'\text{N}$. *Stable Isotope Geochemistry: A Tribute to Samuel Epstein*, 3, 325.

Chauvel, C., Hofmann, A. W., & Vidal, P. (1992). HIMU-EM; the French Polynesian connection. *Earth and Planetary Science Letters*, 110, 99–119.

Chauvel, C., Lewin, E., Carpentier, M., Arndt, N. T., & Marini, J.-C. (2008). Role of recycled oceanic basalt and sediment in generating the Hf–Nd mantle array. *Nature Geoscience*, 1, 64–67.

Chauvel, C., McDonough, W., Guille, G., Maury, R., & Duncan, R. (1997). Contrasting old and young volcanism in Rurutu Island, Austral chain. *Chemical Geology*, 139, 125–143.

Cheng, Q. C., Macdougall, J. D., & Zhu, P. (1999). Isotopic constraints on the Easter Seamount Chain source. *Contributions to Mineralogy and Petrology*, 135, 225–233.

Clague, D. A., Weber, W. S., & Dixon, J. E. (1991). Picritic glasses from Hawaii. *Nature*, 353, 553–556.

Clift, P., & Vannucchi, P. (2004). Controls on tectonic accretion versus erosion in subduction zones: Implications for the origin and recycling of the continental crust. *Reviews of Geophysics*, 42, RG2001. <https://doi.org/10.1029/2003RG000127>

Clog, M., Aubaud, C., Cartigny, P., & Dosso, L. (2013). The hydrogen isotopic composition and water content of southern Pacific MORB: A reassessment of the D/H ratio of the depleted mantle reservoir. *Earth and Planetary Science Letters*, 381, 156–165.

Clog, M., Cartigny, P., & Aubaud, C. (2012). Experimental evidence for interaction of water vapor and platinum crucibles at high temperatures: Implications for volatiles from igneous rocks and minerals. *Geochimica et Cosmochimica Acta*, 83, 135–137.

Cohen, R. S., & O’nions, R. K. (1982). Identification of recycled continental material in the mantle from Sr, Nd and Pb isotope investigations. *Earth and Planetary Science Letters*, 61, 73–84.

Cooper, K. M., Eiler, J. M., Asimow, P. D., & Langmuir, C. H. (2004). Oxygen isotope evidence for the origin of enriched mantle beneath the mid-Atlantic ridge. *Earth and Planetary Science Letters*, 220, 297–316.

Cooper, L. B., Ruscito, D. M., Plank, T., Wallace, P. J., Syracuse, E. M., & Manning, C. E. (2012). Global variations in $\text{H}_2\text{O}/\text{Ce}$: 1. Slab surface temperatures beneath volcanic arcs. *Geochemistry Geophysics Geosystems*, 13, Q03024. <https://doi.org/10.1029/2011GC003902>

Craig, H., & Lupton, J. E. (1976). Primordial neon, helium and hydrogen in oceanic basalts. *Earth and Planetary Science Letters*, 31, 369–385.

Danyushevsky, L. V., Eggins, S. M., Fallon, T. J., & Christie, D. M. (2000). H_2O abundance in depleted to moderately enriched mid-ocean ridge magmas. Part I: Incompatible behaviour, implications for mantle storage, and origin of regional variations. *Journal of Petrology*, 41, 1329–1364.

Dasgupta, R., & Hirschmann, M. M. (2006). Melting in the Earth’s deep upper mantle caused by carbon dioxide. *Nature*, 440, 659–662. <https://doi.org/10.1038/nature04612>

Dasgupta, R., Hirschmann, M. M., & Smith, N. D. (2007). Partial melting experiments of peridotite + CO_2 at 3 GPa and genesis of alkalic ocean island basalts. *Journal of Petrology*, 48, 2093–2124.

Dasgupta, R., Hirschmann, M. M., & Stalker, K. (2006). Immiscible transition from carbonate-rich to silicate-rich melts in the 3 GPa melting interval of eclogite + CO_2 and genesis of silica-undersaturated ocean island lavas. *Journal of Petrology*, 47, 647–671.

Debaille, V., Trønnes, R. G., Brandon, A. D., Waught, T. E., Graham, D. W., & Lee, C.-T. (2009). Primitive off-rift basalts from Iceland and Jan Mayen: Os-isotopic evidence for a mantle source containing enriched subcontinental lithosphere. *Geochimica et Cosmochimica Acta*, 73, 3423–3449.

De Hoog, J. C. M., Taylor, B. E., & Van Bergen, M. J. (2009). Hydrogen-isotope systematics in degassing basaltic magma and application to Indonesian arc basalts. *Chemical Geology*, 266, 256–266.

Devey, C. W., Garbe-Schönberg, C.-D., Stoffers, P., Chauvel, C., & Mertz, D. F. (1994). Geochemical effects of dynamic melting beneath ridges: Reconciling major and trace element variations in Kolbeinsey (and global) mid-ocean ridge basalt. *Journal of Geophysical Research*, 99, 9077–9095.

Dixon, J. E., & Clague, D. A. (2001). Volatiles in basaltic glasses from Loihi Seamount, Hawaii: Evidence for a relatively dry plume component. *Journal of Petrology*, 42, 627–654.

Dixon, J. E., Clague, D. A., Cousens, B., Monsalve, M. L., & Uhl, J. (2008). Carbonatite and silicate melt metasomatism of the mantle surrounding the Hawaiian plume: Evidence from volatiles, trace elements, and radiogenic isotopes in rejuvenated-stage lavas from Niihau, Hawaii. *Geochemistry Geophysics Geosystems*, 9, Q09005. <https://doi.org/10.1029/2008GC002076>

Dixon, J. E., Clague, D. A., & Stolper, E. (1991). Degassing history of water, sulfur, and carbon in submarine lavas from Kilauea Volcano, Hawaii. *Journal of Geology*, 99, 371–394.

Dixon, J. E., Clague, D. A., Wallace, P., & Poreda, R. (1997). Volatiles in alkalic basalts from the North Arch Volcanic Field, Hawaii: Extensive degassing of deep submarine-erupted alkalic series lavas. *Journal of Petrology*, 38, 911–939.

Dixon, J. E., Leist, L., Langmuir, C. H., & Schilling, J.-G. (2002). Recycled dehydrated lithosphere observed in plume-influence mid-ocean ridge basalts. *Nature*, 420, 385–389.

Dixon, J. E., Stolper, E., & Delaney, J. R. (1988). Infrared spectroscopic measurements of H_2O and CO_2 contents in Juan de Fuca Ridge basaltic glasses. *Earth and Planetary Science Letters*, 90, 87–104.

Donnelly, K. E., Goldstein, S. L., Langmuir, C. H., & Spiegelman, M. (2004). Origin of enriched ocean ridge basalts and implications for mantle dynamics. *Earth and Planetary Science Letters*, 226, 347–366.

Dosso, L., Bougault, H., & Joron, J.-L. (1993). Geochemical morphology of the North Mid-Atlantic Ridge, 10° – 24°N : Trace element-isotope complementarity. *Earth and Planetary Science Letters*, 120, 443–462.

Dosso, L., Bougault, H., Langmuir, C., Bollinger, C., Bonnier, O., & Etoubleau, J. (1999). The age and distribution of mantle heterogeneity along the Mid-Atlantic Ridge (31 – 41°N). *Earth and Planetary Science Letters*, 170, 269–286.

Dosso, L., Hanan, B. B., Bougault, H., Schilling, J.-G., & Joron, J.-L. (1991). Sr-Nd-Pb geochemical morphology between 10° and 17° N on the Mid-Atlantic Ridge: A new MORB isotope signature. *Earth and Planetary Science Letters*, 106, 29–43.

Dostal, J., Cousens, B., & Dupuy, C. (1998). The incompatible element characteristics of an ancient subducted sedimentary component in ocean island basalts from French Polynesia. *Journal of Petrology*, 39, 937–952.

Douglass, J., Schilling, J.-G., & Fontignie, D. (1999). Plume-ridge interactions of the Discovery and Shona mantle plumes with the southern Mid-Atlantic Ridge (40°–55°S). *Journal of Geophysical Research*, 104, 2941–2962.

Douglass, J., Schilling, J.-G., & Kingsley, R. H. (1995). Influence of the Discovery and Shona mantle plumes on the southern Mid-Atlantic Ridge: Rare earth evidence. *Geophysical Research Letters*, 22, 2893–2896.

Douglass, J., & Schilling, J.-G. (2000). Systematics of three-component, pseudo-binary mixing lines in 2D isotope ratio space representations and implications for mantle plume-ridge interaction. *Chemical Geology*, 163, 1–23.

Dupuy, C., Barsczus, H. G., Liotard, J. M., & Dostal, J. (1988). Trace element evidence for the origin of ocean island basalts: An example from the Austral Islands (French Polynesia). *Contributions to Mineralogy and Petrology*, 98, 293–302.

Eiler, J. (2001). Oxygen isotope variations of basaltic lavas and upper mantle rocks. *Reviews in Mineralogy and Geochemistry*, 43, 319–364.

Eiler, J. (2003) (Eds.). *Inside the subduction factory, Geophysical Monograph Series* (Vol. 138). Washington, DC: American Geophysical Union.

Eisele, J., Sharma, M., Galer, S. J. G., Blichert-Toft, J., Devey, C. W., & Hofmann, A. W. (2002). The role of sediment recycling in EM-1 inferred from Os, Pb, Hf, Nd, Sr isotope and trace element systematics of the Pitcairn hotspot. *Earth and Planetary Science Letters*, 196, 197–212.

Ellam, R. M., & Stuart, F. M. (2000). The sub-lithospheric source of North Atlantic basalts: Evidence for, and significance of, a common end-member. *Journal of Petrology*, 41, 919–932.

Elliott, T., Thomas, A., Jeffcoate, A., & Niu, Y. (2006). Lithium isotope evidence for subduction-enriched mantle in the source of mid-ocean-ridge basalts. *Nature*, 443, 565–568. <https://doi.org/10.1038/nature05144>

Engel, A. E. J., Engel, C. G., & Havens, R. G. (1965). Chemical characteristics of oceanic basalts and upper mantle. *Geological Society of American Bulletin*, 76, 719–734.

Faccenda, M., Gerya, T. V., & Burlini, L. (2009). Deep slab hydration induced by bending-related variations in tectonic pressure. *Nature Geoscience*, 2, 790–793. <https://doi.org/10.1038/NGEO656>

Farley, K. A., Natland, J. H., & Craig, H. (1992). Binary mixing of enriched and undegassed (primitive?) mantle components (He, Sr, Nd, Pb) in Samoan lavas. *Earth and Planetary Science Letters*, 111, 183–199.

Farnetani, C. G., Legras, B., & Tackley, P. J. (2002). Mixing and deformations in mantle plumes. *Earth and Planetary Science Letters*, 196, 1–15.

Fitton, J. G. (2007). The OIB paradox. In G. R. Foulger & D. M. Jurdy, (Eds.), *Plates, plumes, and planetary processes* (Vol. 430, pp. 387–412). Geological Society of America.

Foley, S. F., Barth, M. G., & Jenner, G. A. (2000). Rutile/melt partition coefficients for trace elements and an assessment of the influence of rutile on the trace element characteristics of subduction zone magmas. *Geochimica et Cosmochimica Acta*, 64, 933–938.

Fontignie, D., & Schilling, J.-G. (1991). $^{87}\text{Sr}/^{86}\text{Sr}$ and REE variations along the Easter Microplate boundaries (south Pacific): Application of multivariate statistical analyses to ridge segmentation. *Chemical Geology*, 89, 209–241.

Gale, A., Dalton, C. A., Langmuir, C. H., Su, Y., & Schilling, J.-G. (2013a). The mean composition of ocean ridge basalts. *Geochemistry Geophysics Geosystems*, 14, 489–518. <https://doi.org/10.1029/2012GC004334>

Gale, A., Laubier, M., Escrig, S., & Langmuir, C. H. (2013b). Constraints on melting processes and plume-ridge interaction from comprehensive study of the FAMOUS and North Famous segments, Mid-Atlantic Ridge. *Earth and Planetary Science Letters*, 365, 209–220. <https://doi.org/10.1016/j.epsl.2013.01.022>

Galer, S. J. G., & O'Nions, R. K. (1986). Magmagenesis and the mapping of chemical and isotopic variations in the mantle. *Chemical Geology*, 56, 45–61.

Geldmacher, J., Hoernle, K., Klügel, A., van den Bogaard, P., & Bindeman, I. (2008). Geochemistry of a new enriched mantle type locality in the northern hemisphere: Implications for the origin of the EM-I source. *Earth and Planetary Science Letters*, 265, 167–182.

Géli, L., Renard, V., & Rommevaux, C. (1994). Ocean crust formation processes at very slow spreading centers: A model for the Mohns Ridge, near 72°N, based on magnetic, gravity, and seismic data. *Journal of Geophysical Research*, 99, 2995–3013.

Gerbode, C., & Dasgupta, R. (2010). Carbonate-fluxed melting of MORB-like pyroxenite at 2.9 GPa and genesis of HIMU ocean island basalts. *Journal of Petrology*, 51, 2067–2088.

Gerlach, T. M. (1991). Comment on "Mid-ocean ridge popping rocks: Implications for degassing at ridge crest" by P. Sarda and D. Graham. *Earth and Planetary Science Letters*, 105, 566–567.

Graham, C. M., Harmon, R. S., & Sheppard, S. M. F. (1984). Experimental hydrogen isotope studies: Hydrogen isotope exchange between amphibole and water. *American Mineralogist*, 69, 128–138.

Grassi, D., & Schmidt, M. W. (2011a). Melting of carbonated pelites at 8–13 GPa: Generating K-rich carbonatites for mantle metasomatism. *Contributions to Mineralogy and Petrology*, 162, 169–191.

Grassi, D., & Schmidt, M. W. (2011b). The melting of carbonated pelites from 70 to 700 km depth. *Journal of Petrology*, 52, 765–789.

Grassi, D., Schmidt, M. W., & Günther, D. (2012). Element partitioning during carbonated pelite melting at 8, 13 and 22 GPa and the sediment signature in the EM mantle components. *Earth and Planetary Science Letters*, 327–328, 84–96.

Gurenko, A. A., & Chaussidon, M. (1997). Boron concentrations and isotopic compositions of the Icelandic mantle: Evidence from glass inclusions in olivine. *Chemical Geology*, 135, 21–34.

Gurenko, A. A., & Kamenetsky, V. S. (2011). Boron isotopic composition of olivine-hosted melt inclusions from Gorgona komatiites, Colombia: New evidence supporting wet komatiite origin. *Earth and Planetary Science Letters*, 312, 201–212.

Haase, K. M., Hartmann, M., & Wallrabe-Adams, H.-J. (1996). The geochemistry of ashes from Vesterisbanken Seamount, Greenland Basin: Implications for the evolution of an alkaline volcano. *Journal of Volcanology and Geothermal Research*, 70, 1–19.

Halliday, A. N., Dickin, A. P., Fallick, A. E., & Fitton, J. G. (1988). Mantle dynamics: A Nd, Sr, Pb, and O isotopic study of the Cameroon Line Volcanic Chain. *Journal of Petrology*, 29, 181–211.

Halliday, A. N., Lee, D. C., Tommasini, S., Davies, G. R., Paslick, C. T., Fitton, J. G., & James, D. E. (1995). Incompatible trace elements in OIB and MORB and source enrichments in the sub-oceanic mantle. *Earth and Planetary Science Letters*, 133, 379–395.

Hamelin, C., Dosso, L., Hanan, B., Barrat, J.-A., & Ondréas, H. (2010). Sr-Nd-Hf isotopes along the Pacific Antarctic Ridge from 41 to 53°S. *Geophysical Research Letters*, 37, L10303. <https://doi.org/10.1029/2010GL042979>

Hamelin, C., Dosso, L., Hanan, B. B., Moreira, M., Kositsky, A. P., & Thomas, M. Y. (2011). Geochemical portrait of the Pacific Ridge: New isotopic data and statistical techniques. *Earth and Planetary Science Letters*, 302, 154–162.

Hanan, B. B., Blichert-Toft, J., Hermond, C., Sayit, K., Agranier, A., Graham, D. W., & Albarede, F. (2013). Pb and Hf isotope variations along the Southeast Indian Ridge and the dynamic distribution of MORB source domains in the upper mantle. *Earth and Planetary Science Letters*, 375, 196–208.

Hanan, B. B., & Graham, D. W. (1996). Lead and helium isotope evidence from oceanic basalts for a common deep source of mantle plumes. *Science*, 272, 991–995.

Hanan, B. B., & Schilling, J.-G. (1989). Easter microplate evolution: Pb-isotope evidence. *Journal of Geophysical Research*, 94, 7432–7448. 1989.

Hanyu, T., & Kaneoka, I. (1997). The uniform and low ${}^3\text{He}/{}^4\text{He}$ ratios of HIMU basalts as evidence for their origin as recycled materials. *Nature*, 390, 273–276.

Hanyu, T., Tatsumi, Y., & Kimura, J.-I. (2011). Constraints on the origin of the HIMU reservoir from He-Ne-Ar isotope systematics. *Earth and Planetary Science Letters*, 307, 377–386.

Hart, S. (1988). Heterogeneous mantle domains: Signatures, genesis and mixing chronologies. *Earth and Planetary Science Letters*, 90, 273–296.

Hart, S. R., Hauri, E. H., Oschmann, L. A., & Whitehead, J. A. (1992). Mantle plumes and entrainment: The isotopic evidence. *Science*, 256, 517–520.

Harte, B. (2010). Diamond formation in the deep mantle: The record of mineral inclusions and their distribution in relation to mantle dehydration zones. *Mineralogical Magazine*, 74, 189–215.

Hauri, E. H. (2002). SIMS analysis of volatiles in silicate glasses, 2: Isotopes and abundances in Hawaiian melt inclusions. *Chemical Geology*, 183, 115–141.

Hauri, E. H., Gaetani, G. A., & Green, T. H. (2006). Partitioning of water during melting of the Earth's upper mantle at H_2O -undersaturated conditions. *Earth and Planetary Science Letters*, 248, 715–734.

Hauri, E. H., & Hart, S. R. (1993). Re-Os isotope systematics of HIMU and EMII oceanic basalts from the south Pacific Ocean. *Earth and Planetary Science Letters*, 114, 353–371.

Hauri, E. H., Whitehead, J. A., & Hart, S. R. (1994). Fluid dynamic and geochemical aspects of entrainment in mantle plumes. *Journal Geophysical Research*, 99, 24275–24300.

Hawkesworth, C. J., Mi, J., Norry, J. C., Roddick, R., & Vollmer, (1979). ${}^{143}\text{Nd}/{}^{144}\text{Nd}$ and ${}^{87}\text{Sr}/{}^{86}\text{Sr}$ ratios from the Azores and their significance in LIL-element enriched mantle. *Nature*, 280, 28–31.

Hekinian, R., Pineau, F., Shlobobreeva, S., Bideau, D., Gracia, E., & Javoy, M. (2000). Deep sea explosive activity on the Mid-Atlantic Ridge near 34°50'N: Magma composition, vesicularity and volatile content. *Journal of Volcanology and Geothermal Research*, 98, 49–77.

Hekinian, R., Thompson, G., & Bideau, D. (1989). Axial and off-axial heterogeneity of basaltic rocks from the East Pacific Rise at 12°35'N–12°51'N and 11°26'N–11°30'N. *Journal Geophysical Research*, 94, 12437–17463.

Hermond, C., Devey, C. W., & Chauvel, C. (1994). Source compositions and melting processes in the Society and Austral plumes (South Pacific Ocean): Element and isotope (Sr, Nd, Pb, Th) geochemistry. *Chemical Geology*, 115, 7–45.

Hermann, J., & Rubatto, D. (2009). Accessory phase control on the trace element signature of sediment melts in subduction zones. *Chemical Geology*, 265, 512–526. <https://doi.org/10.1016/j.chemgeo.2009.05.018>

Hermann, J., & Spandler, C. (2008). Sediment melts at sub-arc depths: An experimental study. *Journal of Petrology*, 49, 717–740. <https://doi.org/10.1093/petrology/egm073>

Hilairet, N., Daniel, I., & Reynard, B. (2006). Equation of state of antigorite, stability field of serpentines, and seismicity in subduction zones. *Geophysical Research Letters*, 33, L02302. <https://doi.org/10.1029/2005GL024728>

Hochstaedter, A. G., Gill, J. B., Kusakabe, M., Newman, S., Pringle, M., Taylor, B., & Fryer, P. (1990). Volcanism in the Sumisu Rift, I. Major element, volatile, and stable isotope geochemistry. *Earth and Planetary Science Letters*, 100, 179–194.

Hofmann, A. W. (1988). Chemical differentiation of the Earth: The relationship between mantle, continental crust, and oceanic crust. *Earth and Planetary Science Letters*, 90, 297–314.

Hofmann, A. W. (1997). Mantle geochemistry: The message from oceanic volcanism. *Nature*, 385, 219–229.

Hofmann, A. W. (2003). Sampling mantle heterogeneity through oceanic basalts: Isotopes and trace elements. In R. W. Carlson, H. D. Holland, & K. K. Turekian (Eds.), *Treatise on geochemistry: The mantle and core* (pp. 61–101). New York, NY: Elsevier.

Hofmann, A. W. (2014). Sampling mantle heterogeneity through oceanic basalts: Isotopes and trace elements. In R. W. Carlson (Ed.), *Treatise on geochemistry, Reference Module in Earth Systems and Environmental Sciences, Vol. 3: The Mantle and Core* (2nd ed., pp. 67–101). Oxford, UK: Elsevier-Pergamon.

Hofmann, A. W., & White, W. M. (1982). Mantle plumes from ancient oceanic-crust. *Earth and Planetary Science Letters*, 57, 421–436.

Honma, H., Kusakabe, M., Kagami, H., Iizumi, S., Sakai, H., Kodama, Y., & Kimura, M. (1991). Major and trace element chemistry and D/H, ${}^{18}\text{O}/{}^{16}\text{O}$, ${}^{87}\text{Sr}/{}^{86}\text{Sr}$ and ${}^{143}\text{Nd}/{}^{144}\text{Nd}$ ratios of rocks from the spreading center of the Okinawa Trough, a marginal back-arc basin. *Geochemistry Journal*, 25, 121–136.

Husker, A., & Davis, P. M. (2009). Tomography and thermal state of the Cocos plate subduction beneath Mexico City. *Journal Geophysical Research*, 114, B04306. <https://doi.org/10.1029/2008JB006039>

Ihinger, P. D., Hervig, R. L., & McMillan, P. F. (1994). Analytical methods for volatiles in glasses. *Reviews in Mineralogy: Volatiles in Magmas*, 30, 67–121.

Ionov, D., Bodinier, J.-L., Mukasa, S., & Zanetti, A. (2002). Mechanisms and sources of mantle metasomatism: Major and trace element compositions of peridotite xenoliths from Spitsbergen in the context of numerical modeling. *Journal of Petrology*, 43, 2219–2259.

Ionov, D., Dupuy, C., O'Reilly, S. Y., Kopylova, M. G., & Genshaft, Y. S. (1993). Carbonated peridotite xenoliths from Spitsbergen: Implications for trace element signature of mantle carbonate metasomatism. *Earth and Planetary Science Letters*, 119, 283–297.

Ishikawa, T., & Nakamura, E. (1993). Boron-isotope systematics of Marine sediments. *Earth and Planetary Science Letters*, 117, 567–580.

Ivandic, M., Grevemeyer, I., Bialas, J., & Petersen, C. J. (2010). Serpentization in the trench-outer rise region offshore of Nicaragua: Constraints from seismic refraction and wide-angle data. *Geophysical Journal of International*, 180, 1253–1264. <https://doi.org/10.1111/j.1365-246X.2009.04474.x>

Izraeli, E. S., Harris, J. W., & Navon, O. (2001). Brine inclusions in diamonds: A new upper mantle fluid. *Earth and Planetary Science Letters*, 187, 323–332.

Jackson, M. G., & Dasgupta, R. (2008). Compositions of HIMU, EM1, and EM2 from global trends between radiogenic isotopes and major elements in ocean island basalts. *Earth and Planetary Science Letters*, 276, 175–186.

Jackson, M. G., Hart, S. R., Koppers, A. A. P., Staudigel, H., Konter, J., Blusztajn, J., ... Russel, J. A. (2007). The return of subducted continental crust in Samoan lavas. *Nature*, 448, 684–687.

Jambon, A., & Zimmermann, J. L. (1990). Water in oceanic basalts: Evidence for dehydration of recycled crust. *Earth and Planetary Science Letters*, 101, 323–331.

Johnson, M. C., & Plank, T. (1999). Dehydration and melting experiments constrain the fate of subducted sediments. *Geochemistry Geophysics Geosystems*, 1(12), 1007. <https://doi.org/10.1029/1999GC000014>

Kamenetsky, V. S., Everard, J. L., Crawford, A. J., Varne, R., Eggins, S. M., & Lanyon, R. (2000). Enriched end-member of primitive MORB melts: Petrology and geochemistry of glasses from Macquarie Island (SW Pacific). *Journal of Petrology*, 41, 411–430.

Katayama, I., Hirose, K., Yurimoto, H., & Nakashima, S. (2003). Water solubility in majoritic garnet in subducting oceanic crust. *Geophysical Research Letters*, 30(22), 2155. <https://doi.org/10.1029/2003GL018127>

Kay, R. W., & Kay, S. M. (1993). Delamination and delamination magmatism. *Tectonophysics*, 219, 177–189.

Kelemen, P. B., Dick, H. J. B., & Quick, J. E. (1992). Formation of harzburgite by pervasive melt/rock reaction in the upper mantle. *Nature*, 358, 635–641.

Kelley, K. A., Kingsley, R., & Schilling, J.-G. (2013). Composition of plume-influenced mid-ocean ridge lavas and glasses from the Mid-Atlantic Ridge, East Pacific Rise, Galápagos Spreading Center, and Gulf of Aden. *Geochemistry Geophysics Geosystems*, 14, 223–242. <https://doi.org/10.1029/2012GC004415>

Kempe, D. R. C., & Schilling, J.-G. (1974). Discovery Tablemount basalt: Petrology and geochemistry. *Contributions to Mineralogy and Petrology*, 44, 101–115.

Kendrick, M. A., Hémond, C., Kamenetsky, V., Danyushevsky, S. L., Devey, C. W., Rodemann, T., ... Perfit, M. R. (2017). Seawater cycled throughout Earth's mantle in partially serpentinized lithosphere. *Nature Geoscience*, 10, 222–228. <https://doi.org/10.1038/NGEO2902>

Keppler, H. (1996). Constraints from partitioning experiments on the composition of subduction-zone fluids. *Nature*, 380, 237–240. <https://doi.org/10.1038/380237a0>

Kessel, R., Schmidt, M. W., Pettke, T., & Ulmer, P. (2005). The trace element signature of subduction zone fluids, melts, and supercritical liquids at 120–180 km depth. *Nature*, 437, 724–727. <https://doi.org/10.1038/nature03971>

Kimura, J.-I., Hacker, B. R., van Keeken, P. E., Kawabata, H., Yoshida, T., & Stern, R. J. (2009). Arc Basalt Simulator version 2, a simulation for slab dehydration and fluid-fluxed mantle melting for arc basalts: Modeling scheme and application. *Geochemistry Geophysics Geosystems*, 10, Q09004. <https://doi.org/10.1029/2008GC002217>

Kincaid, C., & Sacks, I. S. (1997). Thermal and dynamical evolution of the upper mantle in subduction zones. *Journal Geophysical Research*, 102, 12295–12315.

Kingsley, R. H., & Schilling, J.-G. (1998). Plume-ridge interaction in the Easter-Salas y Gomez seamount chain: Easter microplate system: Pb isotope evidence. *Journal Geophysical Research*, 103, 24159–24177.

Kingsley, R. H., Schilling, J.-G., Dixon, J. E., Swart, P., Poreda, R., & Simons, K. (2002). D/H ratios in basalt glasses from the Salas y Gomez mantle plume interacting with the East Pacific Rise: Water from old D-rich recycled crust or primordial water from the lower mantle? *Geochemistry Geophysics Geosystems*, 3(4), 1025. <https://doi.org/10.1029/2001GC000199>

Kiseeva, E. S., Yaxley, G. M., Hermann, J., Litasov, K. D., Rosenthal, A., & Kamenetsky, V. S. (2012). An experimental study of carbonated eclogite at 3.5–5.5 GPa: Implications for silicate and carbonate metasomatism in the cratonic mantle. *Journal of Petrology*, 53, 727–759.

Klemme, S., Blundy, J. D., & Wood, B. J. (2002). Experimental constraints on major and trace element partitioning during partial melting of eclogite. *Geochimica et Cosmochimica Acta*, 66, 3109–3123.

Klemme, S., Prowatke, S., Hametner, K., & Günther, D. (2005). Partitioning of trace elements between rutile and silicate melts: Implications for subduction zones. *Geochimica et Cosmochimica Acta*, 69, 2361–2371.

Klein-BenDavid, O., Izraeli, E. S., Hauri, E., & Navon, O. (2004). Mantle-fluid evolution: A tale of one diamond. *Lithos*, 77, 243–253.

Klein-BenDavid, O., Izraeli, E. S., Hauri, E., & Navon, O. (2007). Fluid inclusions in diamonds from the Diavik mine, Canada and the evolution of diamond-forming fluids. *Geochimica et Cosmochimica Acta*, 71, 723–744.

Kogiso, T., Tatsumi, Y., & Nakano, S. (1997). Trace element transport during dehydration processes in the subducted crust: 1. Experiments and implications for the origin of ocean island basalts. *Earth and Planetary Science Letters*, 148, 193–205.

Krienitz, M.-S., Garbe-Schönberg, D.-D., Romer, R. L., Meixner, A., Haase, K. M., & Stroncik, N. A. (2012). Lithium isotope variations in ocean island basalts—Implications for the development of mantle heterogeneity. *Journal of Petrology*, 53, 2333–2347. <https://doi.org/10.1093/petrology/egs052>

Kyser, T. K., & O'Neil, J. R. (1984). Hydrogen isotope systematics of submarine basalts. *Geochimica et Cosmochimica Acta*, 48, 2123–2133.

Lane, N. (2015). *The vital question: Energy, evolution, and the origin of complex life* (360 p.). New York, NY: WW Norton.

Langmuir, C. H., Bender, J. F., & Batiza, R. (1986). Petrologic and tectonic segmentation of the East Pacific Rise between 5°30'–14°30'N. *Nature*, 322, 422–429.

Langmuir, C. H., Klinkhammer, G. G., & Bougault, H. (1992). *Cruise Report: Evaluation of the relationships among segmentation, hydrothermal activity and petrological diversity on the Mid-Atlantic Ridge (FAZAR)* (Tech. Rep. LDEO-92-3). Palisades, NY: Lamont-Doherty Earth Observatory, Columbia University.

Lassiter, J. C., & Hauri, E. H. (1998). Osmium-isotope variations in Hawaiian lavas: Evidence for recycled oceanic lithosphere in the Hawaiian plume. *Earth and Planetary Science Letters*, 164, 483–496.

Le Roex, A. P., Dick, H. J. B., Gulen, L., Reid, A. M., & Erlank, A. J. (1987). Local and regional heterogeneity in MORB from the Mid-Atlantic Ridge between 54.5°S and 51°S: Evidence for geochemical enrichment. *Geochimica et Cosmochimica Acta*, 51, 541–555.

Le Roux, P. J., Shirey, S. B., Benton, L., Hauri, E. H., & Mock, T. D. (2004). In situ, multiple-multiplier, laser ablation ICP-MS measurement of boron isotopic composition (d11B) at the nanogram level. *Chemical Geology*, 203, 123–138.

Le Roux, P. J., Shirey, S. B., Hauri, E. H., Perfit, M. R., & Bender, J. F. (2006). The effects of variable sources, processes and contaminants on the composition of northern EPR MORB (8–10°N and 12–14°N): Evidence from volatiles (H₂O, CO₂, S) and halogens (F, Cl). *Earth and Planetary Science Letters*, 251, 209–231.

Li, H.-Y., Zhou, Z., Tyan, J. G., Wei, G.-J., & Xu, Y.-G. (2016). Boron isotopes reveal multiple metasomatic events in the mantle beneath the eastern North China Craton. *Geochimica et Cosmochimica Acta*, 194, 77–90. <https://doi.org/10.1016/j.gca.2016.08.027>

Lin, S.-C., & van Keeken, P. E. (2006). Deformation, stirring and material transport in thermochemical plumes. *Geophysical Research Letters*, 33, L20306. <https://doi.org/10.1029/2006GL027037>

Magna, T., Wiechert, U., Stuart, F. M., Halliday, A. N., & Harrison, D. (2011). Combined Li-He isotopes in Iceland and Jan Mayen basalts and constraints on the nature of the North Atlantic mantle. *Geochimica et Cosmochimica Acta*, 75, 922–936.

Martin, E., Bindeman, I. N., Balan, E., Palandri, J., Seligman, A., & Villemant, B. (2017). Hydrogen isotope determination by TC/EA technique in application to volcanic glass as a window into secondary hydration. *Journal of Volcanology and Geothermal Research*. <https://doi.org/10.1016/j.jvolgeores.2017.10.013>

Martin, C., Flores, K. E., & Harlow, G. E. (2016). Boron isotopic discrimination for subduction-related serpentinites. *Geology*, 44, 899–902. <https://doi.org/10.1130/G38102.1>

Marty, B., Sano, Y., & France-Lanord, C. (2001). Water-saturated oceanic lavas from the Manus Basin: Volatile behavior during assimilation-fractional crystallization-degassing (AFCD). *Journal of Volcanology and Geothermal Research*, 108, 1–10.

McCulloch, M. T., & Gamble, J. A. (1991). Geochemical and geodynamical constraints on subduction zone magmatism. *Earth and Planetary Science Letters*, 102, 358–374.

McDonough, W. F. (1990). Constraints on the composition of the continental lithospheric mantle. *Earth and Planetary Science Letters*, 101, 1–18.

McKenzie, D., & O'Nions, R. K. (1983). Mantle reservoirs and ocean island basalts. *Nature*, 301, 229–231.

McKenzie, D., & O'Nions, R. K. (1995). The source regions of ocean island basalts. *Journal of Petrology*, 36, 133–159.

Melson, W. G., Vallier, T., Wright, T. L., Byerly, G., & Nelen, J. (1976). Chemical diversity of abyssal volcanic glass erupted along sea-floor spreading centers. *Journal Geophysical Research*, 79, 351–368.

Mertz, D. F., Devey, C. W., Todt, W., Stoffers, P., & Hofmann, A. W. (1991). Sr-Nd-Pb isotope evidence against plume-asthenosphere mixing north of Iceland. *Earth and Planetary Science Letters*, 107, 243–255.

Mertz, D. F., & Haase, K. M. (1997). The radiogenic isotope composition of the high-latitude North Atlantic mantle. *Geology*, 25, 411–414.

Mibe, K., Kanzaki, M., Kawamoto, T., Matsukage, K. N., Fei, Y., & Ono, S. (2007). Second critical endpoint in the peridotite-H₂O system. *Journal Geophysical Research*, 112, B03201. <https://doi.org/10.1029/2005JB004125>

Mibe, K., Kawamoto, T., Matsukage, K. N., Fei, Y., & Ono, S. (2011). Slab melting versus slab dehydration in subduction-zone magmatism. *Proceedings of National Academy of Sciences of the United States of America*, 108, 8177–8182. <https://doi.org/10.1073/pnas.1010968108>

Michael, P. J. (1988). The concentration, behavior and storage of H₂O in the suboceanic upper mantle: Implications for mantle metasomatism. *Geochimica et Cosmochimica Acta*, 52, 555–566.

Michael, P. J. (1995). Regionally distinctive sources of depleted MORB: Evidence from trace elements and H₂O. *Earth and Planetary Science Letters*, 131, 301–320.

Michael, P. J., & Graham, D. W. (2015). The behavior and concentration of CO₂ in the suboceanic mantle: Inferences from undegassed ocean ridge and ocean island basalts. *Lithos*, 236–237, 338–351.

Moreira, M., & Kurz, M. D. (2001). Subducted oceanic lithosphere and the origin of 'high μ ' basalt helium isotopic signature. *Earth and Planetary Science Letters*, 189, 49–57.

Moriguti, T., & Nakamura, E. (1998). High-yield lithium separation and the precise isotopic analysis for natural rock and aqueous samples. *Chemical Geology*, 145, 91–104.

Navon, O., Hutcheon, I. D., Rossman, G. R., & Wasserburg, G. L. (1988). Mantle-derived fluids in diamond micro-inclusions. *Nature*, 335, 784–789.

Neumann, E.-G., & Schilling, J.-G. (1984). Petrology of basalts from the Mohns-Knipovich Ridge the Norwegian-Greenland Sea. *Contributions to Mineralogy and Petrology*, 85, 209–223.

Newman, S., Epstein, S., & Stolper, E. (1988). Water, carbon dioxide, and hydrogen isotopes in glasses from the ca. 1340 A. D. eruption of the Mono Craters, California: Constraints on degassing phenomena and initial volatile content. *Journal of Volcanology and Geothermal Research*, 35, 75–96.

Nishio, Y., & Nakai, S. (2002). Accurate and precise lithium isotopic determinations of igneous rock samples using multi-collector inductively coupled plasma mass spectrometry. *Analytica Chimica Acta*, 456, 271–281.

Nishio, Y., Nakai, S., Kogiso, T., & Barsczus, H. G. (2005). Lithium, strontium, and neodymium isotopic compositions of oceanic island basalts in the Polynesian region: constraints on a Polynesian HIMU origin. *Geochemical Journal*, 39, 91–103.

Niu, Y., & Batiza, R. (1997). Trace element evidence from seamounts for recycled oceanic crust in the Eastern Pacific mantle. *Earth and Planetary Science Letters*, 148, 471–483.

Niu, Y., Bideau, D., Hékinian, R., & Batiza, R. (2001). Mantle compositional control on the extent of mantle melting, crust production, gravity anomaly, ridge morphology, and ridge segmentation: A case study at the Mid-Atlantic Ridge 33–35°N. *Earth and Planetary Science Letters*, 186, 383–399.

Niu, Y., Collerson, K. D., Batiza, R., Wendt, J. I., & Regelous, M. (1999). Origin of enriched-type mid-ocean ridge basalt at ridges far from mantle plumes: The East Pacific Rise at 11°20'N. *Journal Geophysical Research*, 104, 7067–7087.

Niu, Y., & O'Hara, M. J. (2003). Origin of ocean island basalts: A new perspective from petrology, geochemistry and mineral physics considerations. *Journal Geophysical Research*, 108(B4), 2209. <https://doi.org/10.1029/2002JB002048>

Niu, Y., Regelous, M., Wendt, J. I., Batiza, R., & O'Hara, M. J. (2002). Geochemistry of near-EPR seamounts: Importance of source vs. process and the origin of the enriched mantle component. *Earth and Planetary Science Letters*, 199, 327–345.

Okamoto, K., & Maruyama, S. (2004). The eclogite-garnetite transformation in the MORB + H₂O system. *Physics of the Earth and Planetary Interiors*, 146, 283–296.

O'Leary, J., Kitchen, E. M., & Eiler, J. (2002). Hydrogen isotope geochemistry of Mariana trough lavas. *Eos Transactions American Geophysical Union*, 83(47), T72A-1242.

O'Reilly, S. Y., & Griffin, W. L. (2012). Lecture Notes in Earth System Sciences. In D. Harlov & H. Austrheim (Eds.), *Metasomatism and the chemical transformation of rock: The role of fluids in terrestrial and extraterrestrial processes* (pp. 417–533). Springer Science & Business Media: Berlin, Germany.

Palacz, Z. A., & Saunders, A. D. (1986). Coupled trace element and isotope enrichment in the Cook-Austral-Smoz islands, southwest Pacific. *Earth and Planetary Science Letters*, 79, 270–280.

Pan, Y., & Batiza, R. (1998). Major element chemistry of volcanic glasses from the Easter Seamount Chain: Constraints on melting conditions in the plume channel. *Journal Geophysical Research*, 103, 5287–5304.

Peacock, S. M. (1996). Thermal and petrologic structure of subduction zones. In G. E. Bebout, D. W. Scholl, S. H. Kirby & J. P. Platt (Eds.), *Subduction top to bottom*. Washington, DC: American Geophysical Union. <https://doi.org/10.1029/GM096p0119>

Peacock, S. M. (2001). Are the lower planes of double seismic zones caused by serpentine dehydration in subducting oceanic mantle? *Geology*, 29, 299–302.

Peacock, S. M., & Wang, K. (1999). Seismic consequences of warm versus cool subduction metamorphism: Examples from southwest and north-east Japan. *Science*, 286, 937–939. <https://doi.org/10.1126/science.286.5441.937>

Perfit, M. R., Fornari, D. J., Ridley, W. I., Smith, M. C., Bender, J. F., Langmuir, C. H., & Haymon, R. M. (1994). Small-scale spatial and temporal variations in mid-ocean ridge crest magmatic processes. *Geology*, 22, 375–379.

Pineau, F., & Javoy, M. (1994). Strong degassing at ridge crests: The behaviour of dissolved carbon and water in basalt glasses at 14°N, Mid-Atlantic Ridge. *Earth and Planetary Science Letters*, 123, 179–198.

Pineau, F., Shilobreeva, S., Hékinian, R., Bideau, D., & Javoy, M. (2004). Deep-sea explosive activity on the Mid-Atlantic Ridge near 34 degrees 50'N: A stable isotope (C, H, O) study. *Chemical Geology*, 211, 159–175.

Pineau, F., Shilobreeva, S., Kadik, A., & Javoy, M. (1998). Water solubility and D/H fractionation in the system basaltic andesite-H₂O at 1250°C and between 0.5 and 3 kbars. *Chemical Geology*, 147, 173–184.

Pistiner, J. S., & Henderson, G. M. (2003). Lithium-isotope fractionation during continental weathering processes. *Earth and Planetary Science Letters*, 214, 327–339.

Plank, T., Cooper, L. B., & Manning, C. E. (2009). Emerging geothermometers for estimating slab surface temperatures. *Nature Geoscience*, 2, 611–615. <https://doi.org/10.1038/ngeo614>

Plank, T., & Langmuir, C. H. (1998). The chemical composition of subducting sediment and its consequences for the crust and mantle. *Chemical Geology*, 145, 325–394.

Poli, S., & Schmidt, M. W. (2002). Petrology of subducted slabs. *Annual Review of Earth and Planetary Sciences*, 30, 207–235.

Poreda, R. (1985). Helium-3 and deuterium in back-arc basalts: Lau Basin and the Mariana Trough. *Earth and Planetary Science Letters*, 73, 244–254.

Poreda, R., Schilling, J.-G., & Craig, H. (1986). Helium and hydrogen isotopes in ocean-ridge basalts north and south of Iceland. *Earth and Planetary Science Letters*, 78, 11–17.

Qi, H., Coplen, T. B., Olack, G. A., & Vennemann, T. W. (2014). Caution on the use of NBS 30 biotite for hydrogen-isotope measurements with on-line high-temperature conversion systems. *Rapid Communications in Mass Spectrometry*, 28, 1987–1994. <https://doi.org/10.1002/rcm.6983>

Raga, S., Davies, R. M., Griffin, W. L., Jackson, S., & O'reilly, S. Y. (2003). Trace element analysis of diamond by LAM ICPMS: Preliminary results. Paper presented at 8th International Kimberlite Conference, Extended Abstracts, Victoria, Canada.

Ranero, C. R., Phipps Morgan, J., & Reichert, C. (2003). Bending-related faulting and mantle serpentinization at the Middle America trench. *Nature*, 425, 367–373.

Ranero, C. R., & Sallares, V. (2004). Geophysical evidence for hydration of the crust and mantle of the Nazca plate during bending at the North Chile trench. *Geology*, 32, 549–554.

Rehkämper, M., & Hofmann, A. W. (1997). Recycled ocean crust and sediment in Indian Ocean MORB. *Earth and Planetary Science Letters*, 147, 93–106.

Reynolds, J. R., Langmuir, C. H., Bender, J. F., Kastens, K. A., & Ryan, W. B. F. (1992). Spatial and temporal variability in the geochemistry of basalt from the East Pacific Rise. *Nature*, 359, 493–499.

Reynolds, J. R., & Langmuir, C. H. (2000). Identification and implications of off-axis lava flows around the East Pacific Rise. *Geochemistry Geophysics Geosystems*, 1, 1019. <https://doi.org/10.1029/1999GC000033>

Rideout, M. L., & Schilling, J.-G. (1985). Rare-earth elements, $^{87}\text{Sr}/^{86}\text{Sr}$, and $^{143}\text{Nd}/^{144}\text{Nd}$ mantle source variations. *Initial Report of Deep Sea Drilling Project*, 82, 483–496.

Roden, M. F., Hart, S. R., Frey, F. A., & Melson, W. G. (1984). Sr, Nd and Pb isotopic and REE geochemistry of St. Paul's Rocks: The metamorphic and metasomatic development of an alkali basalt mantle source. *Contributions to Mineralogy and Petrology*, 85, 376–390.

Roy-Barman, M., & Allégre, C. J. (1995). $^{187}\text{Os}/^{186}\text{Os}$ in oceanic island basalts: Tracing oceanic crust recycling in the mantle. *Earth and Planetary Science Letters*, 129, 145–161.

Rüpke, L. H., Morgan, J. P., Hort, M., & Connolly, J. A. D. (2002). Are the regional variations in Central American arc lavas due to basaltic versus peridotitic slab sources of fluids? *Geology*, 30, 1035–1038.

Ruscutto, D. M., Wallace, P. J., Cooper, L. B., & Plank, T. (2012) Global variations in $\text{H}_2\text{O}/\text{Ce}$: 2. Relationships to arc magma geochemistry and volatile fluxes. *Geochemistry Geophysics Geosystems*, 13, Q03025. <https://doi.org/10.1029/2011GC003887>

Ruscutto, D. M., Wallace, P. J., Johnson, E. R., Kent, A. J. R., & Bindeman, I. N. (2010). Volatile contents of mafic magmas from cinder cones in the Central Oregon High Cascades: Implications for magma formation and mantle conditions in a hot arc. *Earth and Planetary Science Letters*, 298, 153–161.

Ryan, J. G., & Chauvel, C. (2014). The subduction-zone filter and the impact of recycled materials on the evolution of the mantle. In *Treatise on Geochemistry* (2nd ed., Vol. 3, pp. 479–508). Elsevier Science. <https://doi.org/10.1016/B978-0-08-095975-7.00211-4>

Ryan, J. G., & Kyle, P. R. (2004). Lithium abundance and lithium isotope variations in mantle sources: Insights from intraplate volcanic rocks from Ross Island and Marie Byrd Land (Antarctica) and other oceanic islands. *Chemical Geology*, 212, 125–142.

Ryan, J. G., & Langmuir, C. H. (1993). The systematics of boron abundances in young volcanic rocks. *Geochimica et Cosmochimica Acta*, 57, 1489–1498.

Saal, A. E., Hauri, E. H., Langmuir, C. H., & Perfit, M. R. (2002). Vapour undersaturation in primitive mid-ocean-ridge basalt and the volatile content of Earth's upper mantle. *Nature*, 419, 451–455.

Saccoccia, P. J., Seewald, J. S., & Shanks, W. C. (2001). New D-H and $^{18}\text{O}/^{16}\text{O}$ fractionation factors for serpentine and talc from 250 to 450°C. Paper presented at American Geophysical Union, Fall Meeting 2001 (abstract #V51B-0991).

Sakai, H., & Tsutsumi, M. (1978). D/H fractionation factors between serpentine and water at 100 to 500°C and 2000 bar water pressure and the D/H ratios of natural serpentines. *Earth and Planetary Science Letters*, 40, 231–242.

Salter, V. J. M., Longhi, J. E., & Bizimis, M. (2002). Near mantle solidus trace element partitioning at pressures up to 3.4 GPa. *Geochemistry Geophysics Geosystems*, 3(2). <https://doi.org/10.1029/2001GC000148>

Salter, V. J. M., & White, W. M. (1998). Hf isotope constraints on mantle evolution. *Chemistry Geology*, 145, 447–460.

Sarda, P., Moreira, M., Staudacher, T., Schilling, J.-G., & Allégre, C. J. (2000). Rare gas systematics on the southernmost Mid-Atlantic Ridge: Constraints on the lower mantle and the Dupal source. *Journal Geophysical Research*, 105, 5973–5996.

Satake, H., & Matsuda, J.-I. (1979). Strontium and hydrogen isotope geochemistry of fresh and metabasalt dredged from the Mid-Atlantic Ridge. *Contributions to Mineralogy and Petrology*, 70, 153–157.

Schilling, J.-G., Kingsley, R., Fontignie, D., Poreda, R., & Xue, S. (1999). Dispersion of the Jan Mayen and Iceland mantle plumes in the Arctic: A He-Pb-Nd-Sr isotope tracer study of basalts from the Kolbeinsey, Mohns, and Knipovich Ridges. *Journal Geophysical Research*, 104, 10543–10569.

Schilling, J.-G., Sigurdsson, H., Davis, A. N., & Hey, R. N. (1985). Easter microplate evolution. *Nature*, 317, 325–331.

Schilling, J.-G., Zajac, M., Evans, R., Johnston, T., White, W., Devine, J. D., & Kingsley, R. (1983). Petrologic and geochemical variations along the mid-Atlantic Ridge from 29°N to 73°N. *American Journal of Science*, 283, 510–586.

Schmidt, M. W., Dardon, A., Chazot, G., & Vannucci, R. (2004a). Rutile-Melt partitioning of Nb and Ta dependent on melt composition and Nb/Ta fractionation in the Earth. *Earth and Planetary Science Letters*, 226, 415–432. <https://doi.org/10.1016/j.epsl.2004.08.010>

Schmidt, M. W., & Poli, S. (1998). Experimentally based water budgets for dehydrating slabs and consequences for arc magma generation. *Earth and Planetary Science Letters*, 163, 361–379.

Schmidt, M. W., & Poli, S. (2014). Devolatilization during subduction. In H. Holland & K. Turekian (Eds.), *Treatise on geochemistry* (2nd ed., Volume 4: The crust). Elsevier Ltd. <https://doi.org/10.1016/B978-0-08-095975-7.00321-1>

Schmidt, M. W., Vielzeuf, D., & Auzanneau, E. (2004b). Melting and dissolution of subducting crust at high pressures: The key role of white micas. *Earth and Planetary Science Letters*, 228, 65–84.

Scholl, D. W., von Huene, R., Vallier, T. L., & Howell, D. G. (1980). Sedimentary masses and concepts about tectonic processes at underthrust ocean margins. *Geology*, 8, 564–568.

Schrauder, M., & Navon, O. (1994). Hydrous and carbonatitic mantle fluids in fibrous diamonds from Jwaneng, Botswana. *Geochimica et Cosmochimica Acta*, 58, 761–771.

Shaw, A. M., Hauri, E. H., Fischer, T. P., Hilton, D. R., & Kelley, K. A. (2008). Hydrogen isotopes in Mariana arc melt inclusions: Implications for subduction dehydration and the deep-Earth water cycle. *Earth and Planetary Science Letters*, 275, 138–145.

Sheppard, S. M., & Epstein, S. (1970). The oxygen and hydrogen isotope geochemistry of clay minerals. *Geochimica et Cosmochimica Acta*, 34, 25–42.

Sheppard, S. M. F., & Gilg, H. A. (1996). Stable isotope geochemistry of clay minerals "The story of sloppy, sticky, lumpy and tough" Cairns-Smith (1971). *Clay Minerals*, 31, 1–24.

Shirey, S. B., Bender, J. F., & Langmuir, C. H. (1987). Three-component isotopic heterogeneity near the Oceanographer transform, Mid-Atlantic Ridge. *Nature*, 325, 217–223.

Shirey, S. B., Cartigny, P., Frost, D. J., Keshav, S., Nestola, F., Nimis, P., ... Walter, M. J. (2013). Diamonds and the geology of mantle carbon. *Reviews in Mineralogy & Geochemistry*, 75, 355–421.

Sigurdsson, H. (1981). First-order major element variation in basalt glasses from the Mid-Atlantic Ridge: 29°N to 73°N. *Journal Geophysical Research*, 86, 9483–9502.

Simons, K. K., Dixon, J. E., Kingsley, R. H., Schilling, J.-G., & Poreda, R. (2002). Volatiles in basaltic glasses from the Easter-Salas y Gomez Seamount Chain and Easter Microplate: Implications for geochemical cycling of volatile elements. *Geochemistry Geophysics Geosystems*, 3(7). <https://doi.org/10.1029/2001GC000173>

Simons, K. K., Harlow, G. E., Brueckner, H. K., Goldstein, S. L., Sorensen, S. S., Hemming, N. G., & Langmuir, C. H. (2010). Lithium isotopes in Guatemalan and Franciscan HP-LT rocks: Insights into the role of sediment-derived fluids during subduction. *Geochimica et Cosmochimica Acta*, 74, 3621–3641.

Sizova, E., Gerya, T., Brown, M., & Perchuck, L. L. (2010). Subduction styles in the Precambrian: Insight from numerical experiments. *Lithos*, 116, 209–229. <https://doi.org/10.1016/j.lithos.2009.05.028>

Sleep, N., & Windley, B. F. (1982). Archean plate tectonics: Constraints and inferences. *Journal of Geology*, 90, 363–379.

Sobolev, A. V., Hofmann, A. W., Kuzmin, D. V., Yaxley, G. M., Arndt, N. T., Chung, S.-L., ... Teklay, T. (2007). The amount of recycled crust in sources of mantle-derived melts. *Science*, 316, 412–417. <https://doi.org/10.1126/science>

Spivack, A. J., & Edmond, J. M. (1987). Boron isotopic exchange between seawater and the oceanic crust. *Geochimica et Cosmochimica Acta*, 51, 1033–1043.

Stachel, T. (2001). Diamonds from the asthenosphere and the transition zone. *European Journal of Mineralogy*, 13, 883–892.

Stakes, D. S. (1991). Oxygen and hydrogen isotope compositions of oceanic plutonic rocks: High temperature deformation and metamorphism of oceanic layer 3. In H. P. Taylor, J. R. O'Neil, & I. R. Kaplan (Eds.), *Stable isotope geochemistry: A tribute to Samuel Epstein*, (Geochemistry Society Special Publication No. 3, pp. 77–90). San Antonio, TX: Geochemical Society.

Stakes, D. S., & O'Neil, J. R. (1982). Mineralogy and stable isotope geochemistry of hydrothermally altered oceanic rocks. *Earth and Planetary Science Letters*, 57, 285–304.

Stalder, R., Foley, S. F., Brey, G. P., & Horn, I. (1998). Mineral-aqueous fluid partitioning of trace elements at 900–1200°C and 3.0 – 5.7 GPa: New experimental data for garnet, clinopyroxene, and rutile, and implications for mantle metasomatism. *Geochimica et Cosmochimica Acta*, 62, 1781–1801.

Stern, C. R. (2011). Subduction erosion: Rates, mechanisms, and its role in arc magmatism and the evolution of the continental crust and mantle. *Gondwana Research*, 20, 284–308.

Stern, R. J. (2002). Subduction zones. *Reviews of Geophysics*, 40(4), 1012. <https://doi.org/10.1029/2001RG000108>

Stern, R. J. (2005). Evidence from ophiolites, blueschists, and ultrahigh-pressure metamorphic terranes that the modern episode of subduction tectonics began in Neoproterozoic time. *Geology*, 33, 557–560. <https://doi.org/10.1130/G21365.1>

Stern, R. J., & Scholl, D. W. (2010). Yin and yang of continental crust creation and destruction by plate tectonic processes. *International Geology Review*, 52, 1–31.

Stracke, A. (2012). Earth's heterogeneous mantle: A product of convection-driven interaction between crust and mantle. *Chemical Geology*, 330–331, 274–299.

Stracke, A., Bizimis, M., & Salters, V. J. M. (2003). Recycling oceanic crust: Quantitative constraints. *Geochemistry Geophysics Geosystems*, 4(3), 8003. <https://doi.org/10.1029/2001GC000223>

Stracke, A., Hofmann, A. W., & Hart, S. R. (2005). FOZO, HIMU, and the rest of the mantle zoo. *Geochemistry, Geophysics, Geosystems*, 6, Q05007. <https://doi.org/10.1029/2004GC000824>

Suárez, G., Gagnepain, J., Cisternas, A., Hatzfeld, D., Molnar, P., Ocola, L., Roecker, S. W., & Viodé, J. P. (1990). Tectonic deformation of the Andes and the configuration of the subducted slab in central Peru: Results from a microseismic experiment. *Geophysics: Journal International*, 103, 1–12.

Sun, S.-S., & McDonough, W. F. (1989). Chemical and isotopic systematics of oceanic basalts: Implications for mantle composition and processes. In A. D. Saunders and M. J. Norry (Eds.), *Magmatism in the ocean basins* (pp. 313–345). London, UK: The Geological Society.

Suzuki, T., & Epstein, S. (1976). Hydrogen isotope fractionation between OH-bearing minerals and water. *Geochimica et Cosmochimica Acta*, 40, 1229–1240.

Syracuse, E. M., van Keken, P. E., & Abers, G. A. (2010). The global range of subduction zone thermal models. *Physics of the Earth and Planetary Interiors*, 183, 73–90.

Tanaka, R., & Nakamura, E. (2005). Boron isotopic constraints on the source of Hawaiian shield lavas. *Geochimica et Cosmochimica Acta*, 69, 3385–3399.

Tappe, S., Foley, A., Atrache, R., Romer, B., Kjarsgaard, L., Heaman, L., & Joyce, (2007). Craton reactivation on the Labrador Sea margins: $^{40}\text{Ar}/^{39}\text{Ar}$ age and Sr-Nd-Hf-Pb isotope constraints from alkaline and carbonatite intrusives. *Earth and Planetary Science Letters*, 256, 433–454.

Thompson, A. B. (1992). Water in the Earth's upper mantle. *Nature*, 358, 295–302.

Thomson, A. R., Kohn, S. C., Bulanova, G. P., Smith, C. B., Araujo, D., Eimf, & Walter, M. J. (2014). Origin of sub-lithospheric diamonds from the Juina-5 kimberlite (Brazil): Constraints from carbon isotopes and inclusion compositions. *Contributions to Mineralogy and Petrology*, 168, 1081.

Thomson, A. R., Walter, M. J., Kohn, S. C., & Brooker, R. A. (2016). Slab melting as a barrier to deep carbon subduction. *Nature*, 529, 76–79. <https://doi.org/10.1038/nature16174>

Tomascak, P. B., Carlson, R. W., & Shirey, S. B. (1999). Accurate and precise determination of Li isotopic compositions by multi-collector sector ICP-MS. *Chemical Geology*, 158, 145–154.

Trønnes, R. G., Planke, S., Sundvoll, B., & Imsland, P. (1999). Recent volcanic rocks from Jan Mayen: Low-degree melt fractions of enriched northeast Atlantic mantle. *Journal of Geophysical Research*, 104, 7153–7168. <https://doi.org/10.1029/1999JB900007>

Turner, S., Tonarini, S., Bindeman, I. N., Leeman, W. P., & Schaefer, B. F. (2007). Boron and oxygen isotope evidence for recycling of subducted components over the past 2.5 Gyr. *Nature*, 447, 702–705. <https://doi.org/10.1038/nature05898>

van Keken, P. E., Hacker, B. R., Syracuse, E. M., & Abers, G. A. (2011). Subduction factory: 4. Depth dependent flux of H_2O from subducting slabs worldwide. *Journal Geophysical Research*, 116, B01401. <https://doi.org/10.1029/2010JB007922>

van Keken, P. E., Hauri, E. H., & Ballentine, C. J. (2002a). Mantle mixing: The generation, reservation, and destruction of chemical heterogeneity. *Annual Review of Earth and Planetary Science*, 30, 493–525.

van Keken, P. E., Kiefer, B., & Peacock, S. M. (2002b). High resolution models of subduction zones: Implications for mineral dehydration reactions and the transport of water into the deep mantle. *Geochemistry Geophysics Geosystems*, 3(10), 1056. <https://doi.org/10.1029/1002GC000256>

Vennemann, T. W., & O'Neil, J. R. (1996). Hydrogen isotope exchange reactions between hydrous minerals and molecular hydrogen: I. A new approach for the determination of hydrogen isotope fractionation at moderate temperatures. *Geochimica et Cosmochimica Acta*, 60, 2437–2451.

Vidal, P., Chauvel, C., & Brousse, R. (1984). Large mantle heterogeneity beneath French Polynesia. *Nature*, 307, 536–538.

Vlastélic, I., Dosso, L., Bougault, H., Aslanian, D., Géli, L., Etoubleau, J., ... Bollinger, C. (2000). Chemical systematics of an intermediate spreading ridge: The Pacific-Antarctic Ridge between 56°S and 66°S. *Journal Geophysical Research*, 105, 2915–2936.

von Huene, R., & Scholl, D. (1993). The return of sialic material to the mantle indicated by terrigenous material subducted at convergent margins. *Tectonophysics*, 219, 163–175.

Wada, I., Behn, M. D., & Shaw, A. M. (2012). Effects of heterogeneous hydration in the incoming plate, slab rehydration, and mantle wedge hydration on slab-derived H_2O flux in subduction zones. *Earth and Planetary Science Letters*, 353–354, 60–71.

Wada, I., & Wang, K. (2009). Common depth of decoupling between the subducting slab and mantle wedge: Reconciling diversity and uniformity of subduction zones. *Geochemistry Geophysics Geosystems*, 10, Q10009. <https://doi.org/10.1029/2009GC002570>

Waggoner, D. G. (1990). *An isotopic and trace element study of mantle heterogeneity beneath the Norwegian-Greenland Sea* (Ph.D. dissertation). University of Rhode Island, Kingston, RI.

Walowski, K. J., Wallace, P. J., Hauri, E. H., Wada, I., & Clyne, M. A. (2015). Slab melting beneath the Cascade Arc driven by dehydration of altered oceanic peridotite. *Nature Geoscience*, 8, 404–408. <https://doi.org/10.1038/NGEO2417>

Weaver, B. L. (1991). The origin of ocean island basalt end-member compositions: Trace element and isotopic constraints. *Earth and Planetary Science Letters*, 104, 381–397.

Weis, D., Frey, F. A., Leyrit, H., & Gautier, I. (1993). Kerguelan Archipelago revisited: Geochemical and isotopic study of the Southeast Province lavas. *Earth and Planetary Science Letters*, 118, 101–119.

Weiss, Y., Class, C., Goldstein, S. L., & Hanyu, T. (2015). Key new pieces of the HIMU puzzle from olivines and diamond inclusions. *Nature*. <https://doi.org/10.1038/nature19113>

Weiss, Y., McNeill, J., Pearson, D. G., Nowell, G. M., & Ottley, C. J. (2016). Highly saline fluids from a subducting slab as the source for fluid-rich diamonds. *Nature*, 524, 339–344. <https://doi.org/10.1038/nature14857>

Wenner, D. B., & Taylor, H. P. Jr. (1974). D/H and O^{18}/O^{16} studies of serpentinization of ultramafic rocks. *Geochimica et Cosmochimica Acta*, 38, 1255–1286.

White, W. M. (1985). Sources of oceanic basalts: Radiogenic isotopic evidence. *Geology*, 13, 115–118.

White, W. M. (2015). Isotopes, DUPAL, LLSVPs, and Anekantavada. *Chemical Geology*, 419, 10–28.

White, W. M., & Duncan, R. (1996). Geochemistry and geochronology of the Society Islands: New evidence for deep mantle recycling. In A. Basu and S. Hart (Eds.), *Earth processes: Reading the isotopic code, AGU Monograph Series* (Vol. 95, pp. 183–206). Washington, DC: American Geophysical Union.

Willbold, M., & Stracke, A. (2006). Trace element composition of mantle end-members; implications for recycling of oceanic and upper and lower continental crust. *Geochemistry Geophysics Geosystems*, 7, Q04004. <https://doi.org/10.1029/2005GC001005>

Woodhead, J. D., & Devey, C. W. (1993). Geochemistry of the Pitcairn seamounts: 1: Source character and temporal trends. *Earth and Planetary Science Letters*, 116, 81–99.

Workman, R. K., & Hart, S. R. (2005). Major and trace element composition of the depleted MORB mantle (DMM). *Earth Planet. Sci. Lett.*, 231, 53–72.

Workman, R. K., Hart, S. R., Jackson, M., Regelous, M., Farley, K. A., Blusztajn, J., ... Staudigel, H. (2004). Recycled metasomatized lithosphere as the origin of the Enriched Mantle II (EM2) end-member: Evidence from the Samoan volcanic chain. *Geochemistry Geophysics Geosystems*, 5, Q04008. <https://doi.org/10.1029/2003GC000623>

Workman, R. K., Hauri, E., Hart, S. R., Wang, J., & Blusztajn, J. (2006). Volatile and trace elements in basaltic glasses from Samoa: Implications for water distribution in the mantle. *Earth and Planetary Science Letters*, 241, 932–951.

Yaxley, G. M., & Brey, G. P. (2004). Phase relations of carbonate-bearing eclogite assemblages from 2.5 to 5.5 GPa: Implications for petrogenesis of carbonatites. *Contributions to Mineralogy and Petrology*, 146, 606–619.

Zack, T., Tomascak, P. B., Rudnick, R. L., Dalpe, C., & McDonough, W. F. (2003). Extremely light Li in orogenic eclogites: The role of isotopic fractionation during dehydration in subducted oceanic crust. *Contributions to Mineralogy and Petrology*, 208, 279–290. 2003.

Zindler, A., & Hart, S. (1986). Chemical geodynamics. *Annual Review of Earth and Planetary Sciences*, 14, 493–571.

Zindler, A., Staudigel, H., & Batiza, R. (1984). Isotope and trace element geochemistry of young Pacific seamounts: Implications from the scale of upper mantle heterogeneity. *Earth and Planetary Science Letters*, 70, 175–195.